



# Developing Lumped-Parameter Models for Porcine-to-Human Cardiac Xenotransplantation

Aoife Healy

19367166

A thesis submitted to University College Dublin  
in fulfilment of the requirements for the degree of

**ME in Mechanical Engineering**

College of Engineering and Architecture  
School of Mechanical and Materials Engineering

*Head of School:* Associate Professor Vincent Hargaden

*Supervisor:* Associate Professor Philip Cardiff

April 2024

## ABSTRACT

Research in porcine-to-human cardiac xenotransplantation is driven by the goal of providing a viable alternative to human-to-human cardiac transplantation, to which the shortage of donor organs is currently the limiting factor. Several challenges still need to be overcome before this can be achieved, including the mechanical challenges introduced by the anatomical differences between pig and human hearts.

Throughout this project, a computationally inexpensive lumped-parameter model of the cardiovascular system was developed and used to investigate the effect of anatomical differences between pig and human hearts on pressure and blood flow characteristics throughout the cardiovascular system.

It is concluded that the anatomical differences with the greatest effect on the mechanics of the cardiovascular system are an increased muscle thickness of the ventricles, resulting in greater pumping power of the heart, decreased diameters of the aortic and pulmonary sinuses, resulting in increased resistance to blood flow through these vessels, and a decrease in Young's modulus of the great vessels, allowing for a greater volume of blood to be accommodated in these vessels.

## STATEMENT OF ORIGINAL AUTHORSHIP

I hereby certify that the submitted work is my own work, was completed while registered as a candidate for the degree stated on the Title Page, and I have not obtained a degree elsewhere on the basis of the research presented in this submitted work.

## ACKNOWLEDGEMENTS

I would like to extend my gratitude to the following people, without whom this project would not have been possible:

My academic supervisor, Associate Professor Philip Cardiff, for his guidance and enthusiasm in this project, offering valuable insights at our every discussion.

My parents for reading and giving me notes on this thesis, offering support and guidance throughout this year, and acting as my first engineering role models.

My friends and colleagues for their help and support throughout this year and my college career.

# CONTENTS

<b>List of Tables</b>	<b>x</b>
<b>List of Figures</b>	<b>xii</b>
<b>Glossary</b>	<b>xvi</b>
<b>List of Acronyms</b>	<b>xxi</b>
<b>Symbols used in mathematical equations</b>	<b>xxiii</b>
<b>1 Introduction</b>	<b>1</b>
1.1 Context . . . . .	1
1.2 Motivation . . . . .	2
1.3 Overall Aim . . . . .	3
1.4 Specific Objectives . . . . .	3
1.5 Thesis Layout . . . . .	4
<b>2 Literature Review</b>	<b>6</b>
2.1 Xenotransplantation . . . . .	6
2.1.1 History of xenotransplantation . . . . .	6

2.1.2	Challenges to overcome . . . . .	8
2.2	Surgical techniques for cardiac transplantation . . . . .	9
2.2.1	Biatrial cardiac transplantation . . . . .	10
2.2.2	Bicaval cardiac transplantation . . . . .	11
2.2.3	Surgical techniques for cardiac xenotransplantation . . . . .	11
2.3	Lumped-parameter models of the cardiovascular system . . . . .	12
2.3.1	Uses of LPMs for investigating pathological conditions . . . . .	14
2.3.2	Making LPMs patient-specific . . . . .	15
2.3.3	Coupling of LPMs with 1D and 3D models . . . . .	16
2.4	Comparison between pig and human heart anatomy . . . . .	17
2.4.1	The great vessels . . . . .	17
2.4.2	The atria . . . . .	18
2.4.3	The ventricles . . . . .	18
2.5	Summary of Literature Review . . . . .	19
<b>3</b>	<b>Methodology</b>	<b>21</b>
3.1	Mathematical model . . . . .	21
3.1.1	Hydraulic-electrical analogy for blood vessel behaviour . . . . .	21
3.1.2	Remodelling compliance . . . . .	23
3.1.3	Heart chambers . . . . .	25
3.1.4	Heart valves . . . . .	28
3.1.5	Making an LPM of the human circulatory system . . . . .	29
3.2	LPM of a standard human to use as a reference . . . . .	30
3.3	Modelling biatrial porcine-to-human cardiac xenotransplantation . . . . .	31
3.3.1	Decrease in aortic and pulmonary sinus diameters . . . . .	31

3.3.2	Decrease in aortic and pulmonary sinus Young's modulus . . . . .	32
3.3.3	Smaller atrial volumes relative to cardiac mass . . . . .	33
3.3.4	Increase in ventricle wall thickness . . . . .	33
3.3.5	Mismatch in size between left and right sides of the porcine heart	34
3.3.6	Summary of LPM parameter changes . . . . .	34
3.4	Modelling bicaval porcine-to-human cardiac xenotransplantation . . . . .	35
3.4.1	Smaller atrial volumes relative to cardiac mass . . . . .	35
3.4.2	Decrease in diameter of the venae cavae . . . . .	36
3.4.3	Decrease in venae cavae Young's modulus . . . . .	37
3.4.4	Summary of LPM parameter changes . . . . .	37
<b>4</b>	<b>The Julia Programming Language and its Application in this Project</b>	<b>39</b>
4.1	Comparison of Julia vs Python processing speed . . . . .	40
4.2	Julia packages used in model creation . . . . .	41
<b>5</b>	<b>Model Verification and Validation</b>	<b>42</b>
5.1	Verification of numerical methods . . . . .	43
5.2	Verification of basic model elements . . . . .	44
5.2.1	Validation of elementary relationships through modelling of basic Windkessel circuits . . . . .	44
5.2.2	Physical interpretation of Windkessel circuit results . . . . .	46
5.3	Validation of the model's ability to represent the cardiovascular system .	47
5.3.1	Pressure and flow characteristics in a healthy human heart . . . . .	47
<b>6</b>	<b>Results and Discussion</b>	<b>53</b>
6.1	Batrial cardiac xenotransplantation . . . . .	53

6.1.1	Effect of decreased aortic sinus radius on the left side of the heart	56
6.1.2	Effect of decreased aorta Young's modulus on the left side of the heart . . . . .	57
6.1.3	Effect of increased left ventricle elastance on the left side of the heart	58
6.1.4	Effect of biatrial cardiac xenotransplantation on the right side of the heart . . . . .	60
6.1.5	Total effect of biatrial cardiac xenotransplantation . . . . .	62
6.2	Bicaval cardiac xenotransplantation . . . . .	64
6.2.1	Effect of decreased venae cavae Young's modulus on the cardiovascular system . . . . .	65
6.2.2	Effect of bicaval xenotransplantation on the right side of the heart	66
6.2.3	Effect of decreased venae cavae Young's modulus on the right side of the heart . . . . .	67
6.2.4	Total effect of bicaval cardiac xenotransplantation . . . . .	68
<b>7</b>	<b>Conclusions and Future Work</b>	<b>70</b>
7.1	Main findings . . . . .	70
7.2	Limitations . . . . .	71
7.3	UN Sustainable Development Goals . . . . .	73
7.4	Ethical implications . . . . .	73
7.5	Possibility for future work . . . . .	74
7.5.1	Comparing model of cardiac xenotransplantation to hearts with different pathological conditions . . . . .	74
7.5.2	Coupling of LPMs and 1D models . . . . .	75
7.5.3	Coupling of LPMs and 3D models . . . . .	75
7.5.4	Valve models . . . . .	76

7.6	Final Thoughts . . . . .	76
	<b>Bibliography</b>	<b>77</b>
	<b>Appendices</b>	<b>85</b>
<b>A</b>	<b>Summary of Equations</b>	<b>87</b>
<b>B</b>	<b>Model parameters used to describe standard human circulatory system, based on Korakianitis and Shi [24]</b>	<b>89</b>
<b>C</b>	<b>Additional graphs for reference</b>	<b>91</b>
C.1	Pressure and flow in the right heart of the reference healthy human . . .	91
C.2	Additional graphs for the investigation of porcine-to-human cardiac xeno- transplantation . . . . .	94
C.2.1	Pressure curves . . . . .	94
C.2.2	Volume curves . . . . .	100
C.2.3	Pressure-Volume loops . . . . .	106
<b>D</b>	<b>Code</b>	<b>110</b>
D.1	Comparison of Julia vs Python processing speed . . . . .	110
D.1.1	Julia . . . . .	110
D.1.2	Python . . . . .	113
D.2	circulatory_system_components.jl . . . . .	117
D.3	Solving Windkessel circuits using <i>ModelingToolkit.jl</i> . . . . .	126
D.4	Building and solving an LPM of the cardiovascular system . . . . .	130

## LIST OF TABLES

3.1	Corresponding electrical and mechanical parameters and units. . . . .	23
3.2	Lumped-parameter components and their governing equations. . . . .	23
3.3	Possible system outputs . . . . .	30
3.4	Effect of decreased aortic and pulmonary sinus diameters on LPM parameters. . . . .	32
3.5	Effect of decreased aortic and pulmonary sinus Young's modulus on LPM parameters. . . . .	33
3.6	Effect of decreased atrial volume on LPM parameters. . . . .	33
3.7	Effect of increased ventricular wall thickness on LPM parameters. . . . .	34
3.8	Effect of size mismatch between the sides of the heart on LPM parameters. . . . .	34
3.9	Summary of LPM parameter changes from the reference healthy human case to model biatrial porcine-to-human cardiac xenotransplantation. . . . .	35
3.10	Effect of decreased atrial volume on LPM parameters. . . . .	36
3.11	Proportion of systemic vein parameters attributable to the venae cavae. . . . .	36
3.12	Effect of decreased venae cavae diameters on LPM parameters. . . . .	37
3.13	Effect of decreased venae cavae Young's modulus on LPM parameters. . . . .	37
3.14	Summary of LPM parameter changes from the reference healthy human case to model bicaval porcine-to-human cardiac xenotransplantation. . . . .	38

4.1	Comparison of Julia and Python processing times for solving ODEs of two, three, and four-element Windkessels. . . . .	40
5.1	Parameters used to define Windkessel circuits [46]. . . . .	45
5.2	Events in the left side of the heart during cardiac cycle. . . . .	49
5.3	Phases of the cardiac cycle, left side of the heart. . . . .	49
5.4	Phases of the cardiac cycle, as seen on the PV loop of the left ventricle. .	50
B.1	Parameters used to define heart chambers . . . . .	89
B.2	Parameters used to define heart valves . . . . .	90
B.3	Parameters used to define systemic and pulmonary circulation . . . . .	90
C.1	Events in the right side of the heart during cardiac cycle. . . . .	93
C.2	Phases of the cardiac cycle, right side of heart. . . . .	93

## LIST OF FIGURES

2.1	Heart diagram.	9
2.2	Biatrial heart transplant technique [55].	10
2.3	Bicaval heart transplant technique [55].	11
2.4	Windkessel effect [53].	13
2.5	Two-, three-, and four-element Windkessel models.	14
3.1	Electrical Components used to describe blood vessel characteristics	22
3.2	Two-Element Windkessel [46].	24
3.3	Compliance element.	25
3.4	Heart chambers activation function.	26
3.5	Elastance in the heart chambers over the cardiac cycle.	27
3.6	Heart chambers.	27
3.7	Heart valves.	28
3.8	LPM of circulatory system.	29
5.1	Solution of a simple two-element Windkessel model at a range of different tolerance levels.	43
5.2	Aortic pressure for 2, 3, and 4 element Windkessel circuits, simulated using <i>LTspice</i> .	45

5.3	Aortic pressure for 2, 3, and 4 element Windkessel circuits, simulated using Julia model. . . . .	46
5.4	Heart diagram. . . . .	47
5.5	Pressure and flow relationships in the left side of the heart, created using Julia model. . . . .	48
5.6	PV loop of the left ventricle with heart diagram for reference. . . . .	50
5.7	PV loop of the left ventricle. . . . .	51
5.8	PV loops of all four heart chambers, created using Julia model. . . . .	52
6.1	Pressure in the aortic sinus of a reference healthy human (blue) and altered model (red). . . . .	54
6.2	Effect of decreased aortic sinus radius on the left side of the heart, showing reference healthy human (blue) and altered model (red). . . . .	56
6.3	Effect of decreased aorta Young's modulus on the left side of the heart, showing reference healthy human (blue) and altered model (red). . . . .	57
6.4	Effect of increased left ventricle elastance on the left side of the heart, showing reference healthy human (blue) and altered model (red). . . . .	58
6.5	Effect of increased left ventricle elastance on blood volumes in different parts of the cardiovascular system, showing reference healthy human (blue) and altered model (red). . . . .	60
6.6	PV loop of the right ventricle of a reference healthy human (blue) and the altered model (red). . . . .	61
6.7	Total effect of batrial cardiac xenotransplantation, showing reference healthy human (blue) and altered model (red). . . . .	63
6.8	Pressure in the aorta of a reference healthy human (blue) and altered model (red). . . . .	64
6.9	Effect of decreased venae cavae Young's modulus on the left side of the heart, showing reference healthy human (blue) and altered model (red). . . . .	65

6.10 Effect of decreased venae cavae Young's modulus on the volume of blood in the systemic veins, showing reference healthy human (blue) and altered model (red). . . . .	66
6.11 Effect of bicaval cardiac xenotransplantation on the right side of the heart, showing reference healthy human (blue) and altered model (red). . . . .	67
6.12 Effect of decreased venae cavae Young's modulus on right side of the heart, showing reference healthy human (blue) and altered model (red). . . . .	68
6.13 Total effect of bicaval cardiac xenotransplantation, showing reference healthy human (blue) and altered model (red). . . . .	69
 C.1 Pressure and flow relationships in the right side of the heart. . . . .	92
C.2 Pressure in the aortic sinus of a reference healthy human (blue) and altered model (red). . . . .	94
C.3 Pressure in the pulmonary sinus of a reference healthy human (blue) and altered model (red). . . . .	95
C.4 Pressure in the left ventricle of a reference healthy human (blue) and altered model (red). . . . .	96
C.5 Pressure in the right ventricle of a reference healthy human (blue) and altered model (red). . . . .	97
C.6 Pressure in the left atrium of a reference healthy human (blue) and altered model (red). . . . .	98
C.7 Pressure in the right atrium of a reference healthy human (blue) and altered model (red). . . . .	99
C.8 Volume of blood in the aortic sinus of a reference healthy human (blue) and altered model (red). . . . .	100
C.9 Volume of blood in the pulmonary sinus of a reference healthy human (blue) and altered model (red). . . . .	101

C.10 Volume of blood in the left ventricle of a reference healthy human (blue) and altered model (red). . . . .	102
C.11 Volume of blood in the right ventricle of a reference healthy human (blue) and altered model (red). . . . .	103
C.12 Volume of blood in the left atrium of a reference healthy human (blue) and altered model (red). . . . .	104
C.13 Volume of blood in the right atrium of a reference healthy human (blue) and altered model (red). . . . .	105
C.14 PV loop of the left ventricle of a reference healthy human (blue) and altered model (red). . . . .	106
C.15 PV loop of the right ventricle of a reference healthy human (blue) and altered model (red). . . . .	107
C.16 PV loop of the left atrium of a reference healthy human (blue) and altered model (red). . . . .	108
C.17 PV loop of the right atrium of a reference healthy human (blue) and altered model (red). . . . .	109

## GLOSSARY

### **Allograft**

A tissue graft from a genetically non-identical donor of the same species.

### **Allotransplantation**

The transplantation of cells, tissues, or organs to a recipient from a genetically non-identical donor of the same species.

### **Anastomosis**

A surgical connection between two tubular structures or channels.

### **Aortic dissection**

A condition caused by the formation of tears in the innermost layer of the aortic wall, causing the division of the lumen into two lumina with separate flow.

### **Aortic regurgitation**

A condition in which the aortic valve fails to fully close, allowing some of the blood that was pumped out of the left ventricle to leak back in.

### **Biatrial cardiac transplantation**

Orthotopic heart transplantation technique that retains the posterior part of the recipient's left and right atria.

### **Bicaval cardiac transplantation**

Orthotopic heart transplantation technique involving two arterial, one left atrial, and two caval anastomoses.

**Biped**

An animal that uses two legs for walking.

**Capacitor**

A device used to store an electric charge.

**Cloning**

The process of producing individual organisms with identical genomes, either by natural or artificial means.

**Coagulopathy**

A condition in which the blood's ability to coagulate (form clots) is impaired.

**Complement regulation**

Regulation of the complement system by complement control proteins.

**Diastole**

The phase of the cardiac cycle when the ventricles relax and fill with blood.

**Dilated cardiomyopathy**

A condition in which heart chamber walls stretch and thin, causing the chambers to become larger.

**Diode**

A semiconductor device with two terminals, typically allowing the flow of current in one direction only.

**Gene transfer**

The movement of genetic material between organisms other than by the transmission of DNA from parent to offspring.

**Gene knockout**

The use of genetic engineering to inactivate or remove one or more specific genes from an organism.

## **Haemodynamics**

Relating to the flow of blood within the organs and tissues of the body.

## **Heterotopic heart transplantation**

A heart transplantation procedure that allows the donor heart to be connected to the native heart in a parallel fashion.

## **Hyperacute rejection**

Rejection that occurs a few minutes after the transplant, when the antigens are completely unmatched.

## **Hypertrophic cardiomyopathy**

a disease in which the muscle in the heart walls becomes thickened.

## **Hypoplastic left heart syndrome**

A birth defect that affects normal blood flow through the heart.

## **Inductor**

A device that stores energy in a magnetic field when electric current flows through it.

## **Lumen**

The inside space of a tubular structure.

## **Mitral stenosis**

A condition in which the mitral valve narrows.

## **Mitral regurgitation**

A condition in which the mitral valve doesn't close fully, and blood leaks back across the valve.

## **Non-ischaemic cardiomyopathy**

A generic term which includes all causes of decreased heart function other than those caused by heart attacks or blockages in the arteries of the heart.

## **Orthotopic heart transplantation**

A heart transplantation procedure that involves excising the recipient heart, and transplanting the donor heart to the recipient via anastomosis.

## **Papillary muscles**

Pillar-like muscles seen within the cavity of the ventricles, attached to their walls. They have an integral role in proper cardiac valvular function.

## **Photoplethysmography**

An optical measurement method often used for heart rate monitoring purposes.

## **Quadruped**

An animal that uses four legs for walking.

## **Resistor**

A device having resistance to the passage of an electric current.

## **Stenosis**

The abnormal narrowing of a passage in the body.

## **Stroke volume**

The volume of blood pumped out of the left ventricle of the heart during each systolic cardiac contraction.

## **Systole**

The phase of the cardiac cycle when the ventricles contract and eject blood.

## **Trabeculae carnae**

Muscle columns in the ventricles of the heart that serve a mechanical role in affecting wall stress and diastolic compliance.

## **Venous return**

The flow of blood from the systemic venous network back to the right atrium.

## **Xenograft**

A tissue graft or organ transplant from a donor of a different species to the recipient.

## **Xenotransplantation**

A procedure that involves the cross-species transplantation, implantation, or infusion of live cells, tissues, or organs.

## **Xenozoonosis**

The transmission of infectious agents between species via xenograft.

## **Young's modulus**

A measure of elasticity, equal to the ratio of the stress acting on a substance to the strain produced.

## **Zero-dimensional model**

A model that varies only with time, and has no spatial variance.

## **Zoonotic disease**

An infection that is spread between humans and animals.

## LIST OF ACRONYMS

**AV** Aortic valve.

**IVC** Inferior vena cava.

**LA** Left Atrium.

**LPM** Lumped parameter model.

**LV** Left Ventricle.

**MV** Mitral valve.

**PA** Pulmonary artery.

**PAR** Pulmonary arterioles.

**PAS** Pulmonary sinus.

**PAT** Pulmonary arteries.

**PCP** Pulmonary capillaries.

**PV** Pulmonary valve; Pressure-volume.

**PVN** Pulmonary veins.

**RA** Right Atrium.

**RV** Right Ventricle.

**SAR** Systemic arterioles.

**SAS** Systemic aortic sinus.

**SAT** Systemic arteries.

**SCP** Systemic capillaries.

**SVC** Superior vena cava.

**SVN** Systemic veins.

**TV** Tricuspid valve.

## SYMBOLS USED IN MATHEMATICAL EQUATIONS

$A$	Area
$C$	Compliance of vessel; Coefficient
$CQ$	Flow coefficient
$E$	Young's modulus of vessel wall; Elastance
$h$	Vessel wall thickness
$I$	Current
$l$	Vessel length
$L$	Inertia of blood in the vessel
$P$	Pressure in a vessel/chamber
$Q$	Blood flow rate through component
$r$	Vessel radius
$R$	Resistance of vessel
$T$	Time; Heart period
$V$	Voltage; Volume of blood in vessel/chamber
$\beta$	Ratio of orifice hole diameter to pipe diameter in orifice valve
$\Delta P$	Pressure drop across component
$\mu$	Fluid dynamic viscosity
$\rho$	Density of blood

## Subscripts

0	Initial value; Offset value; Value for unstressed condition
<i>ar</i>	Arterioles
<i>as</i>	Great artery (aorta and pulmonary artery) sinus
<i>at</i>	Arteries
<i>c</i>	Characteristic
<i>cp</i>	Capillaries
<i>d</i>	Discharge
<i>in</i>	At inlet
<i>max</i>	Maximum value
<i>min</i>	Minimum value
<i>out</i>	At outlet
<i>p</i>	Pulmonary circulation; Peripheral
<i>s</i>	Systemic circulation
<i>s1</i>	Peak of systolic phase
<i>s2</i>	End of systolic phase
<i>vn</i>	Veins

---

## CHAPTER

# ONE

---

## INTRODUCTION

### 1.1 Context

The shortage of human donor organs is currently the limiting factor to completing organ transplants, including heart transplants, in many countries. In Ireland there are currently approximately 600 people on waiting lists for organ transplants [8]. Porcine-to-human cardiac [xenotransplantation](#), or the transplantation of a pig heart into a human, is hoped to offer a viable alternative to human-to-human heart transplants in the future. Although human-to-human [allograft](#) will always be the preferred option, in the absence of human donor organs, xenotransplantation could revolutionise the world of organ transplantation, significantly increasing the number of transplants performed by using organs from animals bred specifically for xenotransplantation.

In recent years two porcine-to-human cardiac xenotransplantations have been carried out by a pioneering group of surgeons at the University of Maryland Medical Centre in the USA (discussed later in Section 2.1). While to date the longest survival time of a patient post-transplant has been circa 2 months, the insights gained from these procedures have been invaluable in determining the challenges that still need to be overcome before xenotransplantation can be considered as a viable alternative to allograft transplantation.

Lumped-parameter, or zero-dimensional models of the cardiovascular system offer a computationally inexpensive way to model and monitor key performance indicators throughout the cardiovascular system. Lumped parameter modelling has previously been used successfully to investigate different pathological conditions (discussed further in Section 2.3.1), however, it has not yet been used to model xenotransplantation. It is hoped that such models can offer some initial insights into the effects of cardiac xenotransplantation on the cardiovascular system before more complex models (for example 3D models using computational fluid dynamics) are developed.

## 1.2 Motivation

After overcoming the issues of immediate rejection of the heart, and the barriers of immunity and infection, factors affecting the long-term success of xenotransplantation must be considered. To determine these factors, a clear understanding of the mechanical challenges introduced by the anatomical difference between pig and human hearts must be understood. Differences such as cardiac chamber volumes and muscle strengths, as well as the dimensions and elastic properties of the blood vessels connected to the heart, must be considered when attempting to determine the influence of the xenotransplant on the overall cardiovascular system.

Lumped-parameter modelling is used to model and monitor important metrics such as blood pressure and flow rates at different points in the circulatory system. They offer a good starting point for gaining an understanding of the circulatory system before more complex geometric models are employed. Lumped-parameter models (**LPMs**) of the circulatory system exploit the commonly used hydraulic-electric analogy to model the system as an electrical circuit, with voltage representing pressure, and current representing blood flow.

## 1.3 Overall Aim

The overall aim of this project is to investigate the effect that the anatomical differences between pig and human hearts have on the mechanics of the cardiovascular system, and the long-term success of the [xenograft](#). It is hoped to gain an understanding of which physical differences between pig and human hearts result in the most critical changes to pressure and blood-flow characteristics within the mechanical system.

A computationally efficient model such as the LPM created for this project has outputs, such as pressure-time and volume-time curves that are familiar to clinicians and easily interpreted. Therefore an LPM that can be easily altered could be used by clinicians to aid their expectations pre-surgery and in the understanding of changes in mechanical parameters post-surgery, as well as aiding with size-matching of pigs and humans.

This project supports the following UN Sustainable Development Goals, which will be further discussed in Section [7.3](#):

- Goal 3 - Good Health and Well-Being.
- Goal 9 - Industry, Innovation and Infrastructure.

## 1.4 Specific Objectives

The specific objectives of this project include:

- Undertake a literature review to gain insights into:
  - The history of xenotransplantation, and the current state of cardiac xenotransplantation research.
  - How LPMs of the cardiovascular system have previously been developed.
  - How LPMs have previously been used to investigate different pathological conditions.
  - The critical anatomical differences between pig and human hearts.

- Become familiar with the Julia programming language, and the packages that will be useful in the development of an LPM of the circulatory system.
- Develop a fully functioning LPM of the human circulatory system in the Julia programming language that can be easily tailored to represent human circulation with a transplanted pig heart, by altering model parameters.
- Determine how to alter the LPM model parameters to best represent the physical changes introduced by porcine-to-human cardiac xenotransplantation.
- Use this model to investigate how the various anatomical differences between pig and human hearts affect key cardiovascular performance indicators by:
  - Investigating each physical change introduced by porcine-to-human cardiac xenotransplantation in isolation to determine those that result in the greatest changes in key metrics.
  - Investigating the total effect of cardiac xenotransplantation on these indicators.

## 1.5 Thesis Layout

This document is split into several chapters.

Chapter 2 covers the literature review and discusses the history and current state of xenotransplantation research, along with the previous development and implementations of LPMs of the cardiovascular system.

Chapter 3 entitled “Methodology” details the mathematical modelling behind the LPM developed for this project. This chapter also discusses the changes to LPM parameters that are made to represent the physical differences between pig and human hearts.

Chapter 4 briefly introduces the Julia programming language and why it was chosen for the creation of the LPM of the cardiovascular system developed for this project.

Chapter 5 details the verification and validation of the model (created using the Julia programming language) that was carried out to determine its ability to represent the cardiovascular system. This included a verification of numerical methods, along with

a verification of the basic elements that the model consists of, and a validation of the model as a whole through comparison with clinical data. Some key model outputs are then discussed for the standard case of a healthy human to gain an understanding of the different stages of the cardiac cycle.

Chapter 6 contains the key results from the investigation of the impact of both biatrial cardiac xenotransplantation and bicaval cardiac xenotransplantation on key mechanical performance indicators in the cardiovascular system.

Finally, Chapter 7 summarises the main findings of this project, along with the limitations of the LPM, and the possibility for future work and research.

---

## CHAPTER

# TWO

---

## LITERATURE REVIEW

### 2.1 Xenotransplantation

#### 2.1.1 History of xenotransplantation

Xenotransplantation can be defined as any procedure that involves the transplantation, implantation, or infusion into a human recipient of live cells, tissues, or organs from a non-human animal source [42]. Xenotransplantation is hoped to offer an alternative to allotransplantation (human-to-human transplantation). The first record of any form of xenotransplantation dates back to the seventeenth century when lamb's blood was used in blood transfusions. One of the first documented organ xenotransplants was a kidney transplant in 1909, in which a macaque kidney was transplanted into a woman, who survived for 32 hours before dying from organ rejection. The invention of effective immunosuppressants in the 1960s saw a renewed interest in organ transplantation, including xenotransplantation.

The first cardiac transplantation was a xenotransplantation of a chimpanzee heart into a human adult male in 1964 [23], and occurred before the first human-to-human cardiac transplantation. Unfortunately, the patient only survived for 90 minutes due

to the chimpanzee heart being too small to handle the large [venous return](#). Three other cardiac xenotransplantations occurred in the late twentieth century, two of which resulted in immediate failure of the xenograft [20]. The third - in 1984 - was to a prematurely born baby with [hypoplastic left heart syndrome](#), who received a baboon heart in the absence of a human infant donor heart. “Baby Fae” survived for 20 days after the operation before passing away. Her case gained significant media attention, sparking an ongoing ethical debate on the subject of xenotransplantation [54].

Although early xenotransplantations used non-human-primate (NHP) xenografts, several limitations including cost and ethical concerns mean the use of NHPs as source animals for xenotransplantations is unsustainable [20]. Pigs have been identified as a source animal for cardiac xenotransplantations due to low breeding and raising costs, lower [xenozoonosis](#) risk, and fewer ethical constraints. Current trials are using pigs with 10-gene edits, which are genetically engineered to prevent [hyperacute rejection](#), [coagulopathy](#) and xenograft overgrowth, and to improve inflammation and [complement regulation](#) [23].

Since January of 2022, two porcine-to-human cardiac xenotransplantations have taken place, both at the University of Maryland Medical Centre, USA. The first of these was on 57-year-old David Bennet, a patient with [non-ischaemic cardiomyopathy](#) (abnormal heart function), who was not a candidate for a traditional [allograft](#) [18]. A biopsy taken on postoperative day 34 showed no evidence of rejection, and the xenograft was functioning normally. The patient was even able to leave his bed for the first time in 109 days. However on postoperative day 49, sudden deterioration of cardiac function occurred [23], and the patient passed away on postoperative day 60. A post-mortem examination revealed several failure mechanisms not normally seen in human allotransplantation [18]. The second such operation occurred in September of 2023 on 59-year-old Lawrence Faucette, a patient with terminal heart disease. Although researchers agreed that he was a more appropriate candidate for such a novel procedure [28], he passed away just under six weeks after the operation.

## 2.1.2 Challenges to overcome

Three main challenges exist that need to be overcome by researchers before cardiac xenotransplantation becomes a viable alternative to allotransplantation [42].

- The first is immunological rejection. Rejection remains an issue in allotransplantation and is even more difficult to address in xenotransplantation due to the evolutionary differences between the two species. [Cloning](#), [gene knockout](#), and [gene transfer](#) are being used to try and overcome this issue.
- The second challenge is the risk of xenozoonosis, which could risk the health of more than just the xenograft recipient, but also the wider population if a [zoonotic disease](#) is infectious.
- The final challenge, which is the focus of this project, is the physiological and anatomical differences between humans and source animals.

## 2.2 Surgical techniques for cardiac transplantation

Figure 2.1 shows a diagram of the heart for reference in the subsequent section.

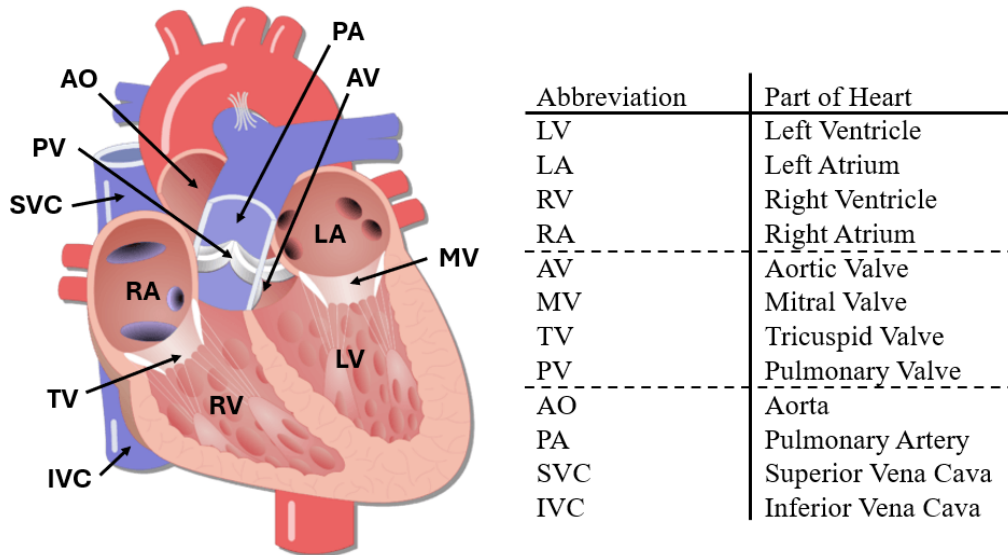
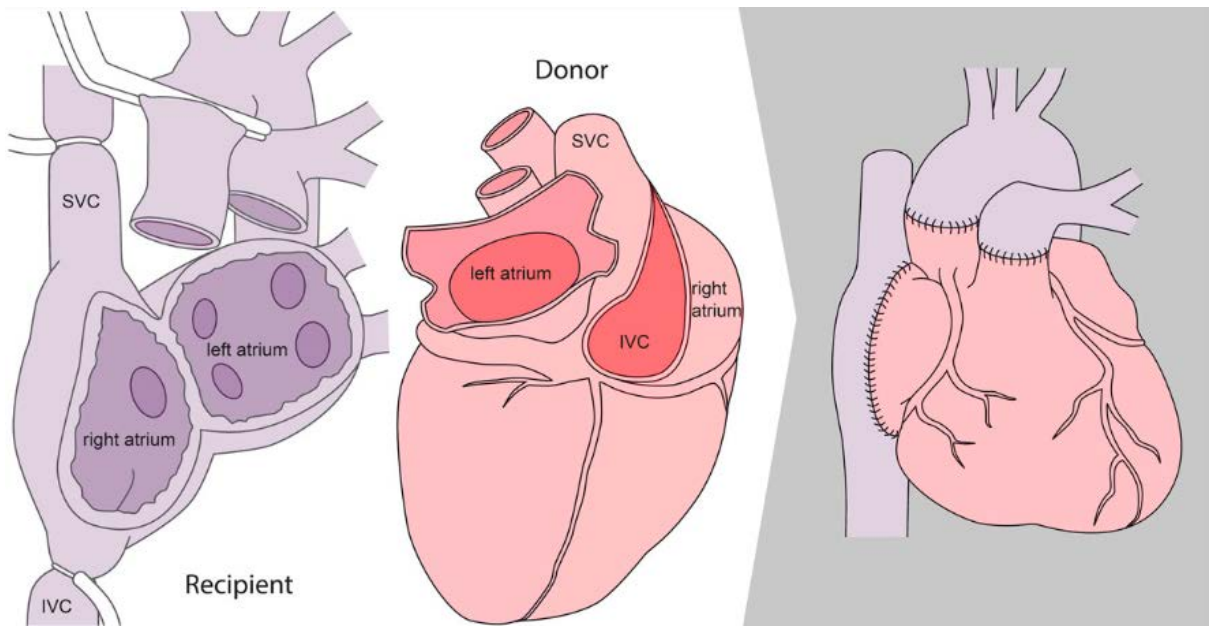


Figure 2.1: Heart diagram.

There are two types of heart transplantation procedures. [Orthotopic heart transplantation](#) is a procedure that involves excising the recipient's heart and transplanting the donor heart to the recipient via [anastomosis](#) [1]. [Heterotopic heart transplantation](#) is a procedure that allows the donor heart to be connected to the native heart in a parallel fashion [14]. Of these two heart transplant procedures, orthotopic cardiac transplantation is by far the most popular choice, with two different techniques (biatrial and bicaval). Heterotopic cardiac transplantation is much more rare, with only a handful of procedures having been performed worldwide.

### 2.2.1 Biatrial cardiac transplantation

The [biatrial cardiac transplantation](#) technique (shown in Figure 2.2) involves retaining the posterior part of the recipient's left and right atria, and anastomosing this wall to the anterior wall of the donor atria [31]. This technique is the “original” technique and is easier to perform surgically.



**Figure 2.2:** Biatrial heart transplant technique [55].

## 2.2.2 Bicaval cardiac transplantation

The [bicaval cardiac transplantation](#) technique (shown in Figure 2.3) was developed in the 1990s and has the advantage of preserving the physiological right atrium conduction system (which controls the electrical heartbeat signals) and geometry [11]. It consists of two arterial, one left atrial, and two caval (vanae cavae) anastomoses, leaving the donor right atrium intact and leaving only a small posterior part of the recipient's left atrial tissue between the pulmonary veins [31]. Due to the increased number of anastomoses, this is a much more challenging surgical technique, however, it results in more favorable early and late outcomes for patients [57].

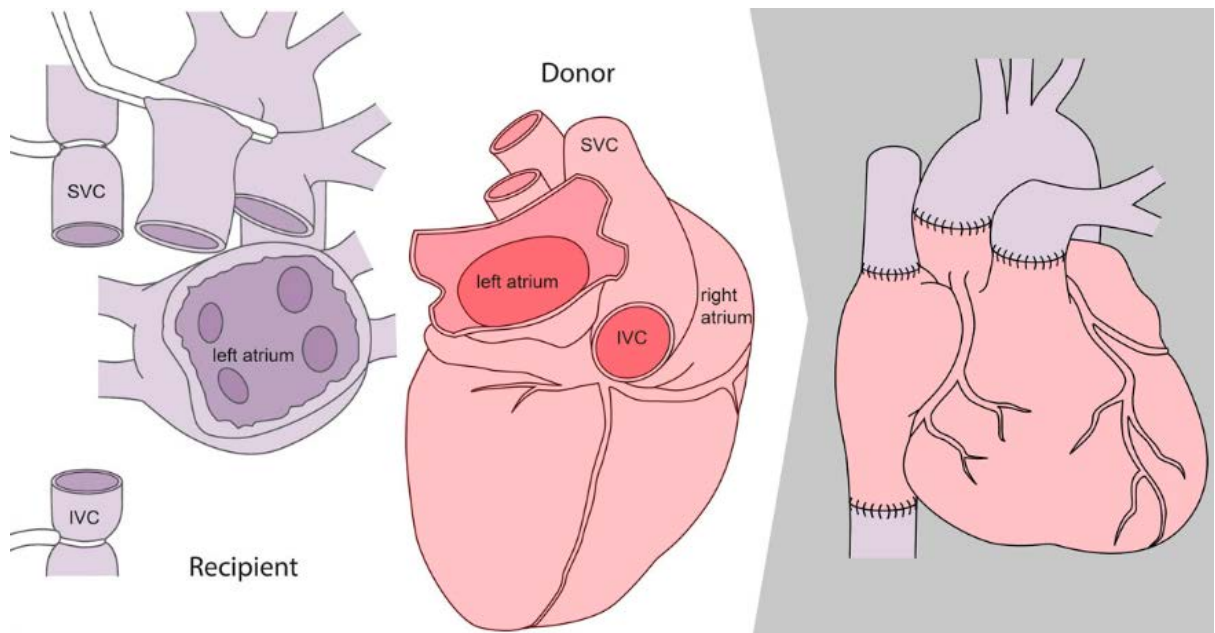


**Figure 2.3:** Bicaval heart transplant technique [55].

## 2.2.3 Surgical techniques for cardiac xenotransplantation

Of the two porcine-to-human cardiac xenotransplantations that have been performed by doctors in the University of Maryland Medical Centre in the past 3 years, only the first currently has papers published detailing the procedure, aftercare, and results of the operation.

The porcine-to-human xenotransplantation performed on 57-year-old David Bennett in January of 2022 was a biatrial cardiac transplantation. This approach was chosen

to allow accommodation for the significant atrial size discrepancies resulting from the patient’s long-standing dilated cardiomyopathy and [mitral regurgitation](#) [44]. In this case, the recipient’s atria were nearly three times larger than those of the donor heart. This size mismatch was addressed through several different surgical innovations and techniques [44].

## 2.3 Lumped-parameter models of the cardiovascular system

LPMs, or [zero-dimensional models](#), of the cardiovascular system assume a uniform distribution of the fundamental variables (pressure, flow, and volume) within any particular compartment (organ, vessel, or part of vessel) of the model at any moment in time [46]. They are referred to as zero-dimensional models because there is no spatial variance of parameters within each compartment, only temporal variance. They can be described by ordinary differential equations. LPMs of the cardiovascular system offer a concise and efficient way to evaluate the [haemodynamic](#) interactions among the heart and vasculature [46]. They use the common hydraulic-to-electric analogy to represent the cardiovascular system as an electric circuit, where a change in blood pressure is represented by voltage and blood flow is represented by current flow. The theory and modelling behind this will be discussed further in Section [3.1.1](#).

The earliest representation of systemic circulation as an electrical system was by Otto Frank in 1899 with his two-element Windkessel model [53]. The Windkessel (loosely translating to ‘air chamber’ in English) effect draws a comparison between the compliance of the large arteries with the Windkessel present in fire engines, which is illustrated in Figure [2.4](#). Blood vessel compliance is the ability of the vessel to expand to accommodate a larger volume of blood without increased resistance or blood pressure [17]. The two-element Windkessel models the time-delay effect that compliance of large arteries has on blood pressure fluctuation.

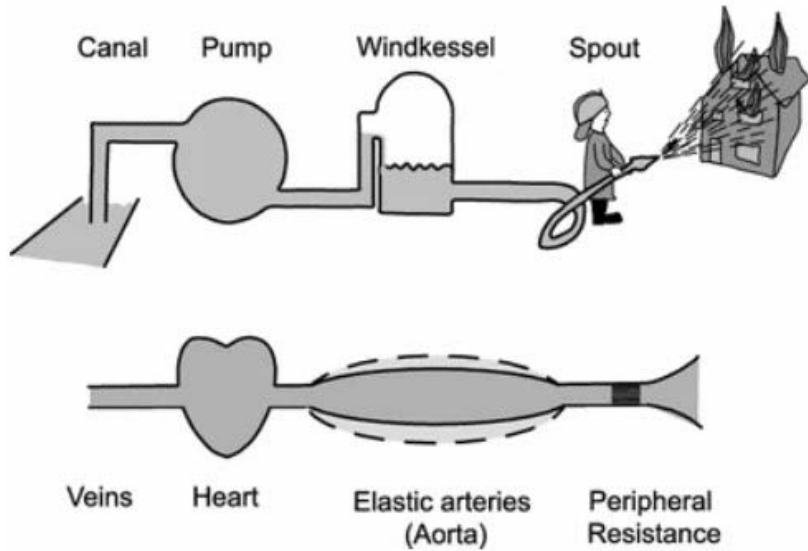


**Figure 2.4:** Windkessel effect [53].

The two-element Windkessel (Fig. 2.5 (a)) consists of a [resistor](#) and [capacitor](#) in series. The resistor represents the resistance of peripheral blood vessels to blood flow, determined by the vessel dimensions. The capacitance represents the compliance of the blood vessels. Similar to a capacitor connected in parallel which acts to smooth spikes in voltage, the compliance of a vessel means it can act as a “blood reservoir”, and can smooth out spikes in pressure.

This early model was improved upon in the three-element Windkessel model (Fig. 2.5 (b)), in which a second resistor is added in series to represent the characteristic impedance of the aorta [53]. This resulted in a more accurate pressure-flow relationship predicted by the model during [systole](#).

The final update to the Windkessel model involved adding an [inductor](#) to the model to represent the inertia of blood flow in the arteries (Fig. 2.5 (c)). This circuit is commonly referred to as the four-element Windkessel model. This inductor has been modelled both in series and parallel with the characteristic impedance. A study by Burattini and Bini [7] used generalised sensitivity function analysis to gain insight into the physiological meaning of the inductor for both models. They determined that the model containing an inductor in series (Fig 2.5 (c)) provided a better representation of blood flow inertia than a model with the inductor in parallel.

Diagrams of the two, three, and four-element Windkessels are illustrated below.

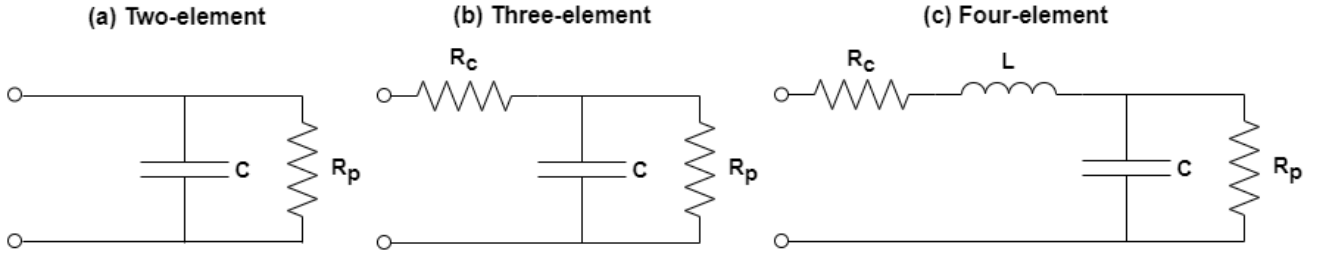


**Figure 2.5:** Two-, three-, and four-element Windkessel models.

Combinations of these RCL circuits are often used to describe sections of the systemic and pulmonary circulation.

### 2.3.1 Uses of LPMs for investigating pathological conditions

LPMs have been widely used to date to simulate pathological conditions, and to investigate the effect of these conditions on the performance of the cardiovascular system. A number of these investigations have been detailed below.

Korakianitis and Shi [24] proposed a new model of heart valve dynamics, where the valve opening is decided by the angular position of the valve leaflets, instead of the pressure difference between the two chambers that each valve connects. They used this valve model in an LPM of the circulatory system to investigate the response of key performance metrics to two separate heart valve diseases, [mitral stenosis](#) and [aortic regurgitation](#).

Rudenick et al [40] use an LPM of [aortic dissection](#) - a condition caused by the formation of tears in the innermost layer of the aortic wall, causing division of the [lumen](#) into two lumina with separate flows - to investigate the effect of wall elasticity on several blood flow characteristics within the aortic dissection.

Laubscher et al [25] aimed to improve on the valve model presented by Korakianitis and Shi, which was limited in terms of patient-specific modelling, by the need to manually tune valvular flow and force coefficients. Laubscher et al proposed a new valve model where pressure loss and motion models are based on basic valve parameters, instead of

valvular flow and force coefficients. They compare their model to Korakianitis and Shi's model in five different cases of increasing valve [stenosis](#).

Bozkurt et al [6] used three patient-specific LPMs of the circulatory system to simulate three cases of mild to severe [dilated cardiomyopathy](#) in children, a condition in which heart chamber walls stretch and thin, causing the chambers to become larger. Their study gave insights into which characteristics of the circulatory system had the greatest influence on the cardiovascular performance of children with this condition.

### 2.3.2 Making LPMs patient-specific

For LPMs to be useful in clinical practice, they must be customisable, so that patient-specific models can be made, ideally without the need for invasive measurements that could cause risk or discomfort to the patient. Several researchers have tackled the problem of customising LPMs.

Duanmu et al [12] used CT images from a patient to measure vessel lengths and diameters to personalise their LPM of the coronary circulation, which they then used to investigate the effect that head loss at vessel inlets has on blood flow characteristics.

Dash et al [10] investigated the feasibility of using non-invasive [photoplethysmography](#) (PPG) signals to estimate model parameters for an LPM of the cardiovascular system, as opposed to more commonly used, but invasive and difficult to obtain, arterial blood pressure (ABP) measurements. They found a strong correlation between parameter estimates from both signals, giving credibility to the hope of using this model for a wide-reaching screening programme for coronary artery disease.

Bozkurt et al [6] used an optimisation process to fit parameters to minimise the difference in mean arterial pressure and cardiac output between clinical data and the output of their LPM. They then used this model to investigate the effect that individual parameters have on cardiovascular performance in patients with mild to severe dilated cardiomyopathy.

Bjørdalsbakke et al [4] developed several cost functions to estimate LPM parameter subsets using synthesized data. They aimed to develop an algorithm for parameter estimation with the goal of easily personalised LPMs.

A review of the literature outlined has given an understanding of how LPMs of the cardiovascular system have previously been used, along with methods that could be used to investigate porcine-to-human cardiac xenotransplantation using LPMs.

### 2.3.3 Coupling of LPMs with 1D and 3D models

LPMs can be coupled with one-dimensional models to provide boundary conditions for the 1D models. 1D models have the added benefit over LPMs of demonstrating the propagation of pressure and flow waves in the vessel network [46], which are believed to contain valuable information regarding cardiac function.

An example of the coupling of 1D and LPM models can be seen in Formaggia et al's investigation of the pressure wave propagation in the arterial tree [15]. In this study, a simple lumped model of the heart was numerically coupled with 1D models representing the 55 largest arteries. Having a lumped model at the boundary condition accounts for the coupling between the heart and the arterial circulation that occurs, which is unaccounted for in models in which the action of the heart is reduced to a prescribed boundary condition.

LPMs can also be coupled with 3D models of parts of the circulatory system, again to provide boundary conditions to these models. Since 3D modelling is very computationally expensive, it is beneficial to limit the parts of the system modelled to only those necessary. In many applications when coupling 3D and LPM models, the lumped-parameter subdomain is intended to provide just a transfer function that incorporates the presence of the peripheral impedance to the simulation of the 3D subdomain [36]. In these cases, the Windkessel models discussed previously can provide a simplified description which can be embedded into the solution of the 3D problem in a relatively straightforward manner.

An example of such a coupling is present in Kim et al's [22] modelling of a 3D aorta, with a lumped parameter heart, described by a time-varying elastance model, which was used to provide the boundary condition at the aorta inlet, and a three-element Windkessel was used to provide the boundary condition at the aorta outlet.

## 2.4 Comparison between pig and human heart anatomy

The porcine heart bears a close resemblance to the human heart in terms of its coronary circulation and haemodynamic similarities [27].

Many of the differences in cardiac anatomy between pigs and humans are the result of the **quadruped** stance of pigs compared to the **biped** stance of humans [27]. The porcine organ has a classic “Valentine heart” shape, reflecting its location within the thorax and to the orientation of the pig’s body. The human heart, in contrast, has a trapezoidal shape [9].

This section discusses the notable differences between pig and human hearts that will be modelling in subsequent sections.

### 2.4.1 The great vessels

The large arteries and veins directly connected to the heart are termed the great vessels, consisting of the:

- Inferior vena cava (**IVC**)
- Superior vena cava (**SVC**)
- Pulmonary artery (**PA**)
- Pulmonary veins
- Root of the aorta

The diameter of the great vessels has been noted to be proportionally smaller in pigs than in humans, particularly for the ascending aorta and main pulmonary artery [44].

The length of the great vessels proximal to major branches is also proportionally shorter in pigs than in humans [44].

In pigs, the left atrium receives oxygenated blood from two pulmonary veins, whereas four pulmonary veins are generally observed in humans [27][9]. The porcine superior and inferior caval veins open into the atrium at right angles to one another, whereas in humans they are directly in line [9].

Van Andel et al's [2] study on the mechanical properties of porcine and human arteries tested the elastic properties of several coronary and internal mammary arteries. This study revealed that overall the porcine arteries were approximately three times more elastic than the human arteries, resulting in porcine blood vessels having a smaller **Young's modulus** than those of humans.

### 2.4.2 The atria

The porcine atria are smaller in size relative to the cardiac mass than the human atria [44]. The porcine left atrium is of similar size to the right atrium, whereas in the human heart, the right atrium is appreciably larger than the left [9]. The atrial septal region of the porcine heart also appears to be longer than that of the human heart [9]. As mentioned previously in Section 2.4.1, the porcine left atrium receives oxygenated blood from two pulmonary veins, whereas the human heart receives blood from four to five pulmonary veins [27].

### 2.4.3 The ventricles

It has been found that the wall thicknesses of the ventricles are much greater in the porcine heart than in a size-matched human heart [27][9]. It has also been observed that both the **trabeculae carnae** (muscles that serve a mechanical role in affecting wall stress and diastolic compliance [19]) and **papillary muscles** (muscles that ensure the proper functioning of the valves [38]) are much coarser and broader than those in the human ventricles [27][9]. A prominent muscular moderator band is situated in a much higher position within the porcine right ventricle compared with that of a human. This is thought

to explain the faster activation of the right ventricle in the pig heart when compared to the human heart [9].

## 2.5 Summary of Literature Review

Having undertaken a literature review surrounding key research areas relevant to this project, the key takeaways are as follows:

- Xenotransplantation has been a concept for hundreds of years, but has not yet achieved long-term success.
- Recent cardiac xenotransplantation research has been focused on 10-gene-edited pigs due to low breeding costs and fewer ethical concerns.
- In the past 3 years, two porcine-to-human cardiac xenotransplantations have taken place, with both patients not living longer than 2 months. The insights gained from these procedures however have given the doctors hope for larger clinical trials.
- There are several surgical techniques for cardiac transplantation, of which the biatrial technique has been favoured in the two recent porcine-to-human cardiac xenotransplantations.
- LPMs of the cardiovascular system are zero-dimensional models that can be used to investigate pressure and flow rates in sections of the cardiovascular system over time. They are relatively computationally inexpensive and offer a good starting point for the investigation of the effect of cardiac xenotransplantation on the cardiovascular network as a mechanical system.
- LPMs make use of the electric-hydraulic analogy to represent parts of the cardiovascular system as electrical elements.
- LPMs of varying complexity have previously been used to investigate a range of pathological conditions, and their impact on the cardiovascular system, but have not yet been used to model cardiac xenotransplantation.

- To date, there has also been significant research into the best ways to make LPMs patient-specific.
- As well as being capable of representing the entire cardiovascular system, LPMs can also be coupled with 1D and 3D models to offer boundary conditions to sections of the cardiovascular system that are to be examined in greater detail.
- There are several anatomical differences between pig and human hearts, the most notable of which being the decreased diameters and Young's moduli of the great vessels, and the increased thickness of the ventricle walls.

---

## CHAPTER

# THREE

---

## METHODOLOGY

### 3.1 Mathematical model

This section discusses the underlying theory and mathematical equations used in the creation of the LPM used in this project. This model was created using the Julia programming language (discussed further in Chapter 4).

A summary of the equations presented in this section can be seen in Appendix A.

#### 3.1.1 Hydraulic-electrical analogy for blood vessel behaviour

In this section, the underlying theory behind the hydraulic-electric analogy, allowing the circulatory system to be modelled as an electrical circuit, will be discussed. The basic parameters of voltage and current represent pressure drop and blood flow respectively. There are three basic electrical elements, the resistor, capacitor, and inductor, which are used to model both systemic and pulmonary circulation. They represent blood vessel resistance, blood vessel compliance, and blood flow inertia respectively.

Both of Kirchhoff's laws apply to circuits created using these elements. Kirchhoff's current law states that the algebraic sum of all currents entering and exiting a node must

equal zero.

$$\sum I_{node} = 0 \quad (3.1)$$

Kirchhoff's voltage law states that the algebraic sum of the potential differences in any loop must be equal to zero.

$$\sum V_{loop} = 0 \quad (3.2)$$

Resistance (R), capacitance (C) and inductance (L) values to be used in the model can be calculated through the following formulae based on the physical properties of the blood vessels.

$$R = \frac{8\mu l}{\pi r^4} \quad C = \frac{3\pi r^3 l}{2Eh} \quad L = \frac{\rho l}{\pi r^2} \quad (3.3)$$

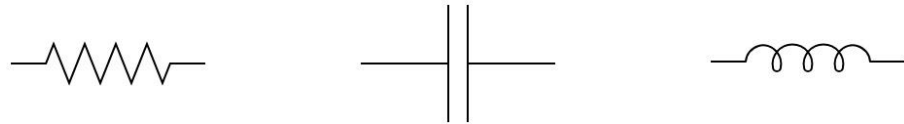


**Figure 3.1:** Electrical Components used to describe blood vessel characteristics

with:

- $\mu$  representing the dynamic viscosity of the fluid,
- $l$  representing the vessel length,
- $r$  representing the vessel radius,
- $E$  representing the Young's modulus of the vessel wall,
- $h$  representing the thickness of the vessel wall,
- $\rho$  representing the density of the blood in the vessels.

The electrical and mechanical parameters used in modelling the cardiovascular system and their corresponding units are shown in Table 3.1.

Electrical Parameter	Electrical Unit	Mechanical Parameter	Mechanical Unit
Voltage	V	Pressure	mmHg
Current	A	Fluid Flow Rate	ml/s
Resistance	$\Omega$	Resistance	mmHg s/ml
Capacitance	F	Compliance	ml/mmHg
Inductance	H	Inertia	mmHg s <sup>2</sup> /ml

**Table 3.1:** Corresponding electrical and mechanical parameters and units.

The governing equations of each of these electrical elements, along with their corresponding mechanical equation are shown in Table 3.2.

	Electrical	Mechanical
<b>Resistor</b>	Ohm's Law: $V = IR$	Poiseuille's Equation: $\Delta P = QR$
<b>Capacitor</b>	$I = C \frac{dV}{dt}$	$Q = C \frac{d\Delta P}{dt}$
<b>Inductor</b>	$V = L \frac{dI}{dt}$	$\Delta P = L \frac{dQ}{dt}$

**Table 3.2:** Lumped-parameter components and their governing equations.

### 3.1.2 Remodelling compliance

As mentioned previously, blood vessel compliance is the ability of the vessel to expand under an applied mechanical load to accommodate a larger volume of blood without increased resistance or blood pressure [17]. For a capacitor to represent a “blood reservoir”, or somewhere where blood is stored, it must be connected in parallel with the other components of the circulation, to a reference pressure (often represented as ground in literature). Examples of this configuration are common in literature where the whole circulatory system is being modelled. An example of this configuration for a simple two-element Windkessel is shown below.

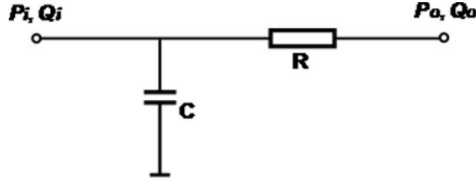


**Figure 3.2:** Two-Element Windkessel [46].

An alternative model to represent the compliance of a blood vessel (as seen in [24]), is modelling it as a vessel or chamber with constant pressure across it (no pressure drop), and varying volume. In this way, it can be connected in series with the other elements of the circulation, and present a more “mechanical” representation of blood vessel compliance. Such a vessel can be described by the following governing equations:

$$P = P_0 + \frac{(V - V_0)}{C} \quad (3.4)$$

$$\frac{dV}{dt} = Q_{in} + Q_{out} \quad (3.5)$$

with:

- $P$  representing the pressure in the vessel,
- $P_0$  representing the offset pressure value of the vessel,
- $V$  representing the volume of blood in the vessel,
- $V_0$  representing the stress-free volume of the vessel,
- $Q_{in}$  representing the blood flow rate at the vessel inlet,
- $Q_{out}$  representing the blood flow rate at the vessel outlet.

This compliance element will be represented in the model schematic as a variable volume container connected to the ground via a spring that compresses with added pressure, increasing the volume of the vessel, as seen in Figure 3.3.

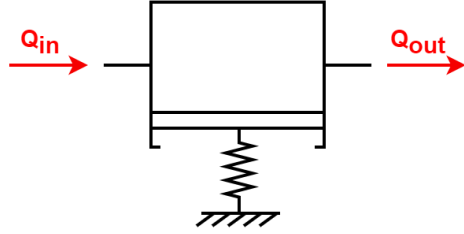


**Figure 3.3:** Compliance element.

### 3.1.3 Heart chambers

Similar to the model for blood vessel compliance, the four heart chambers are modelled as chambers with constant pressure across them (no pressure drop), and varying volume. Therefore, the equations governing the behaviour of the chambers, seen below, closely resemble Equations 3.4 and 3.5:

$$P = P_0 + E(t)(V - V_0) \quad (3.6)$$

$$\frac{dV}{dt} = Q_{in} + Q_{out} \quad (3.7)$$

#### Elastance of the heart chambers

The function  $E(t)$  in equation 3.6 represents the elastance of the chamber walls over the heart's cycle. Elastance represents the ability of the heart walls to resist a change in shape when a mechanical load is applied. It is the reciprocal of compliance which can be seen when comparing Equations 3.4 and 3.6. Elastance can be understood as the “pumping strength” of the heart chamber. The time-varying elastance of the heart chamber walls is as follows:

$$E(t) = E_{min} + \frac{E_{max} - E_{min}}{2} e(t) \quad (3.8)$$

The function  $e(t)$  is an activation function that aims to approximate the contraction of the heart tissue over time. The contraction is driven by electrical signals travelling through the nervous system. The signal  $e(t)$  used in this model is described below in 3.9 [5].

$$e(t) = \begin{cases} 1 - \cos\left(\frac{t}{T_{s1}}\pi\right) & 0 \leq t < T_{s1} \\ 1 - \cos\left(\frac{t - T_{s1}}{T_{s2} - T_{s1}}\pi\right) & T_{s1} \leq t < T_{s2} \\ 0 & T_{s2} \leq t < T \end{cases} \quad (3.9)$$

with:

- $T$  representing the period of one cycle of the heart,
- $T_{s1}$  representing the time of the peak of the systolic phase,
- $T_{s2}$  representing the time of the end of the systolic phase.

Although the elastance function for the ventricles and atria have the same activation function, they occur at different times in the heart cycle. Therefore a time shift must be applied to  $t$  in Equation 3.9 when representing the elastance of the atria, which occurs later in the cycle. This can be illustrated by plotting the activation function of both the ventricles and the atria, as seen below in Figure 3.4, where the contraction of the atria starts at a time offset of 0.92 seconds after the start of the cardiac cycle.

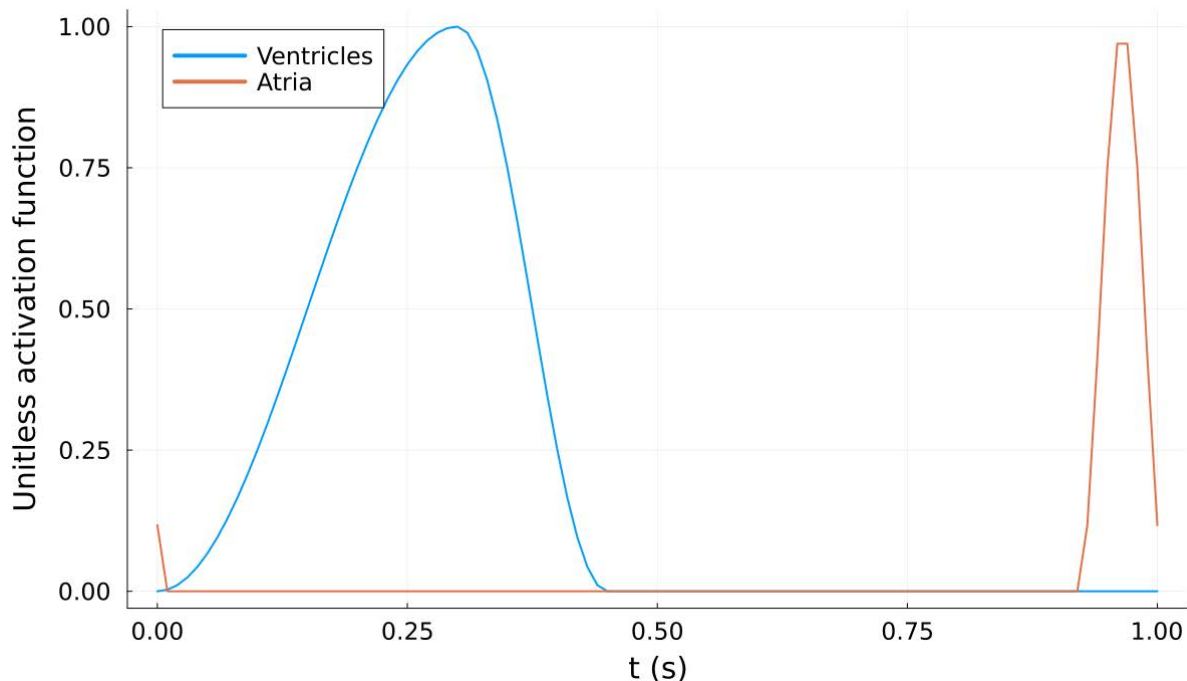


**Figure 3.4:** Heart chambers activation function.

After applying the appropriate  $E_{max}$  and  $E_{min}$  values for each of the heart chambers to the elastance function (Equation 3.8), the magnitudes of elastance in each of the four heart chambers can be calculated, as seen in Figure 3.5.

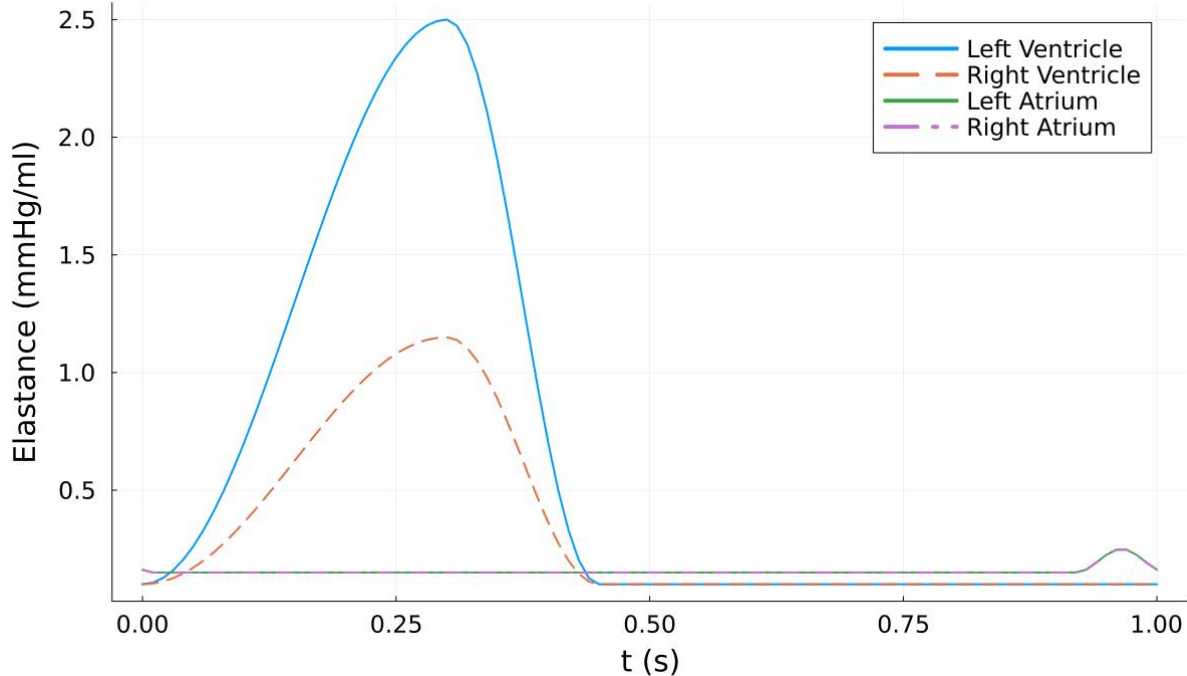


**Figure 3.5:** Elastance in the heart chambers over the cardiac cycle.

The period of the heart cycle in which the ventricles contract (i.e. the ventricle elastance increases above its minimum value) is referred to as **systole**, while **diastole** refers to the period of the heart cycle when the ventricles are at rest (i.e. ventricle elastance is at its minimum) [33].

The heart chambers will be represented in the model schematic as a variable volume chamber with a “piston” driven by the chamber elastance, as seen in Figure 3.7.

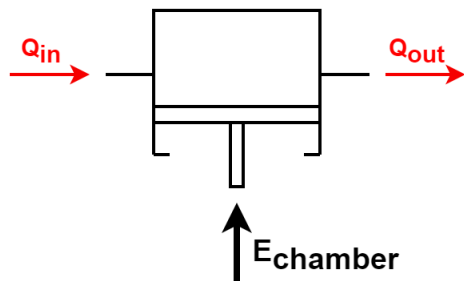


**Figure 3.6:** Heart chambers.

### 3.1.4 Heart valves

The heart valves are modelled as an orifice valve in series with a [diode](#), and will be represented in the model schematic as follows:

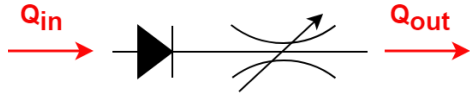


**Figure 3.7:** Heart valves.

The diode models the closing of the valve to prevent backflow through them. When the valve is open, flow characteristics are modelled as an orifice valve. The combination of these two elements has the following governing equation for the blood flow through the valve:

$$Q = \begin{cases} CQ\sqrt{-\Delta P} & \Delta P < 0 \\ 0 & \Delta P > 0 \end{cases} \quad (3.10)$$

where  $\Delta P$  is the pressure difference across the valve, and  $CQ$  is the flow coefficient given by the following equation:

$$CQ = C_d A \sqrt{\frac{2}{\rho(1 - \beta^4)}} \quad (3.11)$$

with:

- $C_d$  representing the valve discharge coefficient (determined by valve geometry),
- $A$  representing the cross-sectional area of the orifice hole,
- $\rho$  representing the density of the blood,
- $\beta$  representing the ratio of the orifice hole diameter to the pipe (in this case heart chamber) diameter.

### 3.1.5 Making an LPM of the human circulatory system

A series of the different elements discussed above can be connected to form an LPM of the entire circulatory system, seen in Figure 3.8 below. This model is based on the model of the circulatory system suggested by Korakianitis and Shi [24] in their investigation of heart valve models.

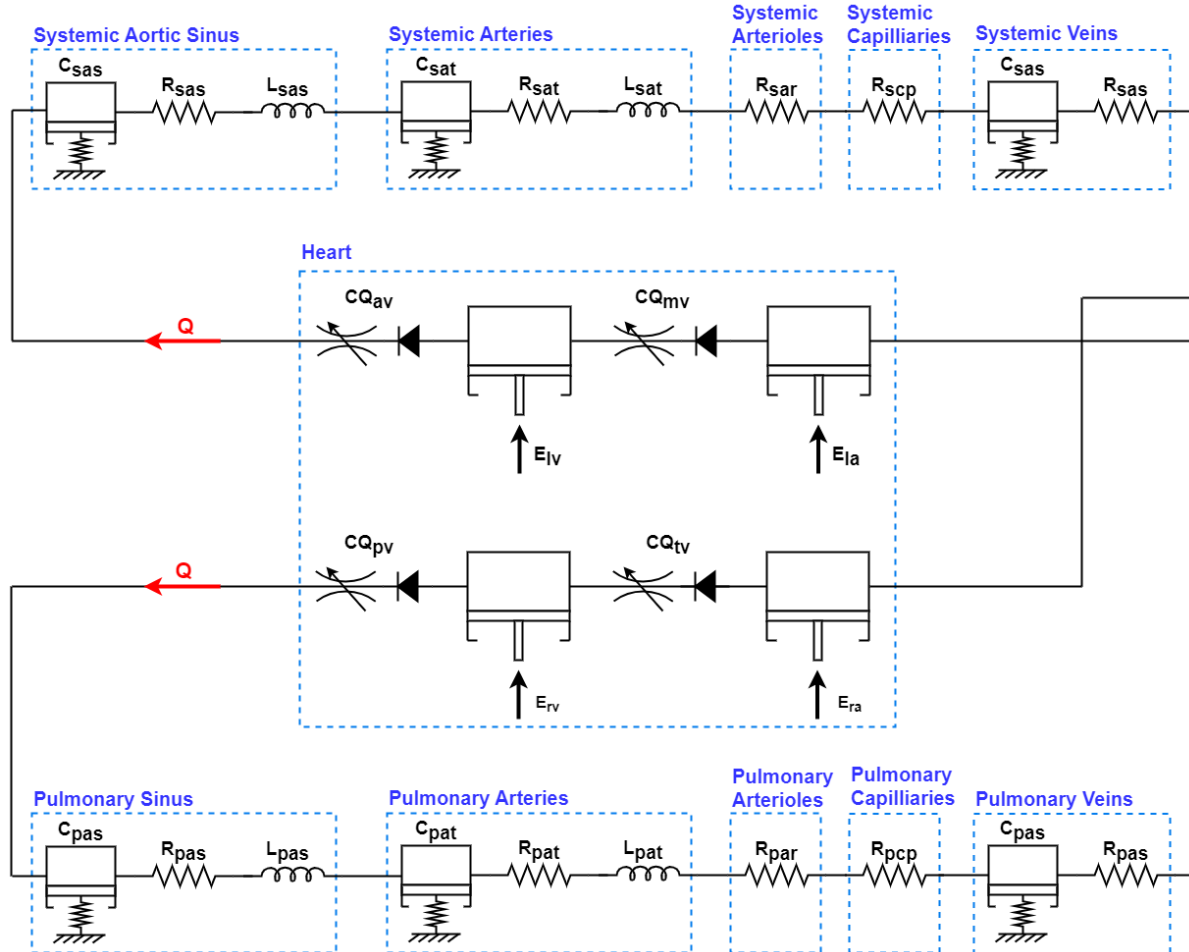


**Figure 3.8:** LPM of circulatory system.

Elements of the model are connected between “nodes”, at which there is a continuity of pressure and blood flow. Each compartment of the model gives rise to two coupled ordinary differential equations (ODEs), representing conservation of mass and conservation of momentum [46]. Connecting all the elements to form a representation of the circulatory system gives rise to a relatively large system of ODEs, which is solved

using the *DifferentialEquations.jl* package (see Section 4.2) and employing the fourth-order Runge-Kutta method.

### Model inputs, outputs and parameters

The input to the model created for this project (illustrated by the schematic in Figure 3.8) is the activation function seen in Equation 3.9 in Section 3.1.3. This represents the electrical signal to the heart and is the only driving force external to the circulatory system included in this model.

This model has a large number of outputs that can be summarised as follows, with check marks indicating the possible outputs for each type of element/point in the system.

	Pressure at/in element	Pressure drop across element	Volume in element	Flow rate through element
Node	✓			✓
Resistance		✓		✓
Inductance		✓		✓
Compliance	✓		✓	
Heart Chamber	✓		✓	
Heart Valve		✓		✓

**Table 3.3:** Possible system outputs

All the parameters necessary to define the circulatory system model are listed in Appendix B.

## 3.2 LPM of a standard human to use as a reference

The parameters used to define the model in Figure 3.8 to represent a standard, healthy human are taken from Korakianitis and Shi [24], and are listed in Appendix B.

### 3.3 Modelling biatrial porcine-to-human cardiac xenotransplantation

The differences between pig and human hearts that have been taken into account when modelling biatrial porcine-to-human cardiac xenotransplantation are as follows:

- The porcine heart has a smaller aortic sinus diameter [44] (Section 3.3.1).
- The porcine heart has a smaller pulmonary sinus diameter [44] (Section 3.3.1).
- The porcine arterial walls are far more elastic (have a smaller Young's modulus) than those of humans [2] (Section 3.3.2).
- The porcine atria have smaller volumes relative to cardiac mass [44] (Section 3.3.3).
- The porcine left ventricle has thicker walls than that of a size-matched human [9] (Section 3.3.4).
- The porcine inter-ventricular septal thickness was greater than that of humans [9] (Section 3.3.4).
- The left side of the porcine heart is larger than the right side, whereas, in the human heart, both the left and right sides of the heart have approximately equal proportions [9] (Section 3.3.5).

The model, which was created in the Julia programming language, can be easily modified by changing parameters detailed in an input file.

#### 3.3.1 Decrease in aortic and pulmonary sinus diameters

The porcine aortic sinus diameter is notably smaller than that of a human. The average aortic diameter of a human adult male is 33.6 mm [30]. The GHRKO (growth hormone receptor knockout) pig donor heart used in the porcine-to-human cardiac xenotransplantation in January 2022 had an aortic diameter of 16.6 mm [44]. The aortic diameter of a human is therefore approximately double that of a pig.

Similarly, the porcine pulmonary sinus diameter is also notably smaller than that of a human. The average pulmonary artery diameter of a human adult male is 32.2 mm [3]. The GHRKO pig donor heart used in the porcine-to-human cardiac xenotransplantation in January 2022 had an aortic diameter of 19.3 mm [44]. The pulmonary sinus diameter of a human is therefore approximately 1.7 times that of a pig.

The modification of the resistance component of the systemic aortic sinus using Equation 3.3 is detailed below. All other changes required are calculated in a similar manner using Equations 3.3.

$$R_{sas,human} = \frac{8\mu l}{\pi} \frac{1}{r_{human}^4} \quad R_{sas,pig} = \frac{8\mu l}{\pi} \frac{1}{(\frac{r_{human}}{2})^4} \quad (3.12)$$

$$= \frac{8\mu l}{\pi} \frac{16}{r_{human}^4} \quad (3.13)$$

$$= 16 \times R_{sas,human} \quad (3.14)$$

The following model parameters are altered from their reference healthy human values (Appendix B) to model a decrease in aortic and pulmonary sinus diameters.

Parameter	SAS Change	PAS Change
$R$	$\times 16$	$\times 8.352$
$C$	$\times 0.125$	$\times 0.204$
$L$	$\times 4$	$\times 2.890$

**Table 3.4:** Effect of decreased aortic and pulmonary sinus diameters on LPM parameters.

### 3.3.2 Decrease in aortic and pulmonary sinus Young's modulus

Porcine arteries are approximately 3 times more elastic than human arteries [2]. This will result in the decrease of the Young's Modulus of the vessel walls in Equation 3.3, and have the following effect on the LPM parameters:

Parameter	SAS Change	PAS Change
$C$	$\times 3$	$\times 3$

**Table 3.5:** Effect of decreased aortic and pulmonary sinus Young's modulus on LPM parameters.

### 3.3.3 Smaller atrial volumes relative to cardiac mass

In their report on the anatomical differences between human and pig hearts and their relevance for cardiac xenotransplantation, Shah et al [44] refer to the fact that pigs have smaller atria volumes relative to cardiac mass, which would affect the stress-free volume,  $V_0$ , of these chambers. In the absence of concrete numerical data to quantify the extent of this decrease in atrial volume, an arbitrary decrease factor is chosen so that the general trends resulting from this decrease can still be investigated.

Parameter	LA Change	RA Change
$V_0$	$\times 0.75$	$\times 0.75$

**Table 3.6:** Effect of decreased atrial volume on LPM parameters.

### 3.3.4 Increase in ventricle wall thickness

The left ventricular wall of an adult pig is much thicker than that of a size-matched human [9]. The average left ventricular mid-diastolic wall thickness of a human adult male is 7.9 mm [52]. The average thickness of the porcine left ventricular free wall at end-systolic and end-diastolic phases was 18.1 and 9.8 mm, respectively [21]. A value of 14 mm is therefore estimated as the left ventricle mid-diastolic wall thickness of the porcine heart, approximately 1.75 times that of the human heart.

There is little data available on porcine right ventricle dimensions, however, it was noted in the literature review that the right ventricular wall thickness does not differ from that of a human to the same extent as the left ventricular wall thickness. Therefore a smaller increase is assumed.

The ventricle thickness affects the elastance of the ventricles, which is the inverse of compliance (See equation for compliance in Equation 3.3). It is therefore assumed that an increase in wall thickness results in a proportional increase in maximum ventricle elastance.

Parameter	LV Change	RV Change
$E_{max}$	$\times 1.75$	$\times 1.1$

**Table 3.7:** Effect of increased ventricular wall thickness on LPM parameters.

### 3.3.5 Mismatch in size between left and right sides of the porcine heart

A four-chamber section of several porcine hearts carried out by Crick et al [9] revealed that the left side of the heart represented approximately two-thirds of the section, whereas an equivalent section of the human heart showed that both the left and right chambers represented approximately equal proportions of the section. To account for this, the stress-free volume ( $V_0$ ) of the left ventricle is increased. The stress-free volume of the right ventricle is left unchanged.

Parameter	LV Change
$V_0$	$\times 1.5$

**Table 3.8:** Effect of size mismatch between the sides of the heart on LPM parameters.

### 3.3.6 Summary of LPM parameter changes

A summary table of all the LPM parameter changes undertaken to model the 9 physical changes introduced by biatrial porcine-to-human cardiac xenotransplantation considered in this study can be seen in Table 3.9 below.

Section of model	Parameter change				
	R	C	L	$V_0$	$E_{max}$
SAS	$\times 16$	$\times 0.375$	$\times 4$	-	-
PAS	$\times 8.352$	$\times 0.611$	$\times 2.890$	-	-
LA	-	-	-	$\times 0.75$	-
RA	-	-	-	$\times 0.75$	-
LV	-	-	-	$\times 1.5$	$\times 1.75$
RV	-	-	-	-	$\times 1.1$

**Table 3.9:** Summary of LPM parameter changes from the reference healthy human case to model biatrial porcine-to-human cardiac xenotransplantation.

## 3.4 Modelling bicaval porcine-to-human cardiac xenotransplantation

Modelling bicaval porcine-to-human xenotransplantation has a small number of added changes needed over the modelling of biatrial porcine-to-human xenotransplantation:

- The porcine atria have smaller volumes relative to cardiac mass [44]. Bicaval cardiac transplantation uses the full donor right atrium as opposed to only half, meaning that the post-transplantation right atrium size after bicaval transplantation will be smaller than that after biatrial transplantation
- Some of the donor venae cavae are used, and connected to the recipient's vanae cavae. Porcine venae cavae have a greater diameter than human vanae cavae, which must be accounted for.

### 3.4.1 Smaller atrial volumes relative to cardiac mass

Previously in Section 3.3.3, the stress-free volume,  $V_0$ , of each atrium was multiplied by an arbitrarily chosen factor of 0.75 to account for the fact that porcine hearts have smaller atrial volumes relative to cardiac mass than the human equivalents. In bicaval cardiac

transplantation, the entirety of the donor right atrium is transplanted, and therefore it is necessary to decrease  $V_0$  of the right atrium even further, as in Table 3.10.

Parameter	LA Change	RA Change
$V_0$	$\times 0.75$	$\times 0.5$

**Table 3.10:** Effect of decreased atrial volume on LPM parameters.

### 3.4.2 Decrease in diameter of the venae cavae

The circulatory system model has only one section representing all the systemic veins in the circulatory system, including the venae cavae (see Figure 3.8 in Section 3.1.5). Before altering the systemic vein parameters to reflect a decrease in the diameter of the venae cavae, it is first necessary to determine what proportion of the compliance and resistance of the systemic veins is attributable to the vanae cavae.

In the absence of literature that models the systemic veins and venae cavae in this way, an estimate is made based on the systemic arteries. If it is assumed that the venae cavae account for a similar proportion of the systemic veins' compliance and resistance as the aortic sinus in the systemic arteries, 5% of the systemic veins' compliance, and 0.5% of the systemic veins' resistance can be attributed to the venae cavae. The resulting values are summarised below in Table 3.11.

Parameter	Value for all systemic veins (Appendix B)	Proportion attributable to venae cavae	Value attributable to venae cavae
$R$	0.075 mmHg s/ml	0.5%	$3.75 \times 10^{-4}$ mmHg s/ml
$C$	20.5 ml/mmHg	5%	1.025 ml/mmHg

**Table 3.11:** Proportion of systemic vein parameters attributable to the venae cavae.

The values that will be altered to account for physical changes in the venae cavae will therefore be a small proportion of the total systemic veins.

The diameters of the venae cavae can differ largely from patient to patient, however, a diameter of 20 mm [34] can be taken as an average value for the inferior vena cava (IVC). A study undertaken by Schwein et al [43] found that the average diameter of the porcine IVC to be 16.4 mm, roughly 85% that of the human IVC. To model this difference in diameter, the following model parameters are altered using Equations 3.3.

Parameter	Change to VC proportion of SVN
$R$	$\times 1.916$
$C$	$\times 0.614$

**Table 3.12:** Effect of decreased venae cavae diameters on LPM parameters.

### 3.4.3 Decrease in venae cavae Young's modulus

Porcine vessels are approximately 3 times more elastic than the human equivalent [2]. This will result in a decrease in the Young's Modulus of the vessel walls in Equation 3.3, and have the following effect on the LPM parameters:

Parameter	Change to VC proportion of SVN
$C$	$\times 3$

**Table 3.13:** Effect of decreased venae cavae Young's modulus on LPM parameters.

### 3.4.4 Summary of LPM parameter changes

These additional changes are added to those required to model biatrial porcine-to-human cardiac xenotransplantation (Table 3.9). A summary table of all the LPM parameter changes undertaken to model the 12 physical changes introduced by bicaval porcine-to-human cardiac xenotransplantation considered in this study can be seen in Table 3.14 below.

Section of model	Parameter change				
	R	C	L	V <sub>0</sub>	E <sub>max</sub>
SAS	×16	×0.375	×4	-	-
PAS	×8.352	×0.611	×2.890	-	-
VC proportion of SVN	×1.916	×1.842	-	-	-
LA	-	-	-	×0.75	-
RA	-	-	-	×0.5	-
LV	-	-	-	×1.5	×1.75
RV	-	-	-	-	×1.1

**Table 3.14:** Summary of LPM parameter changes from the reference healthy human case to model bicaval porcine-to-human cardiac xenotransplantation.

---

## CHAPTER

## FOUR

---

### THE JULIA PROGRAMMING LANGUAGE AND ITS APPLICATION IN THIS PROJECT

Julia is a relatively young programming language that has gained popularity in recent years for computational programming, mathematical analysis, and statistical modelling [32]. Several key features are leading some people to call Julia the “programming language of the future” [50].

- **Processing speed:** Julia has a processing speed comparable to that of C and C++, making it very powerful when dealing with large datasets and high-precision performance [32].
- **Syntax:** Similar to Python and R, Julia is dynamically typed, making it easy to read and write [50], especially for those who do not have a strong background in software development. Another advantage of a dynamically typed language is the ability to change a variable’s type as a program is run [32].
- **Multiple dispatch:** Multiple dispatch refers to a function’s ability to behave differently based on the types of its arguments and is one of the features giving rise to Julia’s superior speed [50].

## 4.1 Comparison of Julia vs Python processing speed

As Julia's processing speed is one of its main merits, a comparison between Julia's and Python's processing speeds was undertaken for the application of solving ODEs, an important application for lumped-parameter modelling.

To make a direct comparison between each languages, ODE-solving packages were not used, and a Runge-Kutta fourth-order function was developed from scratch in each language, to ensure the same function was being solved in each case. These fourth-order Runge-Kutta functions were then used to solve for the aortic pressure across two, three and four-element Windkessel models of the circulation. The code for each of these implementations can be seen in Appendix [D.1](#).

The results of this investigation are detailed below in Table [4.1](#). In each case, the ODEs were solved over 3000 seconds, with a step size of 0.01 seconds. While the execution time varies slightly each time the code is run, the figures shown below give an idea of the general range of run times.

Windkessel	Time to solve (s)	
	Python	Julia
Two-Element	5.1	1.8
Three-Element	9.9	3.1
Four-Element	14.4	4.8

**Table 4.1:** Comparison of Julia and Python processing times for solving ODEs of two, three, and four-element Windkessels.

As can be seen from the results of this investigation, Julia is approximately 3 times faster than Python for this application. It is therefore a more efficient choice for this project, as the LPM of the cardiovascular system detailed in Section [3.1.5](#) gives rise to a relatively large system of ODEs to be solved.

## 4.2 Julia packages used in model creation

The model of the circulatory system created for this project was formulated using the *ModelingToolkit.jl* package. *ModelingToolkit.jl* [29] is a modeling framework for high-performance symbolic-numeric computation in scientific computing and scientific machine learning. It allows users to give a high-level description of a model for symbolic pre-processing to analyze and enhance the model. This package is very useful for the development of LPMs, as it allows the user to define simple elements and connect them to form a complicated system.

The systems of differential equations associated with each component of the model are solved using *DifferentialEquations.jl* [37], using the fourth-order Runge-Kutta method.

Some of the elements in this project's model are based on those developed in *CirculatorySystemModels.jl* [41].

The Julia code used to build the model of the circulatory system, and solve for the desired outputs, can be seen in Appendix D.2 and D.4.

---

CHAPTER

**FIVE**

---

## MODEL VERIFICATION AND VALIDATION

Verification and validation of the model of the cardiovascular system were carried out using the method outlined by Leaning et al [26] in their validation of their human cardiovascular system model. Leaning et al's model was more complex than that used in this project and includes the nervous system and its control over the cardiovascular system. Nonetheless, a number of the initial validation criteria and methods can be applied to the model created for this project.

Leaning et al's method can be broken into three parts:

- Verification of numerical methods. This does not require any reference to real-life data, and is only concerned with the performance of the numerical algorithms.
- Verification that individual components of the system align with expectations from theoretical analysis.
- Validation that the outputs of the system correspond to available experimental data.

## 5.1 Verification of numerical methods

The fourth-order Runge-Kutta method is built into the *DifferentialEquations.jl* package, and was used to solve the system of differential equations in this model. To ensure *DifferentialEquations.jl* is using the Runge-Kutta method as expected, a function for the Runge-Kutta method was developed from first principles [56], and compared to the output from *DifferentialEquations.jl*'s solver. This gave confidence that this package is solving the differential equations as expected, using the effective and widely used fourth-order Runge-Kutta method.

The solver from Julia's *DifferentialEquations.jl* package uses an internal adaptive time-stepping engine to achieve the desired tolerance level. Figure 5.1 shows the solution of a simple two-element Windkessel model at a range of different tolerance levels, indicated by the parameter *reltol*. As can be seen from this graph, the solution converges as the required tolerance decreases, with no visible differences between the solutions when the tolerance is set to  $10^{-3}$  versus  $10^{-6}$ .

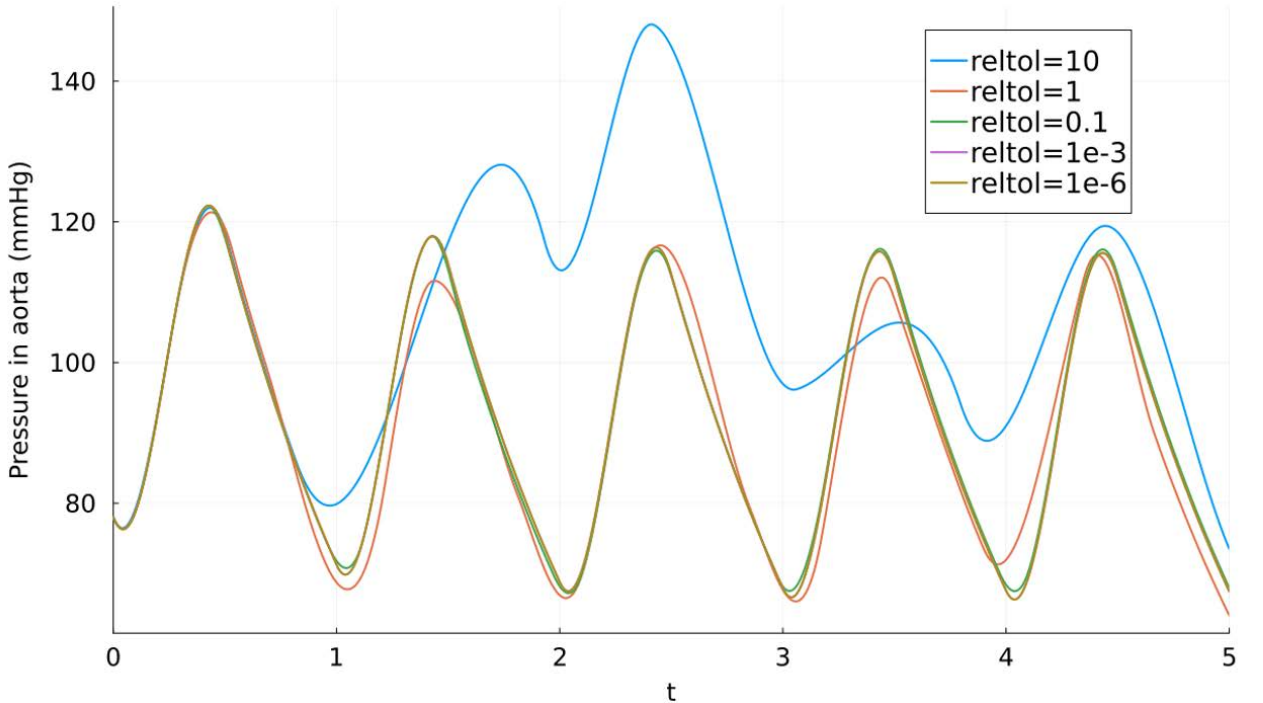


**Figure 5.1:** Solution of a simple two-element Windkessel model at a range of different tolerance levels.

Because the model of the full cardiovascular system is more complicated than the simple two-element Windkessel model, a relative tolerance of  $10^{-9}$  was chosen when solving the model of the circulatory system to minimise numerical errors. While an increased tolerance will increase the time taken for the solution to converge, these models only take seconds to run, so accuracy can be prioritised.

## 5.2 Verification of basic model elements

To build up confidence in the model, a verification of the elementary relationships in the model is carried out.

### 5.2.1 Validation of elementary relationships through modelling of basic Windkessel circuits

The basic two-, three-, and four-element Windkessel representations of the systemic circulation have been used to investigate the effect that each basic element in the model created for this project has on the total pressure difference across the circulation. These investigations are also used to verify the elementary relationships of the circuit elements, against outputs from *LTspice*, a SPICE-based analog electronic circuit simulation software,

These investigations were carried out by using a simple sine wave as an input for blood flow into the systemic circulation. This sine wave was defined using the **stroke volume** of the heart. The stroke volume is defined as the volume of blood pumped out of the left ventricle of the heart during each systolic cardiac contraction [47] and the normal range is 50-100 ml. A stroke volume of 90 ml was assumed for the investigation of Windkessel circuits. This is represented by the area under the blood flow rate curve (grey dashed line) for each cardiac cycle of one second in Figure 5.3.

Figures 5.2 and 5.3 show the aortic pressure derived using two-, three-, and four-element Windkessel models, with the simple sine wave input for blood flow shown for reference, simulated using *LTSpice* and the Julia model respectively. Please note, as

*L*Tspice is an electronic circuit simulator, the units for pressure and blood flow are given in their electrical counterparts (voltage and current respectively). To match the resistances of the circuits, so that the two-element circuit offers a similar overall resistance to the three and four-element circuits, the following circuit parameters were used:

	$R_p$ (mmHg s/ml)	$C$ (ml/mmHg)	$R_c$ (mmHg s/ml)	$L$ (mmHg s <sup>2</sup> /ml)
Two element	0.95	1.05	-	-
Three element	0.9	1.1	0.05	-
Four element	0.9	1.1	0.05	0.0045

**Table 5.1:** Parameters used to define Windkessel circuits [46].

The model outputs of the simple Windkessel circuits (Figure 5.3) were verified against the outputs from the same circuits, simulated using *L*Tspice (Figure 5.2).

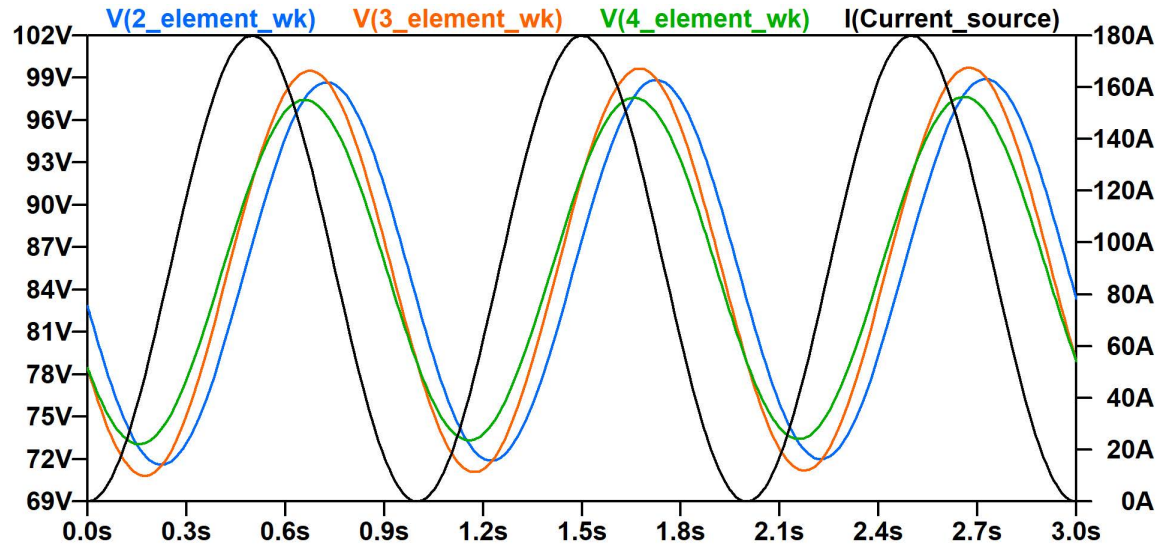


**Figure 5.2:** Aortic pressure for 2, 3, and 4 element Windkessel circuits, simulated using *L*Tspice.

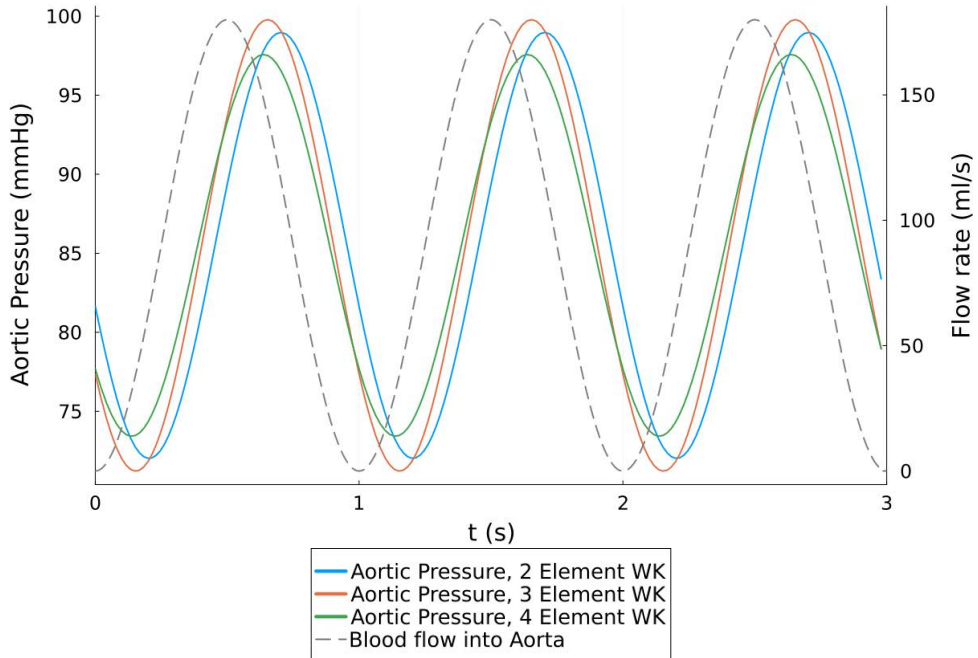


**Figure 5.3:** Aortic pressure for 2, 3, and 4 element Windkessel circuits, simulated using Julia model.

### 5.2.2 Physical interpretation of Windkessel circuit results

As can be seen from Figure 5.3, the peak pressure for each of the three different Windkessel circuit configurations occurs after the peak of the blood flow into the aorta. This is a result of the compliance of the blood vessels, which causes a time delay between blood flow and pressure increase in the aorta through the expanding of blood vessels.

The pressure across the three-element Windkessel has a slightly greater magnitude than that of the resistance-matched two-element Windkessel due to the added resistive element.

An inductive element is added to form the four-element Windkessel to account for the inertia of blood flow through the circulatory system. Inertia acts to resist a change in motion or velocity of a body, having a damping effect on the overall mechanical system. This explains why the amplitude of the pressure wave of the four-element Windkessel (circa 24 mmHg) is smaller than that of the three-element circuit (circa 28 mmHg).

## 5.3 Validation of the model's ability to represent the cardiovascular system

The model used for this project is based on the model used by Shi et al [45] in their construction of cardiovascular models in the CellML language. Their model parameters were based on those used in Korakianitis and Shi's LPM of the circulatory system [24], which are chosen based on data widely referred to in literature. Laubscher et al [25] use a similar model which was validated against experimental data in literature. Comparing the outputs of the model created for this project against waveforms shown in these papers gives confidence that the model outputs are generally representative of the cardiovascular system.

### 5.3.1 Pressure and flow characteristics in a healthy human heart

Figure 2.1 is repeated below as Figure 5.4 for reference in the subsequent section.

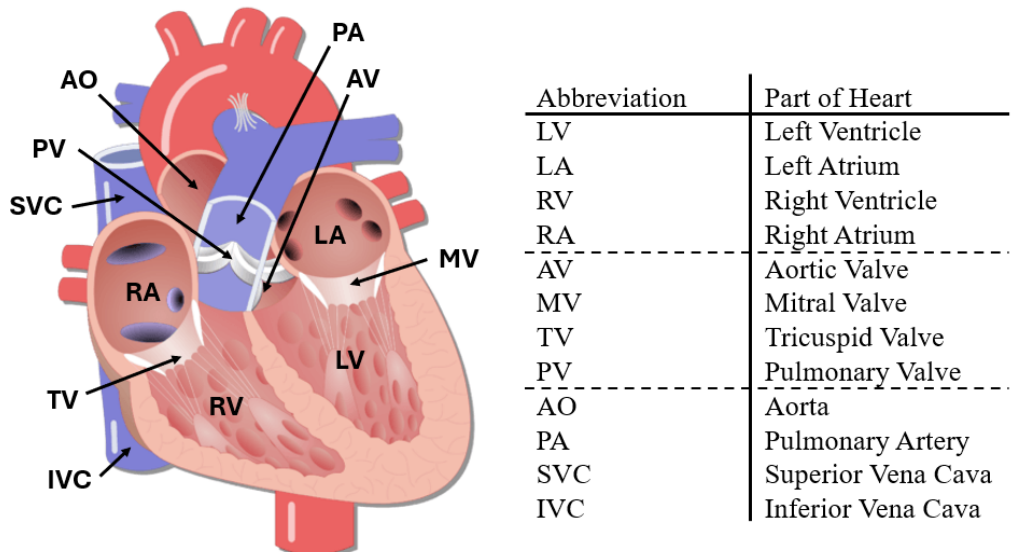
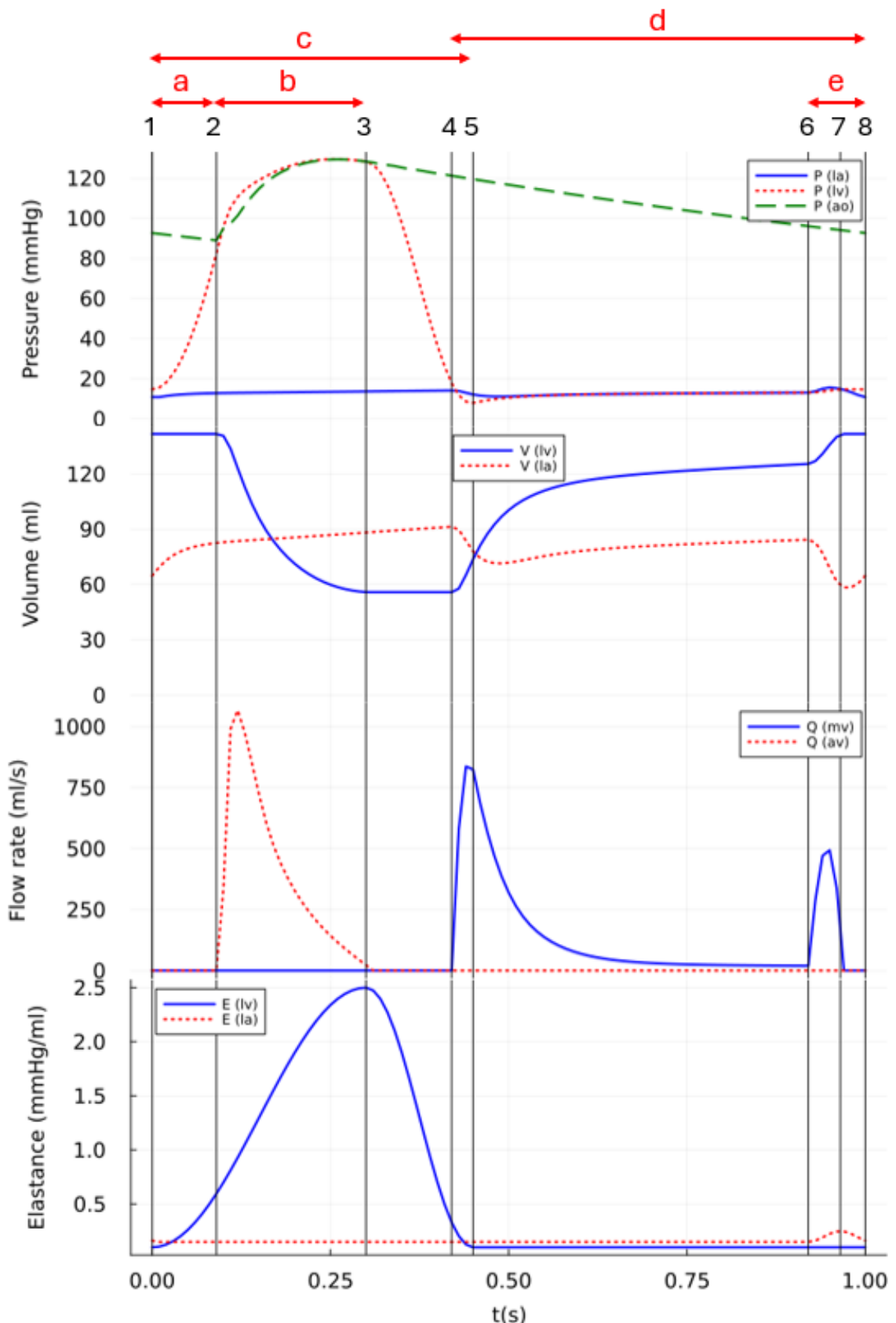


Figure 5.4: Heart diagram.

Figure 5.5 shows the pressures, volumes, flow rates, and elastances in the key sections of the left side of the heart.



**Figure 5.5:** Pressure and flow relationships in the left side of the heart, created using Julia model.

Several key events occur in the left side of the heart during the cardiac cycle, which are numbered in Figure 5.5 and detailed in Table 5.2.

Label	Event
1	Start of the cardiac cycle, start of systolic phase
2	Aortic valve opens
3	Peak of systolic phase, aortic valve closes
4	Mitral valve opens
5	End of systolic phase
6	Start of atrial contraction
7	Peak of atrial contraction, mitral valve closes
8	End of atrial contraction, end of cardiac cycle

**Table 5.2:** Events in the left side of the heart during cardiac cycle.

The left side of the heart has several different phases occurring between the events detailed in Table 5.2. These phases are labelled with letters in Figure 5.5 and detailed in Table 5.3.

Label	Phase
a	Pressure builds in the left ventricle as its elastance increases.
b	Blood is ejected from the left ventricle into the aorta, causing the volume in the left ventricle to drop.
c	Systolic phase, the part of the cycle where the ventricle elastance is above its minimum value i.e. the ventricle is “squeezing”.
d	Left ventricle fills with blood from the atrium via the mitral valve.
e	Contraction of the atrium.

**Table 5.3:** Phases of the cardiac cycle, left side of the heart.

Throughout the cardiac cycle, blood flows into the left atrium via the pulmonary arteries at a relatively constant rate.

The pressure-flow relationships in the right side of the heart can be investigated in a similar manner, which is detailed in Appendix C.

Another graph that clinicians use when investigating the health of the cardiovascular system is the pressure-volume (PV) loop of each of the four heart chambers. The work done by each heart chamber is proportional to the area inside the PV loop. The PV loop of the left ventricle can be seen in Figure 5.6.

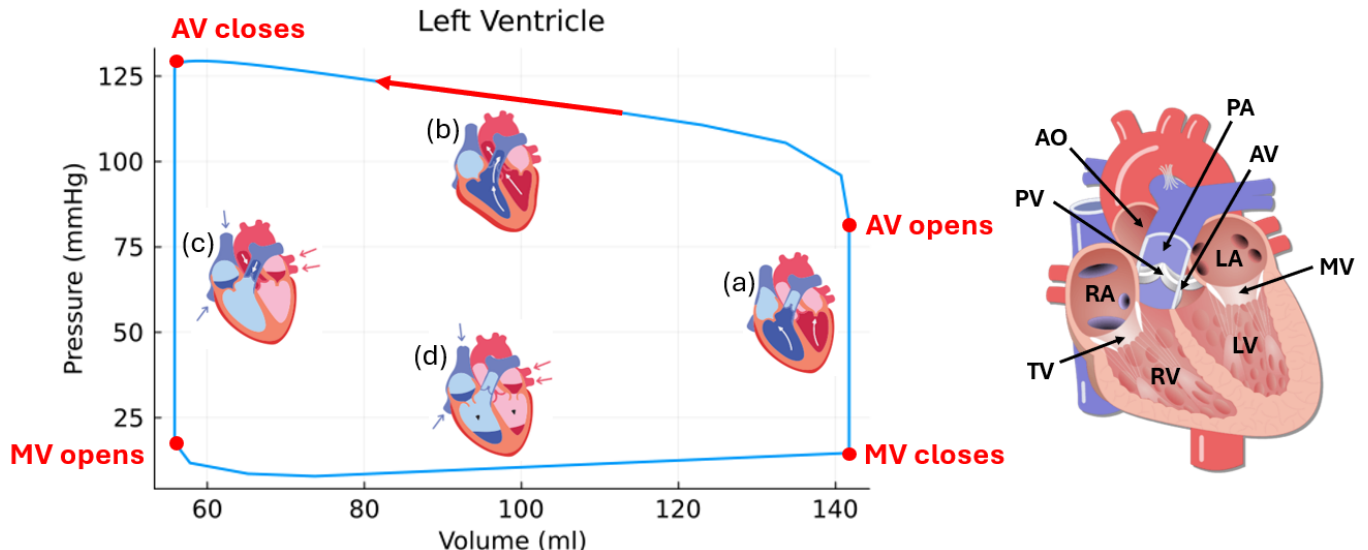


**Figure 5.6:** PV loop of the left ventricle with heart diagram for reference.

As indicated by the heart schematics, there are four phases of the cardiac cycle illustrated by the left ventricle PV loop, described as follows:

	Phase	Description
(a)	Isovolumetric contraction	Occurs between the closing of the mitral valve (MV) and the opening of the aortic valve (AV). The ventricle starts to contract and pressure in the left ventricle builds. (~ 0.05s)
(b)	Ventricular ejection	Occurs between the opening and closing of the AV. The ventricle continues to contract as blood is ejected into the aorta. (~ 0.25s)
(c)	Isovolumetric relaxation	Occurs between the closing of the AV and the opening of the MV. The ventricle relaxes. (~ 0.15s)
(d)	Ventricular filling	Occurs between the opening and closing of the MV. The ventricle fills with blood from the left atrium. (~ 0.55s)

**Table 5.4:** Phases of the cardiac cycle, as seen on the PV loop of the left ventricle.

PV loops are useful to clinicians because several key metrics are easily read from these graphs, as seen in Figure 5.7.

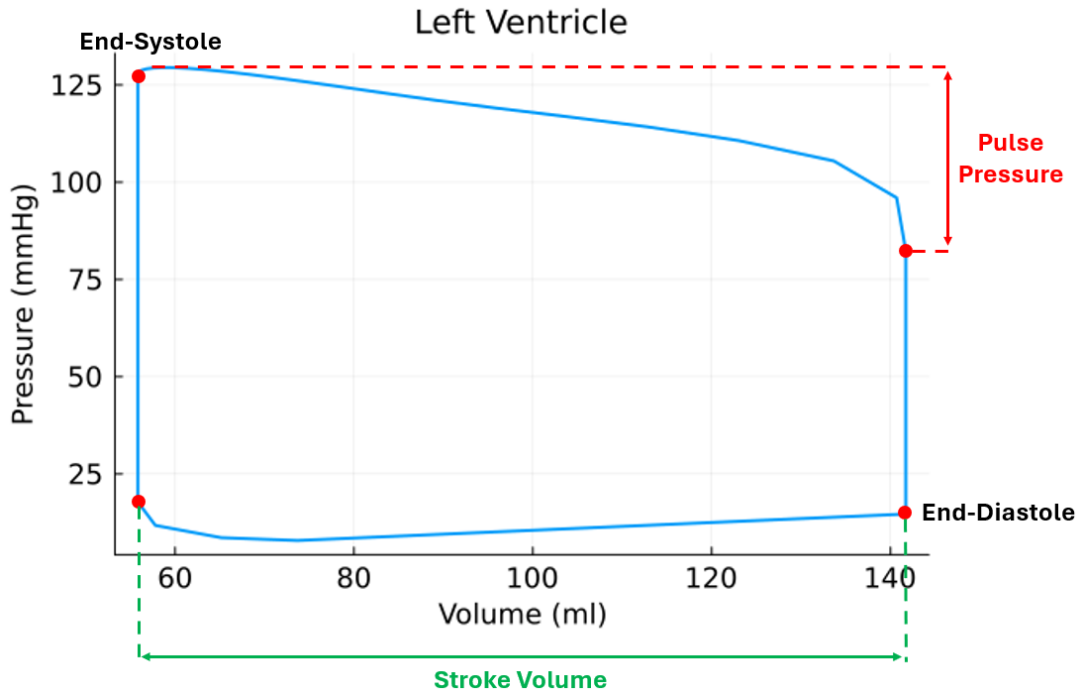


**Figure 5.7:** PV loop of the left ventricle.

- Stroke volume:
  - The stroke volume of a cardiac cycle is the volume of blood pumped out of the left ventricle of the heart during each systolic cardiac contraction.
  - $SV = EDV - ESV$ , where SV is the stroke volume, EDV is the end-diastolic volume and ESV is the end systolic volume.
  - Healthy range: 50-100 ml [47].
  
- Pulse pressure:
  - The pulse pressure of a cardiac cycle is the difference between systolic and diastolic blood pressure.
  - $PP = SP - DP$  where PP is the pulse pressure, SP is the systolic pressure, and DP is the diastolic pressure.
  - Healthy range: 40-60 mmHg [35].

- Ejection fraction:
  - The ejection fraction is a measurement of how much blood the ventricle pumps out with each contraction.
  - $EF(\%) = \frac{SV}{EDV} \times 100$
  - Healthy range: 50-70%

Figure 5.8 shows the PV loops of all four heart chambers for reference.

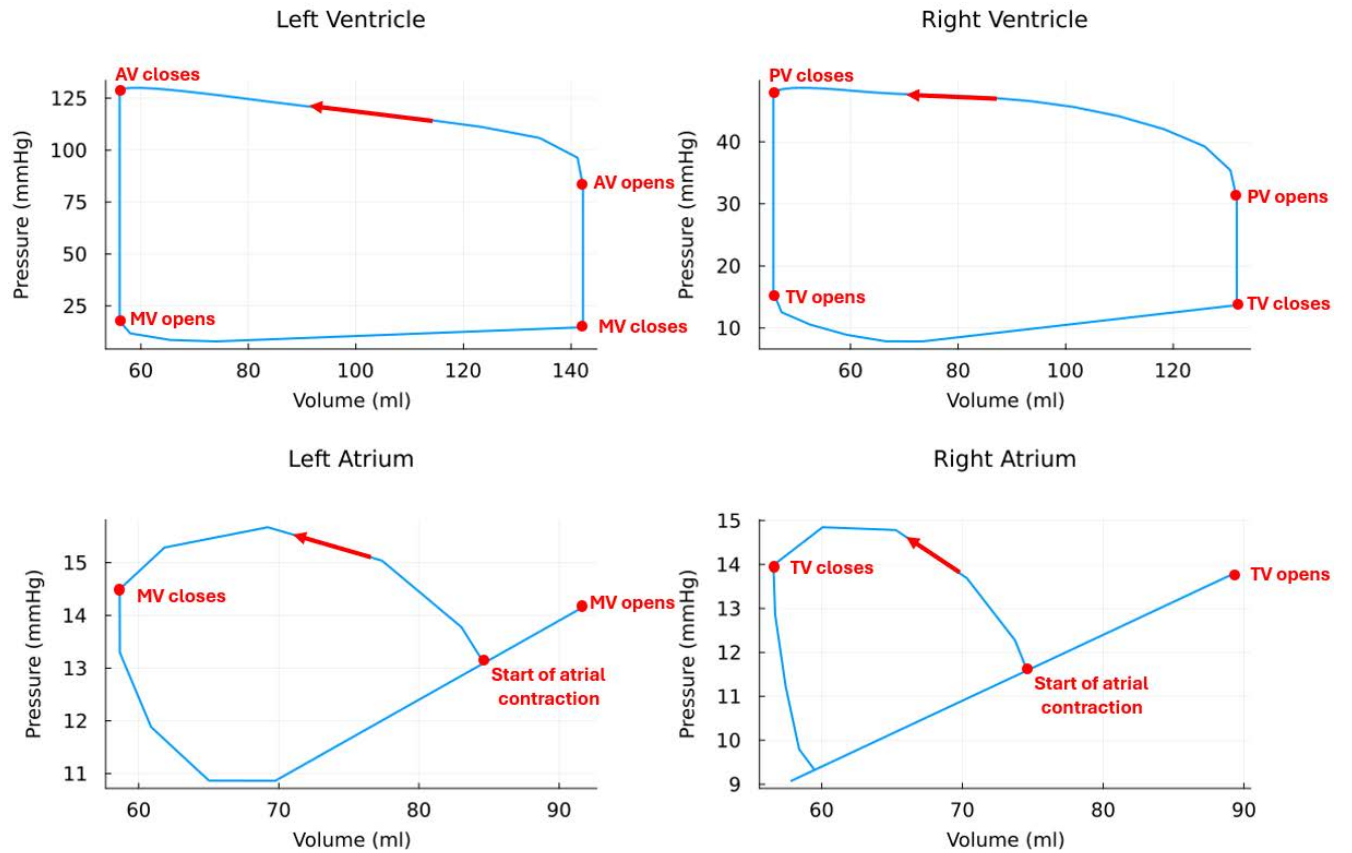


Figure 5.8: PV loops of all four heart chambers, created using Julia model.

---

CHAPTER  
**SIX**

---

## RESULTS AND DISCUSSION

This section contains the results from the investigation of the impact of porcine-to-human cardiac xenotransplantation on key metrics of the cardiovascular system. Biatrial cardiac xenotransplantation is initially investigated, as this was the technique used in the pioneering procedure performed by doctors in Maryland in 2022. Bicaval cardiac xenotransplantation is also investigated, as this is the technique that has provided the most favorable results in allotransplantations.

### 6.1 Biatrial cardiac xenotransplantation

To gain an insight into the effect that biatrial cardiac xenotransplantation on the mechanical performance of the cardiovascular system, the effect that each of the individual changes mentioned in Section 3.3 has on some of the key performance indicators (chosen based on the most common metrics analysed in literature) is investigated. The first important metric investigated was the pressure in the aortic sinus over the cardiac cycle.

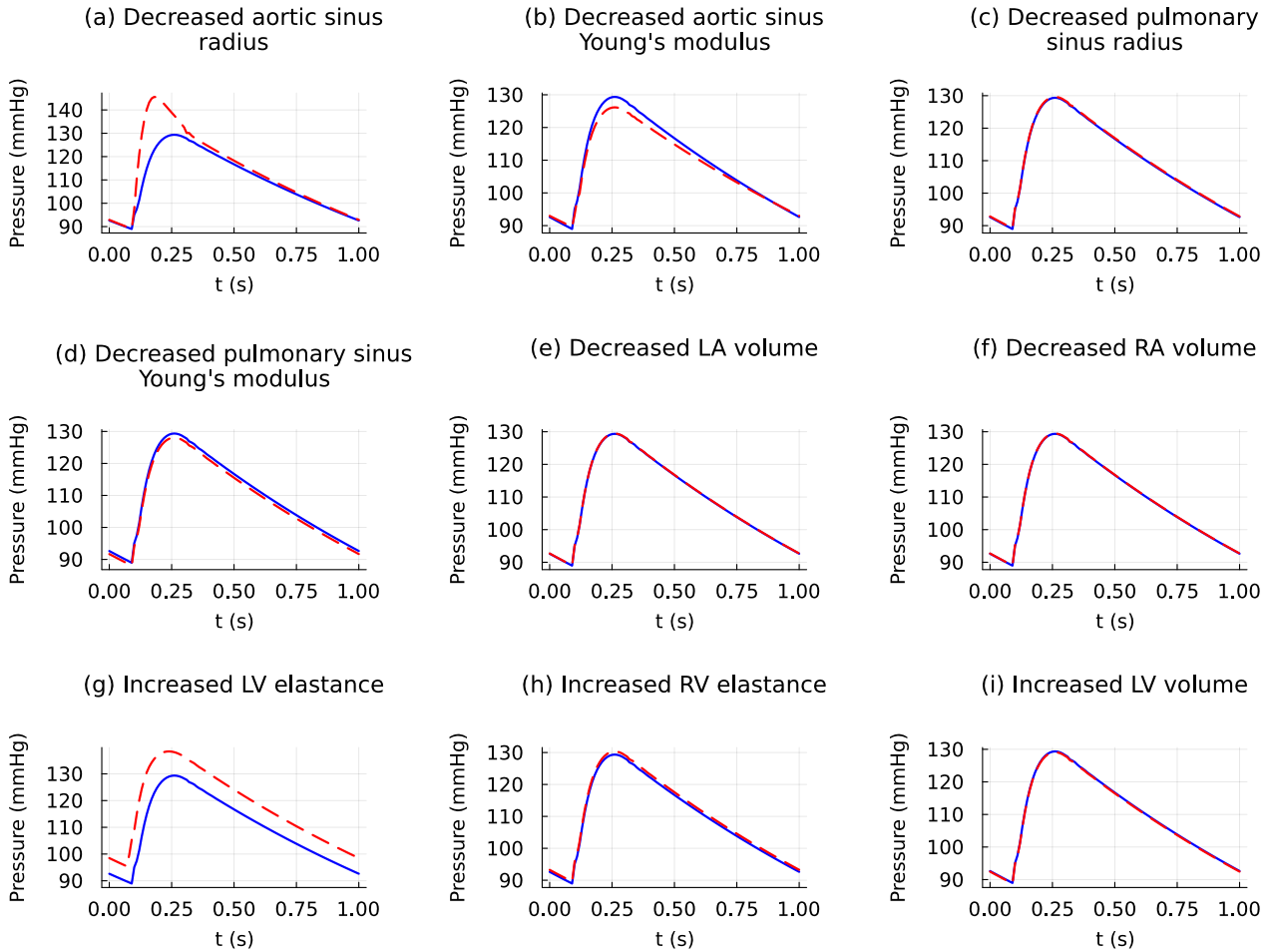


**Figure 6.1:** Pressure in the aortic sinus of a reference healthy human (blue) and altered model (red).

As can be seen from Figure 6.1, most of the physical changes introduced by biatrial cardiac xenotransplantation have negligible effects on the aortic sinus pressure, with only the decreased aortic sinus radius (Fig. 6.1 (a)), decreased aortic sinus Young's modulus (Fig. 6.1 (b)), and increased left ventricular elastance (Fig. 6.1 (g)) resulting in noticeable changes.

Decreasing the radius of the aortic sinus (Fig. 6.1 (a)) results in a much larger peak aortic sinus pressure, with the pressure returning to values similar to those of the reference healthy human once the aortic valve closes, as can be seen by the presence of a sharp divet in the pressure curve at the point where the aortic valve closes. Reducing the radius of the aortic sinus results in an increased resistance, meaning a greater pressure gradient

across the aorta is required to provide enough force to push the same volume of blood through to the rest of the vasculature. A reduced radius also reduces the compliance of the vessel, meaning it cannot expand to accommodate the same amount of blood as in the reference case, further increasing the pressure in the aortic sinus.

Decreasing the Young's Modulus of the aortic sinus walls (Fig. 6.1 (b)) increases the compliance of the vessel. When this change is made in isolation, it results in a decrease in peak aortic pressure, because a more elastic vessel can stretch to accommodate a larger volume of blood without a resulting increase in pressure in the vessel.

Increasing the maximum elastance of the left ventricle (Fig. 6.1 (g)) is effectively increasing the power and strength of the heart. The elastance of a chamber is a measure of the chamber's ability to resist a change in volume with increased pressure, and represents how the heart squeezes, reducing the volume of blood in the left ventricle in order to eject blood into the aorta. Increasing left ventricular elastance will result in increased ventricular pressure, which in turn increases aortic pressure as they are directly connected via the aortic valve.

Although a reduction in aortic pressure is seen in the case of the decreased aortic sinus Young's modulus (Fig. 6.1 (b)), both the decreased aortic sinus radius (Fig. 6.1 (a)), and the increased left ventricular elastance (Fig. 6.1 (g)) result in an increase in aortic pressure of much greater magnitude than the change resulting from the decreased aortic sinus Young's modulus. Therefore it is expected that overall, the pressure in the aorta will rise. The overall effect of biatrial cardiac xenotransplantation on the pressure in the aorta can be seen in Figure 6.7 (i) in Section 6.1.5.

Now that the changes that affect the aortic pressure to the greatest extent have been identified, some other important key performance indicators in the left side of the heart will be investigated under these scenarios.

### 6.1.1 Effect of decreased aortic sinus radius on the left side of the heart

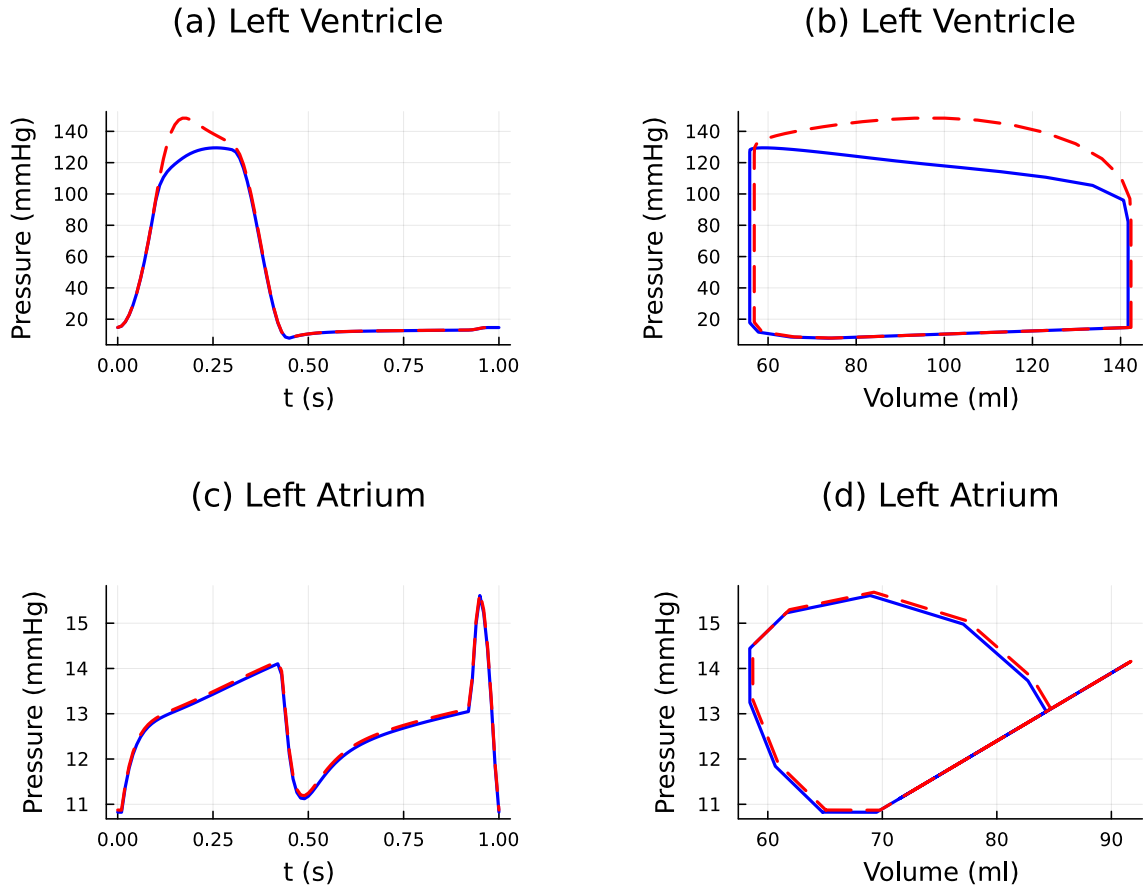


**Figure 6.2:** Effect of decreased aortic sinus radius on the left side of the heart, showing reference healthy human (blue) and altered model (red).

As can be seen from Figure 6.2, the decreased aortic sinus radius has little effect on the pressure and volume in the left atrium (Fig. 6.2 (c) and (d)), however, it has a notable effect on the left ventricle (Fig. 6.2 (a) and (b)). Left ventricular pressure reaches a significantly higher peak than the reference case of a healthy human. Similar to the effect on the aortic sinus pressure, to overcome the increased resistance of the aortic sinus resulting from its decreased radius, the pressure in the left ventricle must be higher to push the same volume of blood through.

From the PV loop of the left ventricle (Fig. 6.2 (b)), we can see that the area of the loop has increased, meaning that the left ventricle is doing more work than in the reference

case. More work is required to increase the pressure in the left ventricle sufficiently to overcome the increased resistance of the aortic sinus.

### 6.1.2 Effect of decreased aorta Young's modulus on the left side of the heart

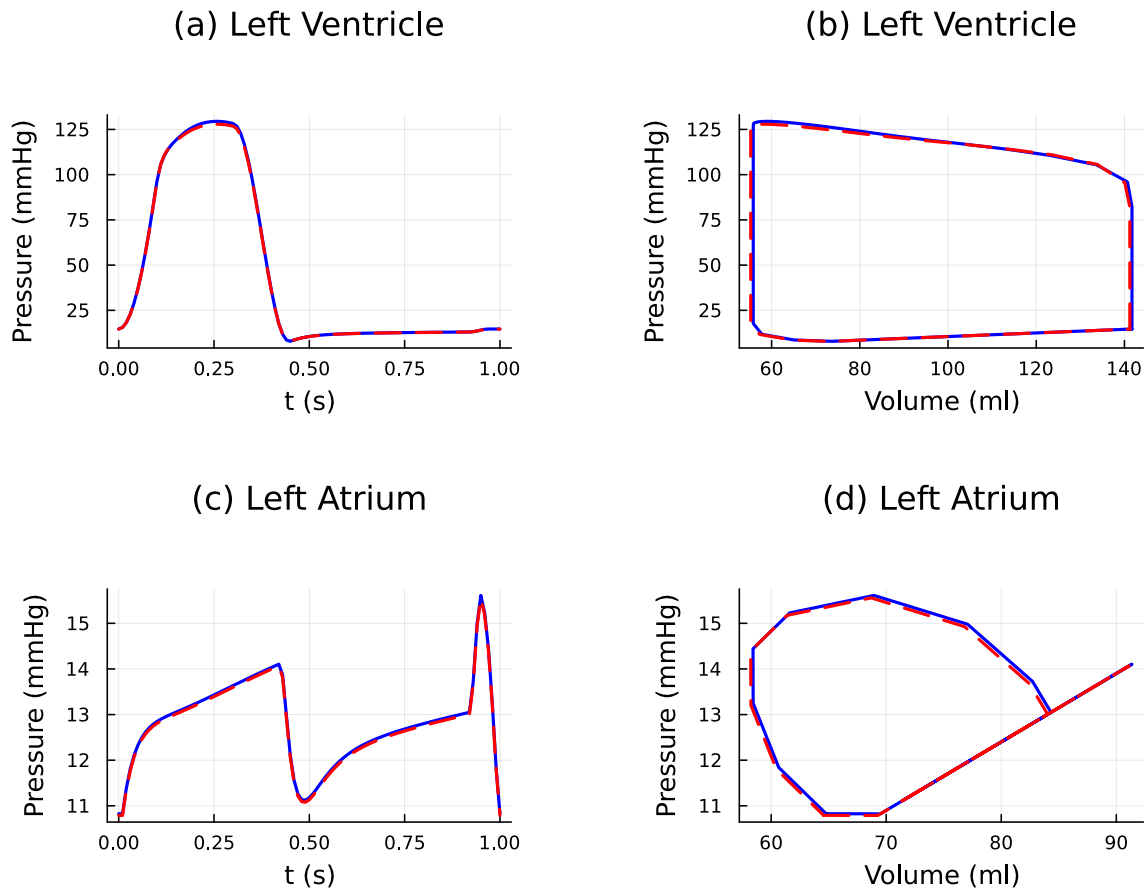


**Figure 6.3:** Effect of decreased aorta Young's modulus on the left side of the heart, showing reference healthy human (blue) and altered model (red).

Figure 6.3 demonstrates that the decreased Young's modulus of the aortic sinus has little effect on the pressures and volumes in the chambers of the left side of the heart. The peak pressure in the left ventricle (Fig. 6.3 (a)) shows a very slight decrease. As the more elastic aortic sinus can stretch to accommodate a greater volume of blood at a given pressure, the pressure in the left ventricle required to push blood through the aortic sinus

will decrease, however, the extent to which the left-ventricular pressure reduces can be deemed negligible.

### 6.1.3 Effect of increased left ventricle elastance on the left side of the heart

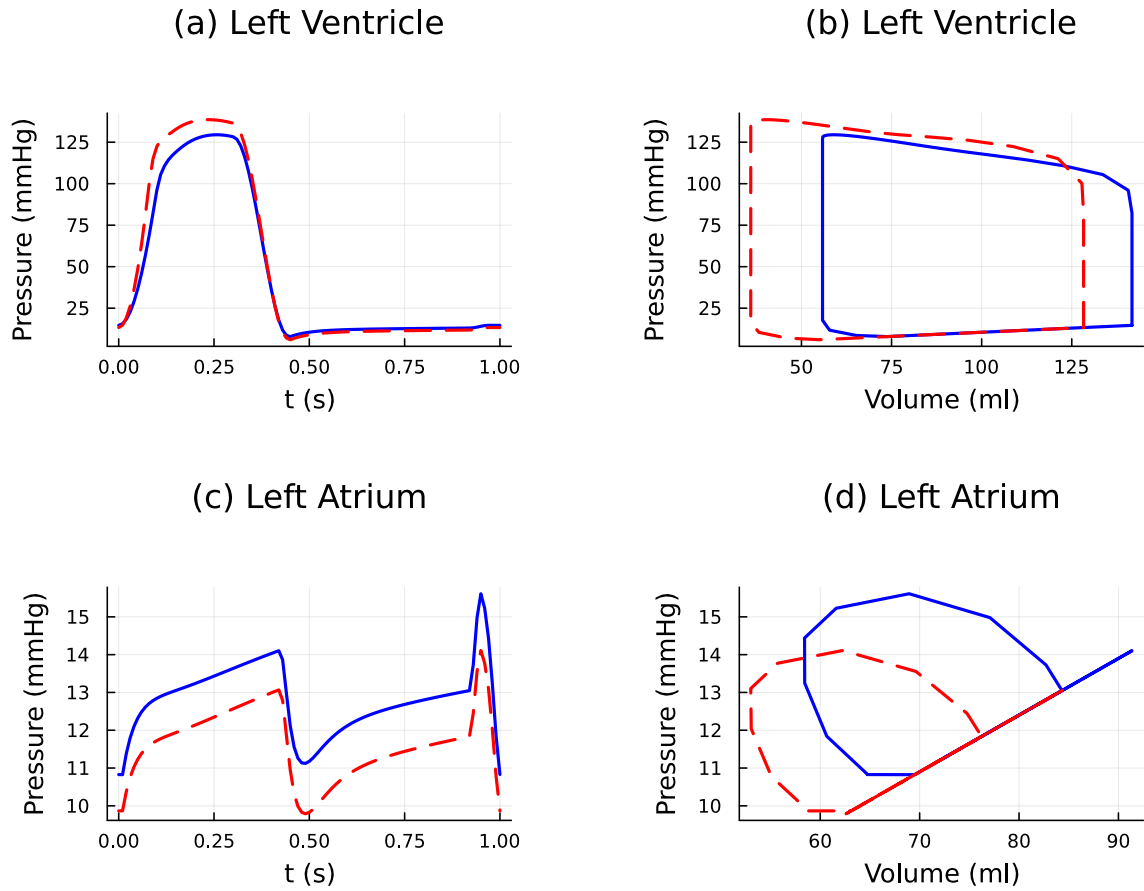


**Figure 6.4:** Effect of increased left ventricle elastance on the left side of the heart, showing reference healthy human (blue) and altered model (red).

Figure 6.4 indicates that the increased left-ventricular elastance has a significant effect on all four of the graphs being investigated. The peak pressure in the left ventricle (Fig. 6.4 (a)) is greater than the reference case with differences first noted near the beginning of the systolic phase. Increasing the maximum elastance of the left ventricle results in a proportional increase in ventricular pressure (see Equations 3.6 and 3.8). The left-ventricular pressure of the altered case differs to a greater extent from the reference case

as the pressure is rising as opposed to falling. This is because the elastance peaks in the latter half of the systolic period (see Figure 3.4), returning quickly to its minimum value after the peak, whereas there is a longer rising period before the elastance peak.

From the left-ventricular PV loop (Fig. 6.4 (b)), it can be seen that the maximum and minimum volumes in the left ventricle reduce when compared to the reference case. Elastance acts to resist an increase in volume with increased pressure, therefore resulting in a reduction in the volume of blood in the left ventricle. The area inside the loop of the altered case is slightly bigger than that of the reference, and the left ventricle stroke volume is also slightly bigger. The shift in the PV loop of the left ventricle results in a higher ejection fraction of approximately 80%. Ejection fractions over 75% can be considered dangerously high in normal clinical cases and can indicate heart conditions such as [hypertrophic cardiomyopathy](#) (a disease in which the heart muscle becomes thickened), which is a common cause of sudden cardiac arrest [13]. As the porcine heart has thicker walls than the human heart, such a change in ejection fraction is not surprising. However, it could have an impact on the long-term viability of the xenograft.

There is a reduction in pressure in the left atrium (Fig. 6.4 (c)). This is a result of the reduced volume in the left atrium, indicated in the left atrium PV loop (Fig. 6.4 (d)). As the left ventricle accepts a smaller volume of blood, the volume of blood required in the left atrium is also reduced. Therefore the overall volume of blood in the left side of the heart decreases.

To investigate the possible redistribution of blood in the cardiovascular system as a result of the decreased volume in the left side of the heart, the volume of blood in different sections of the cardiovascular system was investigated.

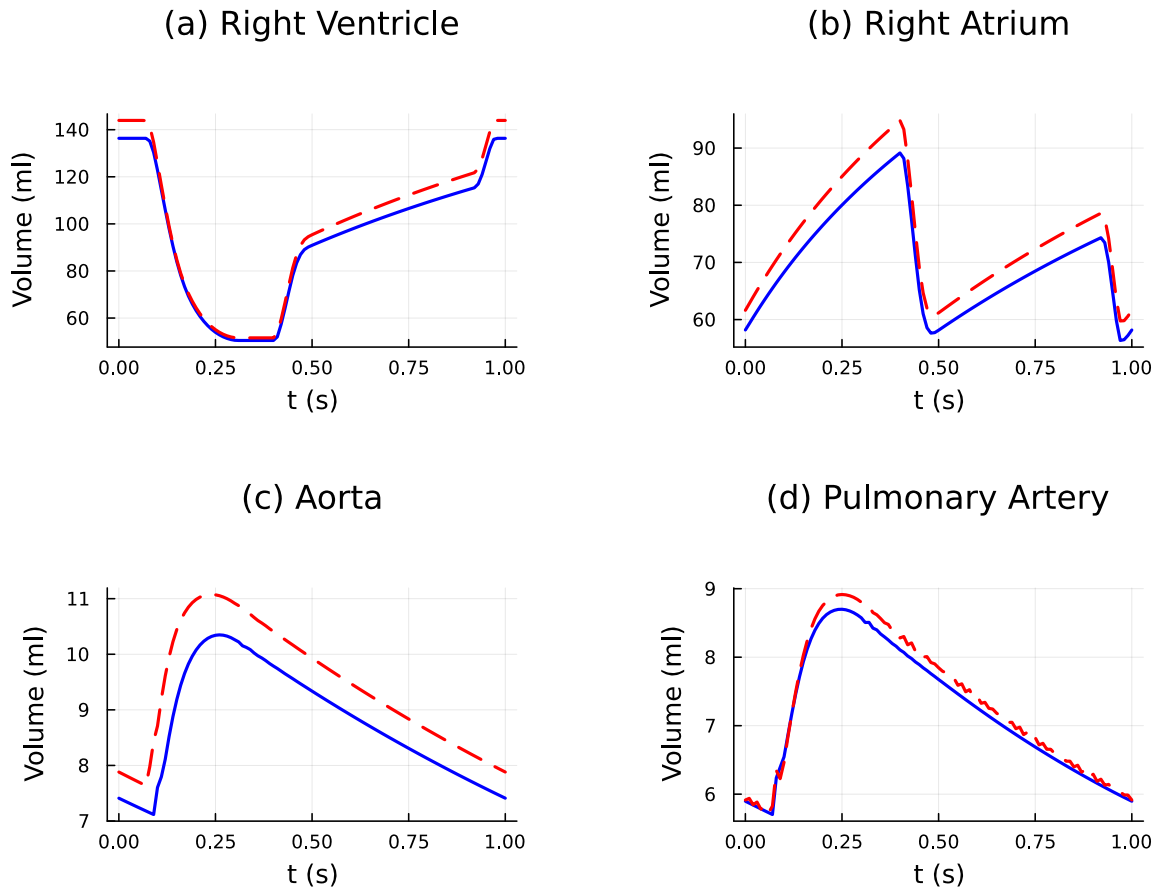


**Figure 6.5:** Effect of increased left ventricle elastance on blood volumes in different parts of the cardiovascular system, showing reference healthy human (blue) and altered model (red).

In Figure 6.5 it can be seen that when the left ventricular elastance is increased in isolation, the volume of blood in the chambers of the right side of the heart, as well as the vasculature, increases to compensate for the decreased volume in the chambers of the left side of the heart.

#### 6.1.4 Effect of biatrial cardiac xenotransplantation on the right side of the heart

The analysis has thus far been focused on the effect of cardiac xenotransplantation on the left side of the heart, as these parameters are more frequently analysed in literature. The right side of the heart has similar responses to the corresponding changes as the left

side of the heart. A decrease in pulmonary sinus radius increases right ventricular and pulmonary sinus pressure. A decrease in pulmonary sinus Young's modulus results in a slight decrease in pulmonary sinus pressure, and an increase in right ventricular elastance has similar impacts on the right side of the heart as an increase in left ventricular elastance had on the left side of the heart, although to a lesser degree due to a smaller elastance increase in the right ventricle (as discussed in Section 3.3.4). A good indication of the effect of each different physical change on the right side of the heart comes from looking at the PV loop of the right ventricle (Figure 6.6).

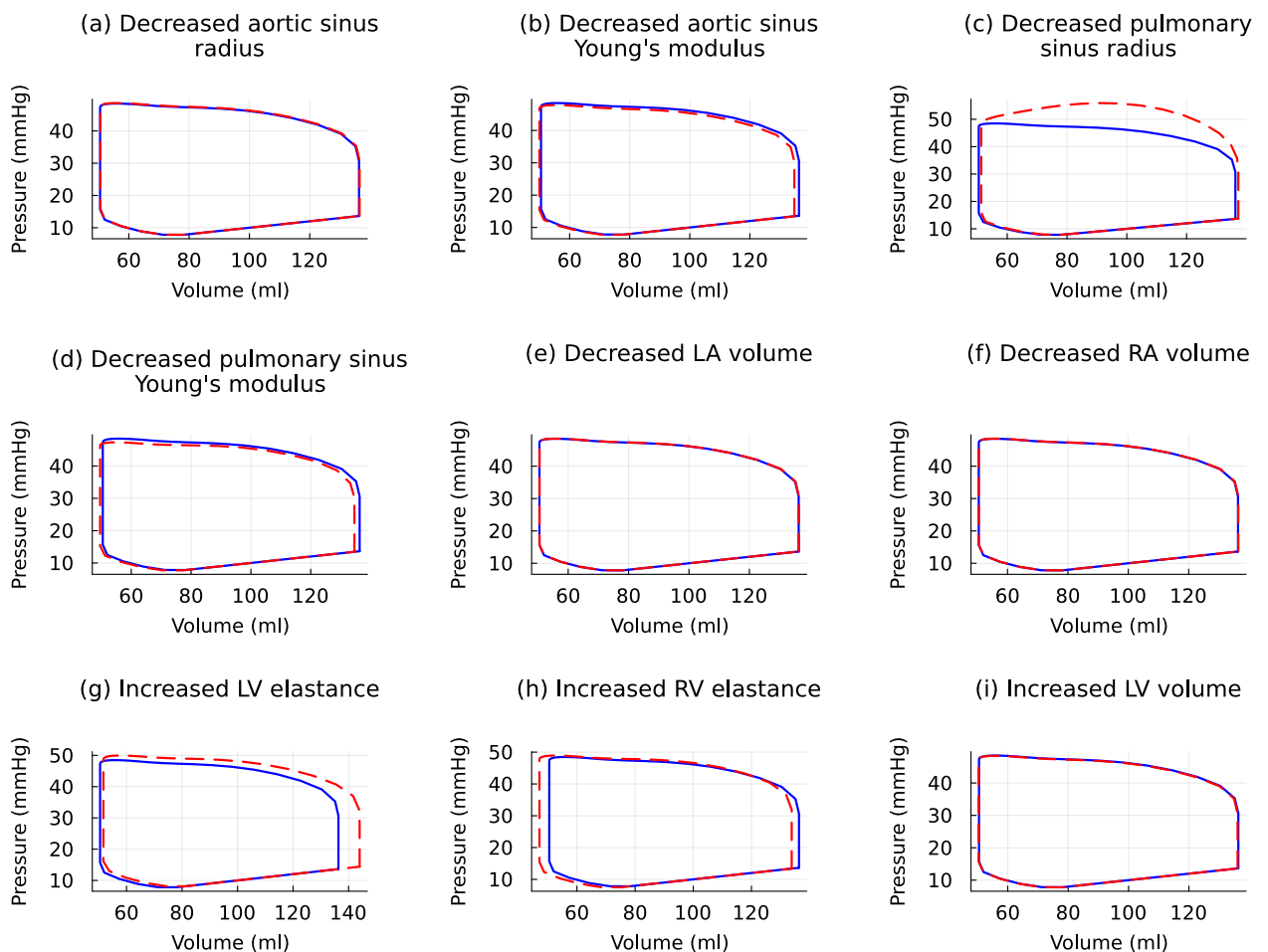


**Figure 6.6:** PV loop of the right ventricle of a reference healthy human (blue) and the altered model (red).

The physical changes that cause the greatest change in the PV loop of the right ventricle are the decreased PA radius (Fig. 6.6 (c)) and decreased PA Young's Modulus (Fig. 6.6 (d)), along with the increased elastance of both ventricles (Fig. 6.6 (g) and

(h)). The effect of the increased elastance of the right ventricle (Fig. 6.6 (h)) is less than the corresponding effects of the increased left ventricle elastance in the left side of the heart (Fig. 6.4 (b)) because the elastance of the right ventricle is not increased to the same extent as that of the left ventricle. The increase in left ventricle elastance however, results in more work being done by the right ventricle (Fig. 6.6 (g)), as can be seen by the increased area of the loop. This is due to the increase in the maximum volume of blood in the right ventricle, as blood is redistributed throughout the cardiovascular system to account for the decreased volume of blood in the left side of the heart (as discussed in Section 6.1.3).

### 6.1.5 Total effect of biatrial cardiac xenotransplantation

The total effect of biatrial cardiac xenotransplantation on the heart, taking into account all nine physical changes as seen in Figure 6.1, and the corresponding model modifications detailed in Table 3.9, can be seen in Figure 6.7.

Figure 6.7 again demonstrates that the physical changes that have the greatest effect on the left side of the heart are the decrease in aortic sinus radius, and the increase in left ventricle elastance, with the graphs of the left side of the heart in Figure 6.7 appearing to be a superposition of these two effects, with all other physical changes seeming negligible in comparison.

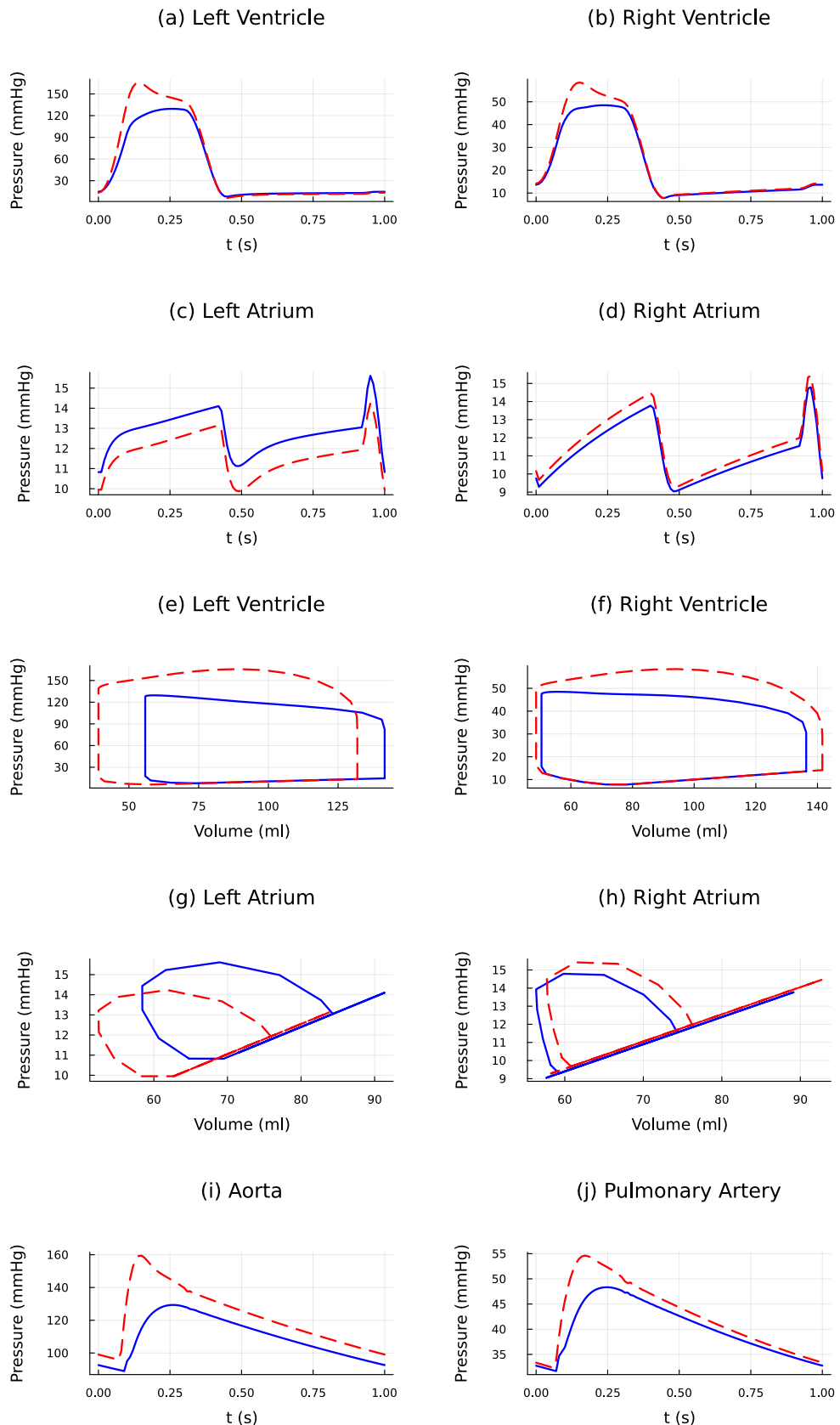


**Figure 6.7:** Total effect of biatrial cardiac xenotransplantation, showing reference healthy human (blue) and altered model (red).

## 6.2 Bicaval cardiac xenotransplantation

As discussed in Section 3.4, there are three additional changes made to the model in order to model bicaval cardiac xenotransplantation:

- A larger decrease in the volume of the right atrium.
- A decrease in radius of both the inferior and superior venae cavae.
- A decrease in the Young's modulus of the venae cavae walls.

The effect that these additional changes have on the aortic pressure when applied to the model in isolation can be seen in Figure 6.8.

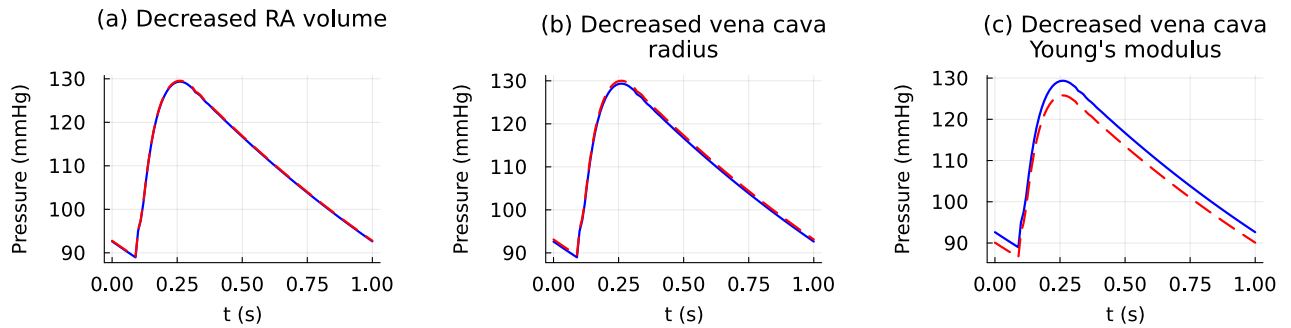


**Figure 6.8:** Pressure in the aorta of a reference healthy human (blue) and altered model (red).

From these graphs, it can be seen that the change that alters the aortic pressure most significantly is the decrease in venae cavae Young's modulus. This change was therefore investigated in more detail.

### 6.2.1 Effect of decreased venae cavae Young's modulus on the cardiovascular system

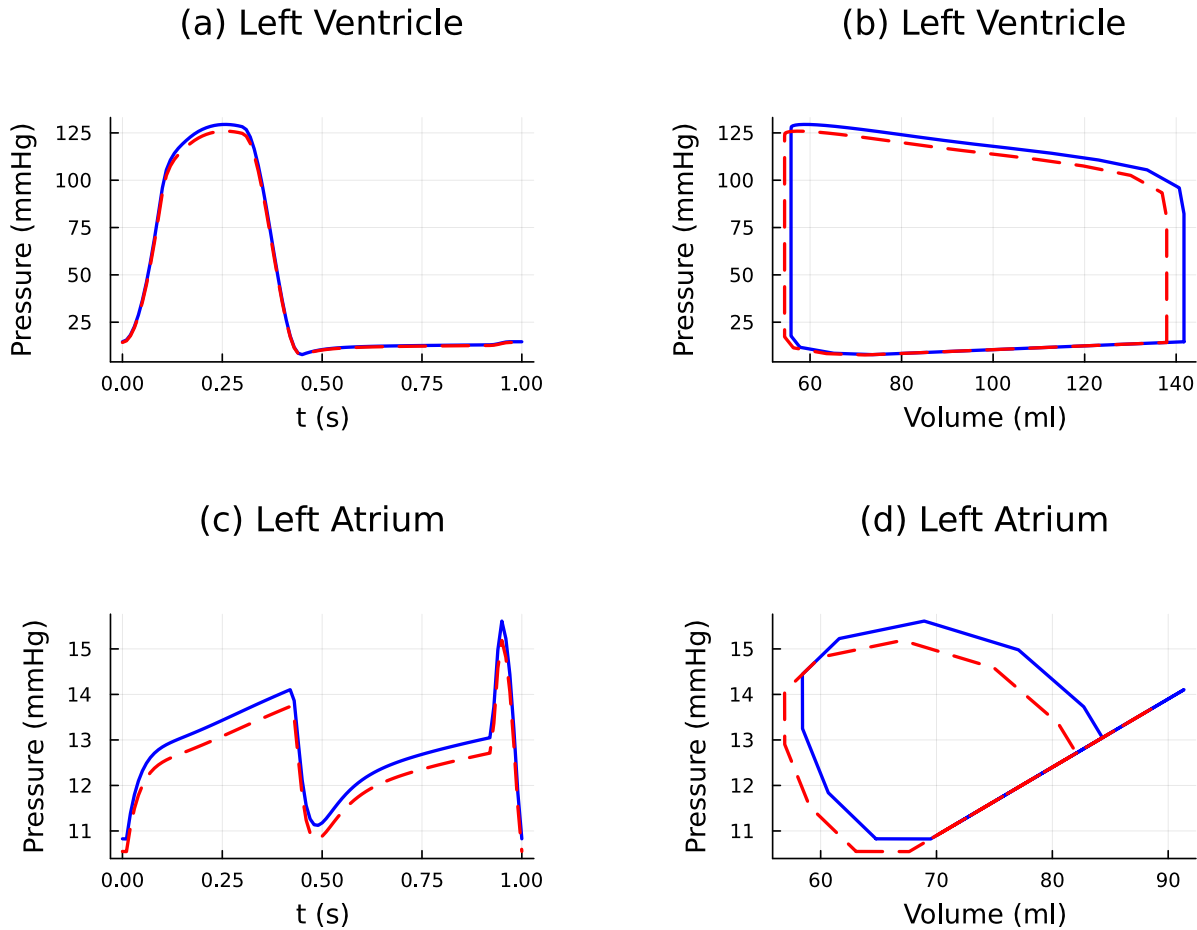


**Figure 6.9:** Effect of decreased venae cavae Young's modulus on the left side of the heart, showing reference healthy human (blue) and altered model (red).

Figure 6.9 indicates that a decrease in venae cavae Young's modulus when changed in isolation, will result in a decrease in both the pressure and volume in both chambers in the left side of the heart. The decrease in pressure can be seen as a direct result of the decrease in volume.

The venae cavae are the largest veins in the body and therefore hold a substantial amount of blood [51]. A decreased Young's modulus results in an increased compliance of the venae cavae, meaning they can stretch to accommodate a larger volume of blood.

This can be seen below in Figure 6.10, showing the volume of blood in all of the systemic veins.

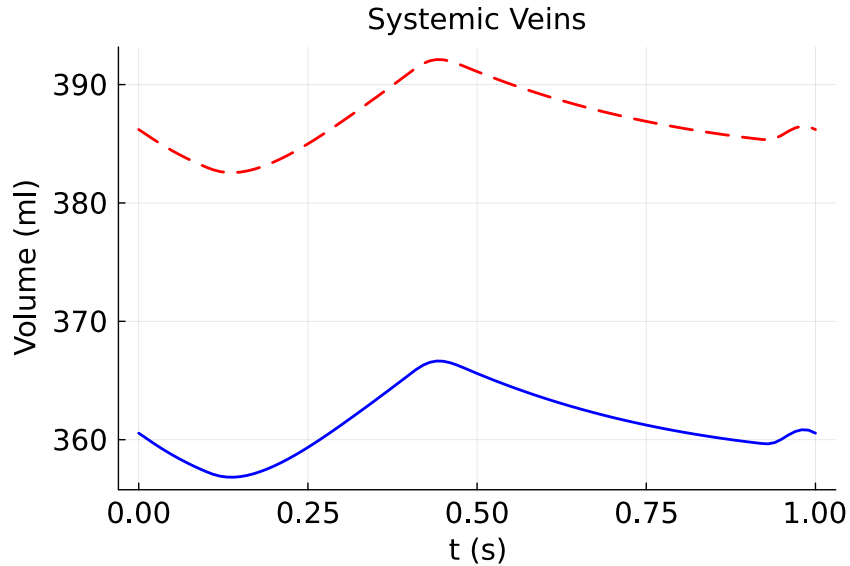


**Figure 6.10:** Effect of decreased venae cavae Young's modulus on the volume of blood in the systemic veins, showing reference healthy human (blue) and altered model (red).

A decrease in the Young's modulus of the venae cavae results in a redistribution of blood throughout the cardiovascular system, due to the venae cavae being capable of holding a larger volume of blood. There is therefore a decrease in the volume of blood in many sections of the cardiovascular system, resulting in a corresponding decrease in pressure.

### 6.2.2 Effect of bicaval xenotransplantation on the right side of the heart

Section 6.2.1 discussed the effect of bicaval xenotransplantation on the left side of the heart. While the impact on the left side of the heart is important to note, as it is these performance indicators that clinicians most often use to determine the overall health of the heart and cardiovascular system, the added physical changes introduced by bicaval transplantation over biatrial transplantation all occur on the right side of the heart. Therefore an investigation into the effect of these changes on the right side of the heart

was also undertaken. An initial investigation into the impact of the three added physical changes involved looking at the PV loops of the right ventricle, shown in Figure 6.11.

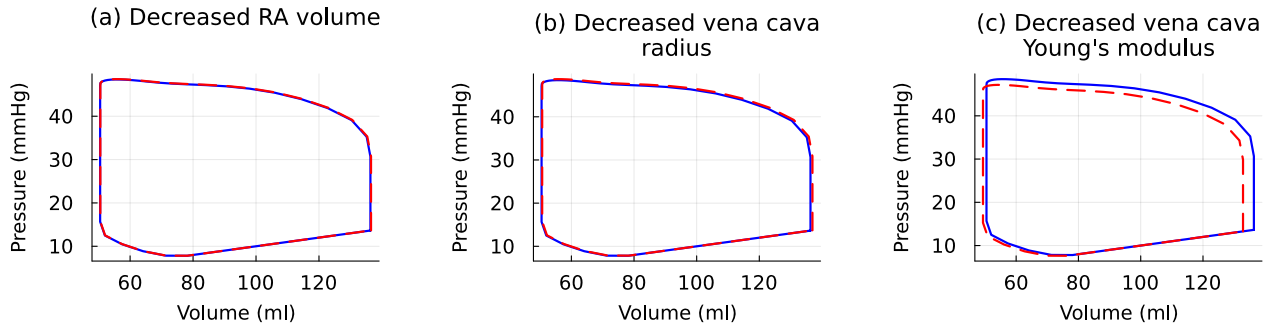


**Figure 6.11:** Effect of bicaval cardiac xenotransplantation on the right side of the heart, showing reference healthy human (blue) and altered model (red).

Similar to the response of the left side of the heart, the decrease in right atrium volume and vena cava radius have negligible effects on the performance of the right ventricle. The decreased vena cava Young's modulus results in a slight decrease in both volume and pressure in the right ventricle, therefore this change is investigated in more detail.

### 6.2.3 Effect of decreased venae cavae Young's modulus on the right side of the heart

The effect of the decreased vena cava Young's modulus on the right side of the heart is similar to the response of the left side of the heart. The right ventricle, right atrium, and pulmonary sinus all see a decrease in overall pressure. As seen from the PV loops of both the right ventricle and right atrium, both chambers also see a decrease in the volume of blood contained in them, which is most likely the primary cause for the pressure decreases seen in Figure 6.12. This decrease in volume in the heart chambers is again a result of the increased compliance of the vena cava, and its ability to expand to accommodate a larger volume of blood, as previously illustrated in Figure 6.10.

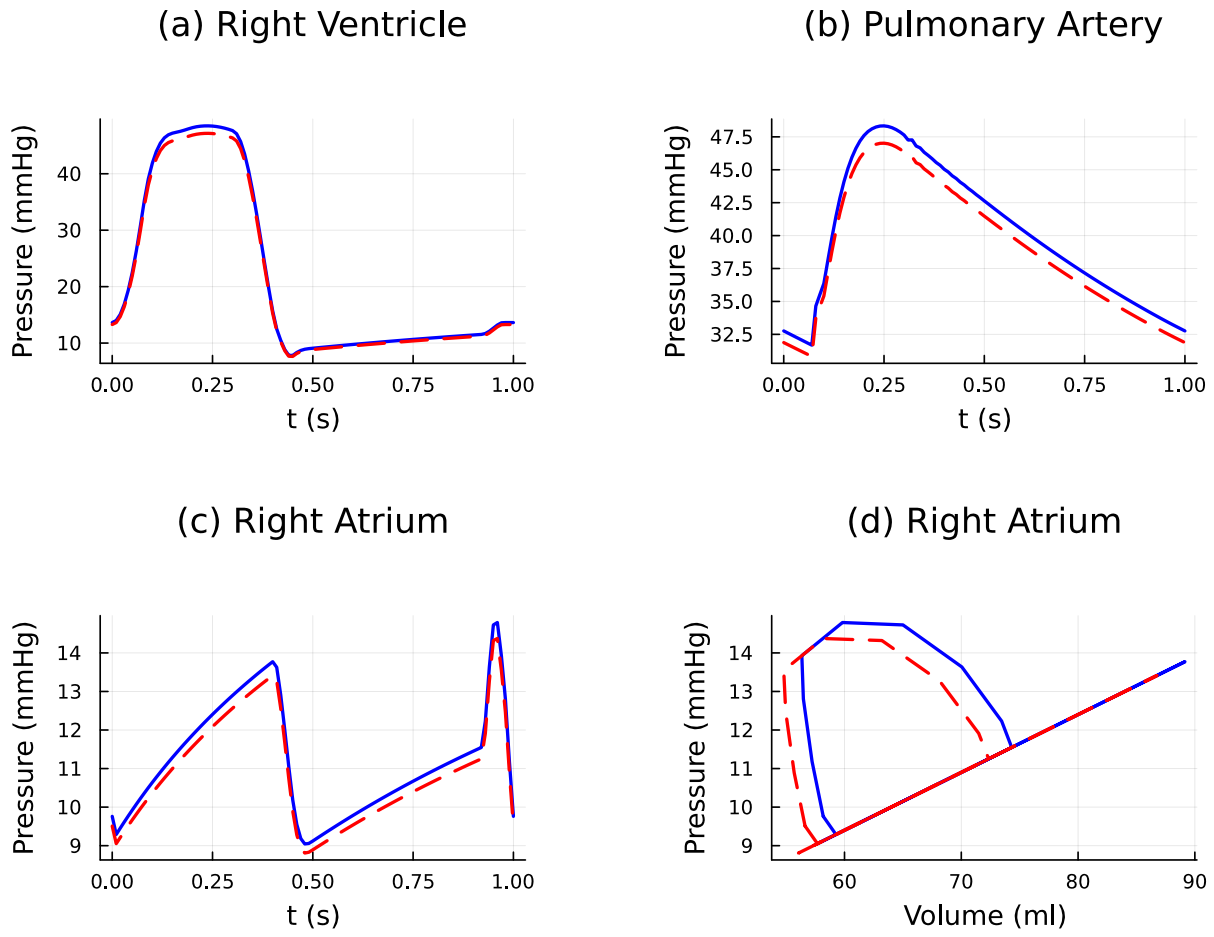


**Figure 6.12:** Effect of decreased venae cavae Young's modulus on right side of the heart, showing reference healthy human (blue) and altered model (red).

#### 6.2.4 Total effect of bicaval cardiac xenotransplantation

The total effect of bicaval cardiac xenotransplantation on the heart, taking into account all of the changes detailed in Table 3.14 can be seen below in Figure 6.13. As in the biatrial case, the physical changes that have the greatest effect on the heart remain the decrease in aortic and pulmonary sinus radii and the increase in ventricular elastances. Therefore Figure 6.13 looks very similar to Figure 6.7, which shows the total impact of biatrial cardiac xenotransplantation on the cardiovascular system.

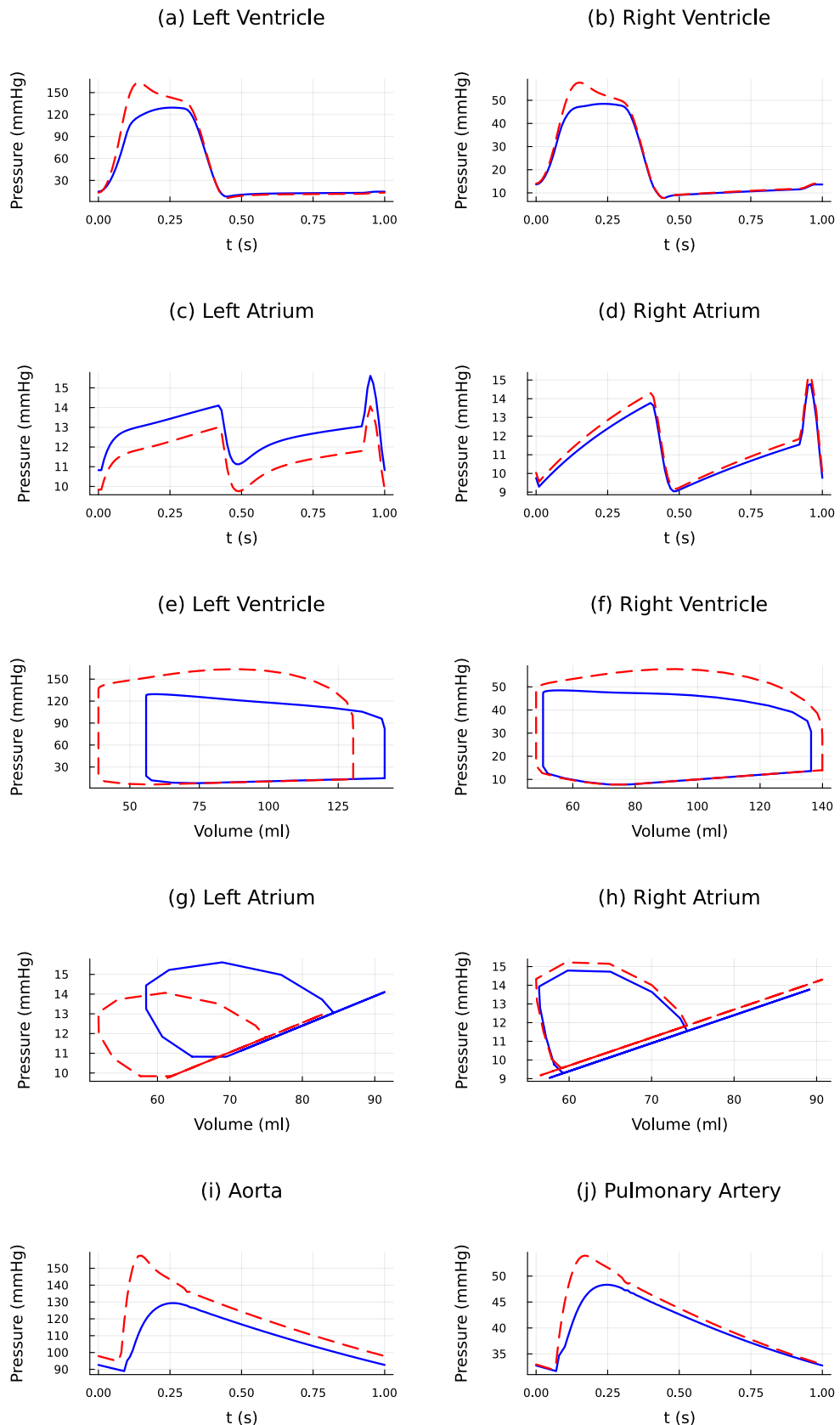


**Figure 6.13:** Total effect of bicaval cardiac xenotransplantation, showing reference healthy human (blue) and altered model (red).

---

CHAPTER  
SEVEN

---

## CONCLUSIONS AND FUTURE WORK

### 7.1 Main findings

In the study of the effect of biatrial cardiac xenotransplantation, nine anatomical differences between pig and human hearts were investigated. Of these differences, only three resulted in non-negligible changes in the aortic sinus pressure, warranting further investigation.

- **A decrease in aortic sinus diameter** increases the resistance of the aortic sinus. This resulted in a notable increase in pressure (without a corresponding increase in blood volume) in the left ventricle due to the need for an increased pressure gradient across the aortic sinus to push the same amount of blood through.
- **A decrease in the Young's modulus of the aortic sinus** results in a slight decrease in pressure in the aortic sinus, due to the increased compliance of the vessel allowing the same volume of blood to be accepted into the aortic sinus while maintaining a lower pressure. Apart from the effect on the pressure in the aortic sinus, the decrease in aortic sinus Young's modulus has negligible effects on other parts of the cardiovascular system.

- An increase in left ventricular elastance (or the pumping strength of the left ventricle) results in an increase in pressure and a decrease in volume in the left ventricle. Elastance acts to resist an increase in volume with increased pressure, therefore resulting in a reduction in the volume of blood in the left ventricle. There is also a reduction in the volume of blood in the left atrium, resulting in a notable decrease in pressure in this chamber. The reduction in the volume of blood in the left side of the heart is accounted for by the redistribution of blood throughout the cardiovascular system, with increased blood volumes in the right side of the heart and the vasculature, resulting in a corresponding increase in pressure in these sections of the system.

The investigation into the effect of bicaval cardiac xenotransplantation introduced three extra anatomical differences to be accounted for, of which the decrease in venae cavae Young's modulus was the only one that resulted in non-negligible changes in the indicators studied.

Decreased venae cavae Young's modulus results in a decrease in pressure and volume in all four heart chambers as well as the aorta and the pulmonary artery. Due to the size of the venae cavae, they can hold a substantial amount of blood, and decreasing their Young's modulus results in a larger volume of blood being accommodated in the venae cavae, and a resulting redistribution of blood throughout the cardiovascular system, leading to a smaller volume of blood in other sections of the system.

## 7.2 Limitations

While the LPM used in this project offers a computationally inexpensive way to investigate the effects of cardiac xenotransplantation on the cardiovascular system, with outputs that are familiar to clinicians, several limitations must be considered.

As LPMs are “zero-dimensional models”, their response is based on idealised mathematical equations that respond only to time. Any changes in geometry between two models must be described through changes in the fixed model parameters. In each

of the 28 sections in the model, all model outputs such as pressure, volume and blood flow are assumed to have no spatial variance throughout the section.

The LPM cannot therefore predict a response to sharp geometrical features. For example in the investigation of the effect of the decreased aortic sinus diameter in Section 6.1.1, the decreased diameter was accounted for by increasing the resistance and inertia values and decreasing the compliance value of the aortic sinus. This results in an increase in pressure in both the aortic sinus, as well as in the systemic arteries to which the aortic sinus is directly connected. However, such a drastic increase in diameter from the aortic sinus to the ascending aorta would most likely result in a sharp decrease in pressure in the ascending aorta relative to the aortic sinus due to the blood being expelled into a vessel with a much larger diameter. While the pressure in the ascending aorta and other systemic arteries may indeed be higher in the case of cardiac xenotransplantation, it is important to note that geometrical features like these are not accounted for in lumped-parameter modelling, and therefore in a real-life scenario, the pressure and flow characteristics might not change to the same extent as predicted.

This model is purely a mechanical system and does not account for any changes in the cardiovascular system that are caused by sources external to the system. For example, in Section 6.1.3, the decrease in volume in the left side of the heart was accounted for through an increase in the volume of blood in other parts of the cardiovascular system. However, the kidneys can regulate the volume of blood in the cardiovascular system by excreting or retaining extra water when necessary. Reactions such as this could occur in the case of cardiac xenotransplantation, however they are beyond the scope of this model.

As the purpose of this model is to provide an idea of possible trends in key performance indicators in the mechanical system that may arise as a result of porcine-to-human cardiac xenotransplantation, the absolute values are less important than the general trends observed.

## 7.3 UN Sustainable Development Goals

The 17 Sustainable Development Goals (SDGs) are at the heart of the UN's 2030 Agenda for Sustainable Development, which was adopted by all UN member states in 2015 and provides a shared blueprint for peace and prosperity for people and the planet, now and into the future [49]. This project supports the following SDGs:

- **Goal 3 - Good Health and Well-Being :** This project aims to support the ongoing effort to make porcine-to-human cardiac xenotransplantation a viable alternative to allotransplantation. If this is realised, porcine-to-human cardiac xenotransplantation could address the current shortage of organ donors, and increase access to transplants, thus promoting good health and well-being.
- **Goal 9 - Industry, Innovation and Infrastructure:** Porcine-to-cardiac xenotransplantation is an area of great innovation in the medical field. This project uses LPMs to better understand the mechanical challenges introduced by cardiac xenotransplantation to the cardiovascular system. While LPMs have previously been used to model pathological conditions of the cardiovascular system, the application of LPMs to model cardiac xenotransplantation is novel.

In summary, this project contributes to advancing the Sustainable Development Goals by leveraging innovation and scientific research to improve healthcare outcomes and address global challenges related to organ shortages.

## 7.4 Ethical implications

While there are no direct ethical implications of this project, which is solely based on *in-silico* experimentation, the modelling of xenotransplantation aims to support the end goal of making xenotransplantation more viable. There are several ethical concerns associated with xenotransplantation, the most notable of which are listed below:

- **Welfare of the source animals:** Pigs raised for organ transplantation will be kept in the manner of laboratory animals, under confined, sterile conditions that

minimise the risk of pathogen proliferation [39]. This results in the pigs being unable to actualise their psychological and biological natures.

- **Spreading of zoonotic diseases:** Pigs carry endogenous retroviruses that can cause humans to become very sick. One of these retroviruses was likely responsible for the swine flu epidemic in 2009 [39]. Therefore the risk of infection applies not only to the xenotransplant recipient but also to the wider public.
- **Continuous surveillance of research participants:** To minimise the risk of spreading zoonotic diseases, early recipients of xenotransplants will have to consent to lifelong monitoring for infectious organisms. This would go against the right of research subjects to withdraw from research participation at any time for any reason, a right which is endorsed worldwide in ethical guidelines governing human subjects [16].
- **Distribution of donor organs:** If xenotransplantation is deemed a viable alternative to allotransplantation in the future, a new ethical concern will arise over the distribution of donor organs. As allotransplantation will always be the preferred option, doctors will need to make difficult decisions regarding which patients will receive available human hearts, and which patients will receive a xenotransplant. These decisions will become even more difficult when we take into account the fact that in some cultures and religions (particularly Islam), pigs are considered dirty, and people from these cultures will likely not accept a porcine xenograft.

## 7.5 Possibility for future work

### 7.5.1 Comparing model of cardiac xenotransplantation to hearts with different pathological conditions

Throughout this investigation, the impacts of the physical changes introduced by porcine-to-human cardiac xenotransplantation have been compared to the reference case of a healthy human heart. However, the hearts of patients who require heart transplantation

will most likely not be in a healthy condition. It would therefore be beneficial to compare the change in key metrics when a pig heart is transplanted into a patient who, prior to the surgery, has abnormal heart function due to different pathological conditions.

### 7.5.2 Coupling of LPMs and 1D models

While LPMs offer a good starting point for understanding pressure and flow rates over time in different parts of the circulatory system, they are limited by their inability to describe the spatial variance of these parameters throughout these sections, with the assumption of a uniform distribution of the fundamental variables within any particular compartment.

One-dimensional models of different parts of the vasculature have the added benefit of demonstrating the propagation of pressure and flow waves across the length of a blood vessel without a significant additional computational cost [46]. 1D modelling is therefore a logical next step to follow from lumped-parameter modelling.

Sections of the LPM proposed in this paper could be used to provide boundary conditions to a 1D model of sections of the vasculature. For example, a 1D model of the aorta and other major arteries could use the lumped left-heart model to describe conditions at the inlet, and a three-element Windkessel (describing systemic arterioles, capillaries and veins) to describe conditions at the outlet.

### 7.5.3 Coupling of LPMs and 3D models

Similar to the coupling of LPMs with 1D models, they can also be used to describe the conditions at the boundaries of 3D models. 3D models can offer detailed descriptions of fluid flow throughout the cardiovascular system, with temporal variance as well as variance in the three spatial directions. This can give valuable insights into detailed fluid dynamics, such as possible areas where blood re-circulation can occur under different pathological conditions. 3D models can also use fluid-structure interaction algorithms which can be utilized to examine how the human circulatory system functions by simulating blood flow and capturing mechanical responses within blood vessels [48].

Sections of the LPM proposed in this paper could be used to provide boundary conditions to a 3D model of sections of the circulatory system. For example, a 3D model of the left side of the heart could use the LPMs of the pulmonary and systemic circulation (or an even more simplified version of these) at the inlet and outlet of the left side of the heart respectively.

#### 7.5.4 Valve models

During this study, the effect of the difference between pig and human valves on blood flow characteristics has not been thoroughly investigated. This is primarily due to the lack of information on anatomical differences between pig and human valves in literature that could be directly translated into model parameter changes using Equation 3.11.

Therefore, if future research into porcine-heart anatomy gives a clearer idea of the differences between pig and human valves, the change in valve dynamics should be investigated further. Furthermore, alternative valve models could be investigated that take into account the opening and closing mechanics as opposed to the simple on-off approach taken in this model.

### 7.6 Final Thoughts

This study has revealed that porcine-to-cardiac xenotransplantation can result in a significant change in key mechanical metrics of the cardiovascular system when compared to the reference case of a healthy human, as a result of the anatomical differences between pig and human hearts. Models such as the LPM model developed for this project have the possibility of aiding clinicians as they determine how these metric changes will affect the long-term success of the xenograft.

## BIBLIOGRAPHY

- [1] Talha Ahmed and Ankit Jain. “Heart Transplantation”. eng. In: *StatPearls*. Treasure Island (FL): StatPearls Publishing, 2024. URL: <http://www.ncbi.nlm.nih.gov/books/NBK557571/> (visited on 02/25/2024).
- [2] Carolien J. van Andel, Peter V. Pistecky, and Cornelius Borst. “Mechanical properties of porcine and human arteries: implications for coronary anastomotic connectors”. eng. In: *The Annals of Thoracic Surgery* 76.1 (July 2003), 58–64, discussion 64–65. ISSN: 0003-4975. DOI: [10.1016/s0003-4975\(03\)00263-7](https://doi.org/10.1016/s0003-4975(03)00263-7).
- [3] Tim Berger et al. “Pulmonary artery diameter: means and normal limits—assessment by computed tomography angiography”. In: *Interactive CardioVascular and Thoracic Surgery* 34.4 (Apr. 2022), pp. 637–644. ISSN: 1569-9285. DOI: [10.1093/icvts/ivab308](https://doi.org/10.1093/icvts/ivab308). URL: <https://doi.org/10.1093/icvts/ivab308> (visited on 03/14/2024).
- [4] Nikolai L. Bjørdalsbakke et al. “Parameter estimation for closed-loop lumped parameter models of the systemic circulation using synthetic data”. In: *Mathematical Biosciences* 343 (Jan. 2022), p. 108731. ISSN: 0025-5564. DOI: [10.1016/j.mbs.2021.108731](https://doi.org/10.1016/j.mbs.2021.108731). URL: <https://www.sciencedirect.com/science/article/pii/S002555642100136X> (visited on 12/13/2023).
- [5] Selim Bozkurt. “Mathematical modeling of cardiac function to evaluate clinical cases in adults and children”. In: *PLoS ONE* 14.10 (Oct. 2019), e0224663. ISSN: 1932-6203. DOI: [10.1371/journal.pone.0224663](https://doi.org/10.1371/journal.pone.0224663). URL: <https://www.ncbi.nlm.nih.gov/pmc/articles/PMC6822734/> (visited on 12/14/2023).

- [6] Selim Bozkurt et al. “Patient-Specific Modelling and Parameter Optimisation to Simulate Dilated Cardiomyopathy in Children”. In: *Cardiovascular Engineering and Technology* 13.5 (2022), pp. 712–724. ISSN: 1869-408X. DOI: [10.1007/s13239-022-00611-9](https://doi.org/10.1007/s13239-022-00611-9). URL: <https://www.ncbi.nlm.nih.gov/pmc/articles/PMC9616749/> (visited on 12/13/2023).
- [7] Roberto Burattini and Silvia Bini. “Physiological interpretation of inductance and low-resistance terms in four-element windkessel models: Assessment by generalized sensitivity function analysis”. In: *Medical Engineering & Physics* 33.6 (July 2011), pp. 739–754. ISSN: 1350-4533. DOI: [10.1016/j.medengphy.2011.01.012](https://doi.org/10.1016/j.medengphy.2011.01.012). URL: <https://www.sciencedirect.com/science/article/pii/S1350453311000166> (visited on 12/13/2023).
- [8] Jennie Cotter. *St. Vincent’s University Hospital calls for more individuals to become Organ Donors on the 60th anniversary year of transplantation in Ireland and Organ Donor Awareness Week*. en. May 2023. URL: <https://www.stvincents.ie/st-vincents-university-hospital-calls-for-more-individuals-to-become-organ-donors-on-the-60th-anniversary-year-of-transplantation-in-ireland-and-organ-donor-awareness-week-the-first-kidney-transp/> (visited on 01/01/2024).
- [9] S. J. Crick et al. “Anatomy of the pig heart: comparisons with normal human cardiac structure”. eng. In: *Journal of Anatomy* 193 ( Pt 1).Pt 1 (July 1998), pp. 105–119. ISSN: 0021-8782. DOI: [10.1046/j.1469-7580.1998.19310105.x](https://doi.org/10.1046/j.1469-7580.1998.19310105.x).
- [10] Ashutosh Dash et al. “Non-invasive detection of coronary artery disease from photoplethysmograph using lumped parameter modelling”. In: *Biomedical Signal Processing and Control* 77 (Aug. 2022), p. 103781. ISSN: 1746-8094. DOI: [10.1016/j.bspc.2022.103781](https://doi.org/10.1016/j.bspc.2022.103781). URL: <https://www.sciencedirect.com/science/article/pii/S1746809422003032> (visited on 12/13/2023).
- [11] Angelo Maria Dell’Aquila et al. “Bicaval versus standard technique in orthotopic heart transplant: assessment of atrial performance at magnetic resonance and transthoracic echocardiography”. In: *Interactive Cardiovascular and Thoracic Surgery*

*Surgery* 14.4 (Apr. 2012), pp. 457–462. ISSN: 1569-9293. DOI: [10.1093/icvts/ivr084](https://doi.org/10.1093/icvts/ivr084). URL: <https://www.ncbi.nlm.nih.gov/pmc/articles/PMC3309807/> (visited on 04/14/2024).

- [12] Zheng Duanmu et al. “A patient-specific lumped-parameter model of coronary circulation”. In: *Scientific Reports* 8 (Jan. 2018), p. 874. ISSN: 2045-2322. DOI: [10.1038/s41598-018-19164-w](https://doi.org/10.1038/s41598-018-19164-w). URL: <https://www.ncbi.nlm.nih.gov/pmc/articles/PMC5772042/> (visited on 12/13/2023).
- [13] *Ejection Fraction: What Do the Numbers Mean?* / Penn Medicine. en-US. Apr. 2022. URL: <https://www.pennmedicine.org/updates/blogs/heart-and-vascular-blog/2022/april/ejection-fraction-what-the-numbers-mean> (visited on 04/04/2024).
- [14] Erwan Flécher et al. “Heterotopic heart transplantation: where do we stand?” eng. In: *European Journal of Cardio-Thoracic Surgery: Official Journal of the European Association for Cardio-Thoracic Surgery* 44.2 (Aug. 2013), pp. 201–206. ISSN: 1873-734X. DOI: [10.1093/ejcts/ezt136](https://doi.org/10.1093/ejcts/ezt136).
- [15] Luca Formaggia et al. “Numerical modeling of 1D arterial networks coupled with a lumped parameters description of the heart”. eng. In: *Computer Methods in Biomechanics and Biomedical Engineering* 9.5 (Oct. 2006), pp. 273–288. ISSN: 1025-5842. DOI: [10.1080/10255840600857767](https://doi.org/10.1080/10255840600857767).
- [16] Susan Gilbert. *Xenotransplantation: Three Areas of Concern*. en-US. Jan. 2022. URL: <https://www.thehastingscenter.org/xenotransplantation-three-areas-of-concern/> (visited on 04/11/2024).
- [17] Chaya Gopalan and Erik Kirk. “Chapter 2 - The blood vessels”. In: *Biology of Cardiovascular and Metabolic Diseases*. Ed. by Chaya Gopalan and Erik Kirk. Academic Press, Jan. 2022, pp. 35–51. ISBN: 978-0-12-823421-1. DOI: [10.1016/B978-0-12-823421-1.00004-4](https://doi.org/10.1016/B978-0-12-823421-1.00004-4). URL: <https://www.sciencedirect.com/science/article/pii/B9780128234211000044> (visited on 12/10/2023).

- [18] Bartley P. Griffith et al. “Genetically Modified Porcine-to-Human Cardiac Xenotransplantation”. In: *New England Journal of Medicine* 387.1 (July 2022). Publisher: Massachusetts Medical Society \_eprint: <https://doi.org/10.1056/NEJMoa2201422>, pp. 35–44. ISSN: 0028-4793. DOI: [10.1056/NEJMoa2201422](https://doi.org/10.1056/NEJMoa2201422). URL: <https://doi.org/10.1056/NEJMoa2201422> (visited on 12/05/2023).
- [19] David L. Halaney et al. “The Effect of Trabeculae Carneae on Left Ventricular Diastolic Compliance: Improvement in Compliance With Trabecular Cutting”. In: *Journal of Biomechanical Engineering* 139.3 (Mar. 2017), pp. 0310121–0310128. ISSN: 0148-0731. DOI: [10.1115/1.4035585](https://doi.org/10.1115/1.4035585). URL: <https://www.ncbi.nlm.nih.gov/pmc/articles/PMC7104769/> (visited on 02/27/2024).
- [20] Nicholas R. Hess and David J. Kaczorowski. “The history of cardiac xenotransplantation: early attempts, major advances, and current progress”. In: *Frontiers in Transplantation* 2 (2023). ISSN: 2813-2440. URL: <https://www.frontiersin.org/articles/10.3389/frtra.2023.1125047> (visited on 12/10/2023).
- [21] S. Y. Huang et al. “Effects of birth season, breed, sex, and sire family on cardiac morphology determined in pigs (*Sus scrofa domestica*) by use of echocardiography”. eng. In: *Comparative Medicine* 51.6 (Dec. 2001), pp. 545–549. ISSN: 1532-0820.
- [22] H. J. Kim et al. “On Coupling a Lumped Parameter Heart Model and a Three-Dimensional Finite Element Aorta Model”. en. In: *Annals of Biomedical Engineering* 37.11 (Nov. 2009), pp. 2153–2169. ISSN: 1573-9686. DOI: [10.1007/s10439-009-9760-8](https://doi.org/10.1007/s10439-009-9760-8). URL: <https://doi.org/10.1007/s10439-009-9760-8> (visited on 03/31/2024).
- [23] Jiwon Koh et al. “Historical Review and Future of Cardiac Xenotransplantation”. In: *Korean Circulation Journal* 53.6 (May 2023), pp. 351–366. ISSN: 1738-5520. DOI: [10.4070/kcj.2022.0351](https://doi.org/10.4070/kcj.2022.0351). URL: <https://www.ncbi.nlm.nih.gov/pmc/articles/PMC10244184/> (visited on 11/26/2023).
- [24] Theodosios Korakianitis and Yubing Shi. “Numerical simulation of cardiovascular dynamics with healthy and diseased heart valves”. In: *Journal of Biomechanics* 39.11 (Jan. 2006), pp. 1964–1982. ISSN: 0021-9290. DOI: [10.1016/j.jbiomech](https://doi.org/10.1016/j.jbiomech).

2005 . 06 . 016. URL: <https://www.sciencedirect.com/science/article/pii/S0021929005002927> (visited on 12/13/2023).

- [25] Ryno Laubscher et al. “Dynamic simulation of aortic valve stenosis using a lumped parameter cardiovascular system model with flow regime dependent valve pressure loss characteristics”. eng. In: *Medical Engineering & Physics* 106 (Aug. 2022), p. 103838. ISSN: 1873-4030. DOI: [10.1016/j.medengphy.2022.103838](https://doi.org/10.1016/j.medengphy.2022.103838).
- [26] M.S. Leaning et al. “Modelling a complex biological system: the human cardiovascular system — 2. Model validation, reduction and development”. In: *Transactions of the Institute of Measurement and Control* 5 (Apr. 1983). ISSN: 2. DOI: [10.1177/014233128300500203](https://doi.org/10.1177/014233128300500203). URL: <https://journals.sagepub.com/doi/10.1177/014233128300500203> (visited on 03/01/2024).
- [27] Pavlos P. Lelovas, Nikolaos G. Kostomitsopoulos, and Theodoros T. Xanthos. “A comparative anatomic and physiologic overview of the porcine heart”. eng. In: *Journal of the American Association for Laboratory Animal Science: JAALAS* 53.5 (Sept. 2014), pp. 432–438. ISSN: 2769-6677.
- [28] Tanya Lewis. *Milestone Pig-to-Human Heart Transplant May Pave the Way for Broader Trial*. en. URL: <https://www.scientificamerican.com/article/milestone-pig-to-human-heart-transplant-may-pave-the-way-for-broader-trial/> (visited on 12/05/2023).
- [29] Yingbo Ma et al. *Modeling Toolkit: A Composable Graph Transformation System For Equation-Based Modeling*. 2021. arXiv: [2103.05244 \[cs.MS\]](https://arxiv.org/abs/2103.05244).
- [30] Song Shou Mao et al. “Normal Thoracic Aorta Diameter on Cardiac Computed Tomography in Healthy Asymptomatic Adult; Impact of Age and Gender”. In: *Academic radiology* 15.7 (July 2008), pp. 827–834. ISSN: 1076-6332. DOI: [10.1016/j.acra.2008.02.001](https://doi.org/10.1016/j.acra.2008.02.001). URL: <https://www.ncbi.nlm.nih.gov/pmc/articles/PMC2577848/> (visited on 03/16/2024).
- [31] Sofia Martin-Suarez et al. “Orthotopic Heart Transplantation: Bicaval Versus Biatrial Surgical Technique”. en. In: *Heart Transplantation*. IntechOpen, Oct. 2018. ISBN: 978-1-78923-802-0. DOI: [10.5772/intechopen.76803](https://doi.org/10.5772/intechopen.76803). URL: <https://www.intechopen.com/chapters/63063> (visited on 02/25/2024).

- [32] Soumen Pal et al. “A next-generation dynamic programming language Julia: Its features and applications in biological science”. In: *Journal of Advanced Research* (Nov. 2023). ISSN: 2090-1232. DOI: [10.1016/j.jare.2023.11.015](https://doi.org/10.1016/j.jare.2023.11.015). URL: <https://www.sciencedirect.com/science/article/pii/S2090123223003521> (visited on 03/13/2024).
- [33] Joshua D. Pollock and Amgad N. Makaryus. “Physiology, Cardiac Cycle”. eng. In: *StatPearls*. Treasure Island (FL): StatPearls Publishing, 2023. URL: <http://www.ncbi.nlm.nih.gov/books/NBK459327/> (visited on 12/29/2023).
- [34] M. R. Prince et al. “The diameter of the inferior vena cava and its implications for the use of vena caval filters”. eng. In: *Radiology* 149.3 (Dec. 1983), pp. 687–689. ISSN: 0033-8419. DOI: [10.1148/radiology.149.3.6647844](https://doi.org/10.1148/radiology.149.3.6647844).
- [35] *Pulse Pressure: Calculator, Variation, and More*. en. Dec. 2017. URL: <https://www.healthline.com/health/pulse-pressure> (visited on 04/04/2024).
- [36] A. Quarteroni, A. Veneziani, and C. Vergara. “Geometric multiscale modeling of the cardiovascular system, between theory and practice”. In: *Computer Methods in Applied Mechanics and Engineering* 302 (Apr. 2016), pp. 193–252. ISSN: 0045-7825. DOI: [10.1016/j.cma.2016.01.007](https://doi.org/10.1016/j.cma.2016.01.007). URL: <https://www.sciencedirect.com/science/article/pii/S0045782516000098> (visited on 03/31/2024).
- [37] Christopher Rackauckas and Qing Nie. “DifferentialEquations.jl – A Performant and Feature-Rich Ecosystem for Solving Differential Equations in Julia”. In: *The Journal of Open Research Software* 5.1 (2017). Exported from <https://app.dimensions.ai> on 2019/05/05. DOI: [10.5334/jors.151](https://doi.org/10.5334/jors.151). URL: <https://app.dimensions.ai/details/publication/pub.1085583166%20and%20http://openresearchsoftware.metajnl.com/articles/10.5334/jors.151/galley/245/download/>.
- [38] Natalie L. Rich and Yusuf S. Khan. “Anatomy, Thorax, Heart Papillary Muscles”. eng. In: *StatPearls*. Treasure Island (FL): StatPearls Publishing, 2024. URL: <http://www.ncbi.nlm.nih.gov/books/NBK557802/> (visited on 02/27/2024).

- [39] Bernard E. Rollin. “Ethical and Societal Issues Occasioned by Xenotransplantation”. In: *Animals : an Open Access Journal from MDPI* 10.9 (Sept. 2020), p. 1695. ISSN: 2076-2615. DOI: [10.3390/ani10091695](https://doi.org/10.3390/ani10091695). URL: <https://www.ncbi.nlm.nih.gov/pmc/articles/PMC7552641/> (visited on 04/11/2024).
- [40] Paula A. Rudenick et al. “Assessment of Wall Elasticity Variations on Intraluminal Haemodynamics in Descending Aortic Dissections Using a Lumped-Parameter Model”. In: *PLoS ONE* 10.4 (Apr. 2015), e0124011. ISSN: 1932-6203. DOI: [10.1371/journal.pone.0124011](https://doi.org/10.1371/journal.pone.0124011). URL: <https://www.ncbi.nlm.nih.gov/pmc/articles/PMC4399844/> (visited on 12/13/2023).
- [41] Torsten Schenkel and Harry Saxton. *CirculatorySystemModels*. DOI: [10.5281/zenodo.7497881](https://doi.org/10.5281/zenodo.7497881). URL: <https://github.com/TS-CUBED/%20CirculatorySystemModel>.
- [42] S. Schicktanz. “Xenotransplantation”. In: *Encyclopedia of Applied Ethics (Second Edition)*. Ed. by Ruth Chadwick. San Diego: Academic Press, Jan. 2012, pp. 565–574. ISBN: 978-0-12-373932-2. DOI: [10.1016/B978-0-12-373932-2.00052-1](https://doi.org/10.1016/B978-0-12-373932-2.00052-1). URL: <https://www.sciencedirect.com/science/article/pii/B9780123739322000521> (visited on 12/09/2023).
- [43] Adeline Schwein et al. “Endovascular Porcine Model of Iliocaval Venous Thrombosis”. en. In: *European Journal of Vascular and Endovascular Surgery* 63.4 (Apr. 2022), pp. 623–630. ISSN: 10785884. DOI: [10.1016/j.ejvs.2021.12.022](https://doi.org/10.1016/j.ejvs.2021.12.022). URL: <https://linkinghub.elsevier.com/retrieve/pii/S1078588421009758> (visited on 03/18/2024).
- [44] Aakash Shah et al. “Anatomical Differences Between Human and Pig Hearts and Their Relevance for Cardiac Xenotransplantation Surgical Technique”. In: *JACC Case Reports* 4.16 (July 2022), pp. 1049–1052. ISSN: 2666-0849. DOI: [10.1016/j.jaccas.2022.06.011](https://doi.org/10.1016/j.jaccas.2022.06.011). URL: <https://www.ncbi.nlm.nih.gov/pmc/articles/PMC9434648/> (visited on 02/25/2024).
- [45] Yubing Shi, Patricia Lawford, and D. Rodney Hose. “Construction of lumped-parameter cardiovascular models using the CellML language”. EN. In: *Journal of Medical Engineering & Technology* (Oct. 2018). Publisher: Taylor & Francis. ISSN:

0309-1902. URL: <https://www.tandfonline.com/doi/full/10.1080/03091902.2019.1576792> (visited on 03/12/2024).

- [46] Yubing Shi, Patricia Lawford, and Rodney Hose. “Review of Zero-D and 1-D Models of Blood Flow in the Cardiovascular System”. en. In: *BioMedical Engineering OnLine* 10.1 (Apr. 2011), p. 33. ISSN: 1475-925X. DOI: [10.1186/1475-925X-10-33](https://doi.org/10.1186/1475-925X-10-33). URL: <https://doi.org/10.1186/1475-925X-10-33> (visited on 12/13/2023).
- [47] David Sidebotham and Ian J. Le Grice. “Chapter 1 - Physiology and Pathophysiology”. In: *Cardiothoracic Critical Care*. Ed. by David Sidebotham et al. Philadelphia: Butterworth-Heinemann, Jan. 2007, pp. 3–27. ISBN: 978-0-7506-7572-7. DOI: [10.1016/B978-075067572-7.50004-7](https://doi.org/10.1016/B978-075067572-7.50004-7). URL: <https://www.sciencedirect.com/science/article/pii/B9780750675727500047> (visited on 12/18/2023).
- [48] Faiz Syed, Sahar Khan, and Milan Toma. “Modeling Dynamics of the Cardiovascular System Using Fluid-Structure Interaction Methods”. In: *Biology* 12.7 (July 2023), p. 1026. ISSN: 2079-7737. DOI: [10.3390/biology12071026](https://doi.org/10.3390/biology12071026). URL: <https://www.ncbi.nlm.nih.gov/pmc/articles/PMC10376821/> (visited on 04/01/2024).
- [49] *THE 17 GOALS / Sustainable Development*. URL: <https://sdgs.un.org/goals> (visited on 04/04/2024).
- [50] Bekhruz Tuychlev. *The Rise of the Julia Programming Language — Is it Worth Learning in 2023?* en. May 2023. URL: <https://www.datacamp.com/blog/the-rise-of-julia-is-it-worth-learning-in-2022> (visited on 03/13/2024).
- [51] *Vena Cava: Function and Anatomy*. en. URL: <https://my.clevelandclinic.org/health/body/22619-vena-cava> (visited on 03/25/2024).
- [52] Jeroen Walpot et al. “Left Ventricular Mid-Diastolic Wall Thickness: Normal Values for Coronary CT Angiography”. eng. In: *Radiology. Cardiothoracic Imaging* 1.5 (Dec. 2019), e190034. ISSN: 2638-6135. DOI: [10.1148/ryct.2019190034](https://doi.org/10.1148/ryct.2019190034).

- [53] Nico Westerhof, Jan-Willem Lankhaar, and Berend E. Westerhof. “The arterial Windkessel”. en. In: *Medical & Biological Engineering & Computing* 47.2 (Feb. 2009), pp. 131–141. ISSN: 1741-0444. DOI: [10.1007/s11517-008-0359-2](https://doi.org/10.1007/s11517-008-0359-2). URL: <https://doi.org/10.1007/s11517-008-0359-2> (visited on 12/10/2023).
- [54] *What Happened When a Baby Girl Got a Heart Transplant From a Baboon*. en. Oct. 2015. URL: <https://time.com/4086900/baby-fae-history/> (visited on 12/10/2023).
- [55] Markus J. Wilhelm et al. “Fiftieth anniversary of the first heart transplantation in Switzerland in the context of the worldwide history of heart transplantation”. en. In: *Swiss Medical Weekly* 150.0506 (Feb. 2020). Number: 0506, w20192–w20192. ISSN: 1424-3997. DOI: [10.4414/smw.2020.20192](https://doi.org/10.4414/smw.2020.20192). URL: <https://smw.ch/index.php/smw/article/view/2727> (visited on 02/25/2024).
- [56] L. Zheng and X. Zhang. “Chapter 8 - Numerical Methods”. In: *Modeling and Analysis of Modern Fluid Problems*. Ed. by Liancun Zheng and Xinxin Zhang. Mathematics in Science and Engineering. Academic Press, Jan. 2017, pp. 361–455. ISBN: 978-0-12-811753-8. DOI: [10.1016/B978-0-12-811753-8.00008-6](https://doi.org/10.1016/B978-0-12-811753-8.00008-6). URL: <https://www.sciencedirect.com/science/article/pii/B9780128117538000086> (visited on 03/01/2024).
- [57] Casper F. Zijderhand et al. “Batrial Versus Bicaval Orthotopic Heart Transplantation: A Systematic Review and Meta-Analysis”. eng. In: *The Annals of Thoracic Surgery* 110.2 (Aug. 2020), pp. 684–691. ISSN: 1552-6259. DOI: [10.1016/j.athoracsur.2019.12.048](https://doi.org/10.1016/j.athoracsur.2019.12.048).

# Appendices

---

APPENDIX

---

A

---

SUMMARY OF EQUATIONS

$$\sum I_{node} = 0 \quad (3.1)$$

$$\sum V_{loop} = 0 \quad (3.2)$$

$$R = \frac{8\mu l}{\pi r^4} \quad C = \frac{3\pi r^3 l}{2Eh} \quad L = \frac{\rho l}{\pi r^2} \quad (3.3)$$

$$P = P_0 + \frac{(V - V_0)}{C} \quad (3.4)$$

$$\frac{dV}{dt} = Q_{in} + Q_{out} \quad (3.5)$$

$$P = P_0 + E(t)(V - V_0) \quad (3.6)$$

$$\frac{dV}{dt} = Q_{in} + Q_{out} \quad (3.7)$$

$$E(t) = E_{min} + \frac{E_{max} - E_{min}}{2} e(t) \quad (3.8)$$

$$e(t) = \begin{cases} 1 - \cos\left(\frac{t}{T_{s1}}\pi\right) & 0 \leq t < T_{s1} \\ 1 - \cos\left(\frac{t - T_{s1}}{T_{s2} - T_{s1}}\pi\right) & T_{s1} \leq t < T_{s2} \\ 0 & T_{s2} \leq t < T \end{cases} \quad (3.9)$$

$$Q = \begin{cases} CQ\sqrt{-\Delta P} & \Delta P < 0 \\ 0 & \Delta P > 0 \end{cases} \quad (3.10)$$

$$CQ = C_d A \sqrt{\frac{2}{\rho(1 - \beta^4)}} \quad (3.11)$$

$$R_{sas,human} = \frac{8\mu l}{\pi} \frac{1}{r_{human}^4} \quad R_{sas,pig} = \frac{8\mu l}{\pi} \frac{1}{(\frac{r_{human}}{2})^4} \quad (3.12)$$

$$= \frac{8\mu l}{\pi} \frac{16}{r_{human}^4} \quad (3.13)$$

$$= 16 \times R_{sas,human} \quad (3.14)$$

---

APPENDIX

B

---

MODEL PARAMETERS USED TO DESCRIBE STANDARD  
HUMAN CIRCULATORY SYSTEM, BASED ON  
KORAKIANITIS AND SHI [24]

	$V_0$ ml	$P_0$ mmHg	$E_{min}$ mmHg/ml	$E_{max}$ mmHg/ml	$T_{s1}$ s	$T_{s2}$ s	$T_{shift}$ s
Left Ventricle (LV)	5	1	0.1	2.5	0.3	0.45	0
Right Ventricle (RV)	10	1	0.1	1.15	0.3	0.45	0
Left Atrium (LA)	4	1	0.15	0.25	0.045	0.09	0.92
Right Atrium (RA)	4	1	0.15	0.25	0.045	0.09	0.92

**Table B.1:** Parameters used to define heart chambers

	$CQ$ ml/(s mmHg $^{\frac{1}{2}}$ )
Mitral Valve (MV)	400
Tricuspid Valve (TV)	400
Aortic Valve (AV)	350
Pulmonary Valve (PV)	350

**Table B.2:** Parameters used to define heart valves

	$R$ mmHg s/ml	$C$ ml/mmHg	$L$ mmHg s $^2$ /ml
SAS	0.003	0.08	$6.2 \times 10^{-5}$
SAT	0.05	1.6	0.0017
SAR	0.5	-	-
SCP	0.52	-	-
SVN	0.075	20.5	-
PAS	0.002	0.18	$5.2 \times 10^{-5}$
PAT	0.01	3.8	0.0017
PAR	0.05	-	-
PCP	0.025	-	-
PVN	0.006	20.5	-

**Table B.3:** Parameters used to define systemic and pulmonary circulation

---

APPENDIX

C

---

ADDITIONAL GRAPHS FOR REFERENCE

**C.1 Pressure and flow in the right heart of the reference healthy human**

There are a number of events that occur in the right side of the heart during the cardiac cycle, numbered in Figure C.1 are detailed in Table C.1.

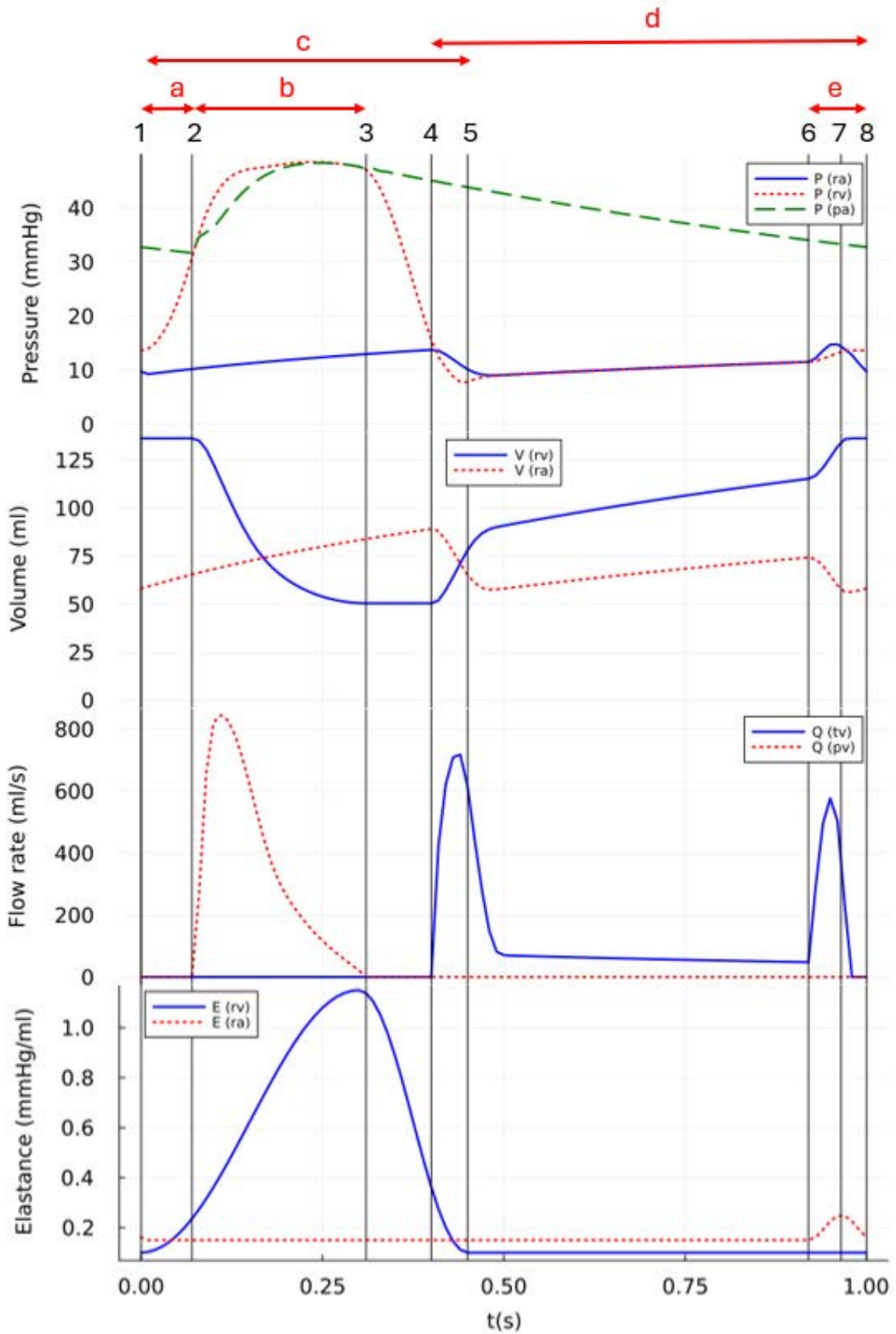


**Figure C.1:** Pressure and flow relationships in the right side of the heart.

Label	Event
1	Start of cardiac cycle, start of systolic phase
2	Pulmonary valve opens
3	Peak of systolic phase, pulmonary valve closes
4	Tricuspid valve opens
5	End of systolic phase
6	Start of atrial contraction
7	Peak of atrial contractions
8	End of atrial contraction, end of cardiac cycle

**Table C.1:** Events in the right side of the heart during cardiac cycle.

The right side of the heart has a number of different phases that occur between the different events detailed in Table C.1. These phases are labelled with letters in Figure C.1

Label	Phase
a	Pressure builds in the right ventricle as its elastance increases.
b	Blood is ejected from the right ventricle into the pulmonary artery, causing the volume in the right ventricle to drop.
c	Systolic phase, the part of the cycle where the ventricle elastance is above its minimum value i.e. the ventricle is “squeezing”.
d	Right ventricle fills with blood from the atrium via the tricuspid valve.
e	Contraction of the atrium.

**Table C.2:** Phases of the cardiac cycle, right side of heart.

Throughout the cardiac cycle, blood flows into the right atrium via the venae cavae at a relatively constant rate.

## C.2 Additional graphs for the investigation of porcine-to-human cardiac xenotransplantation

### C.2.1 Pressure curves

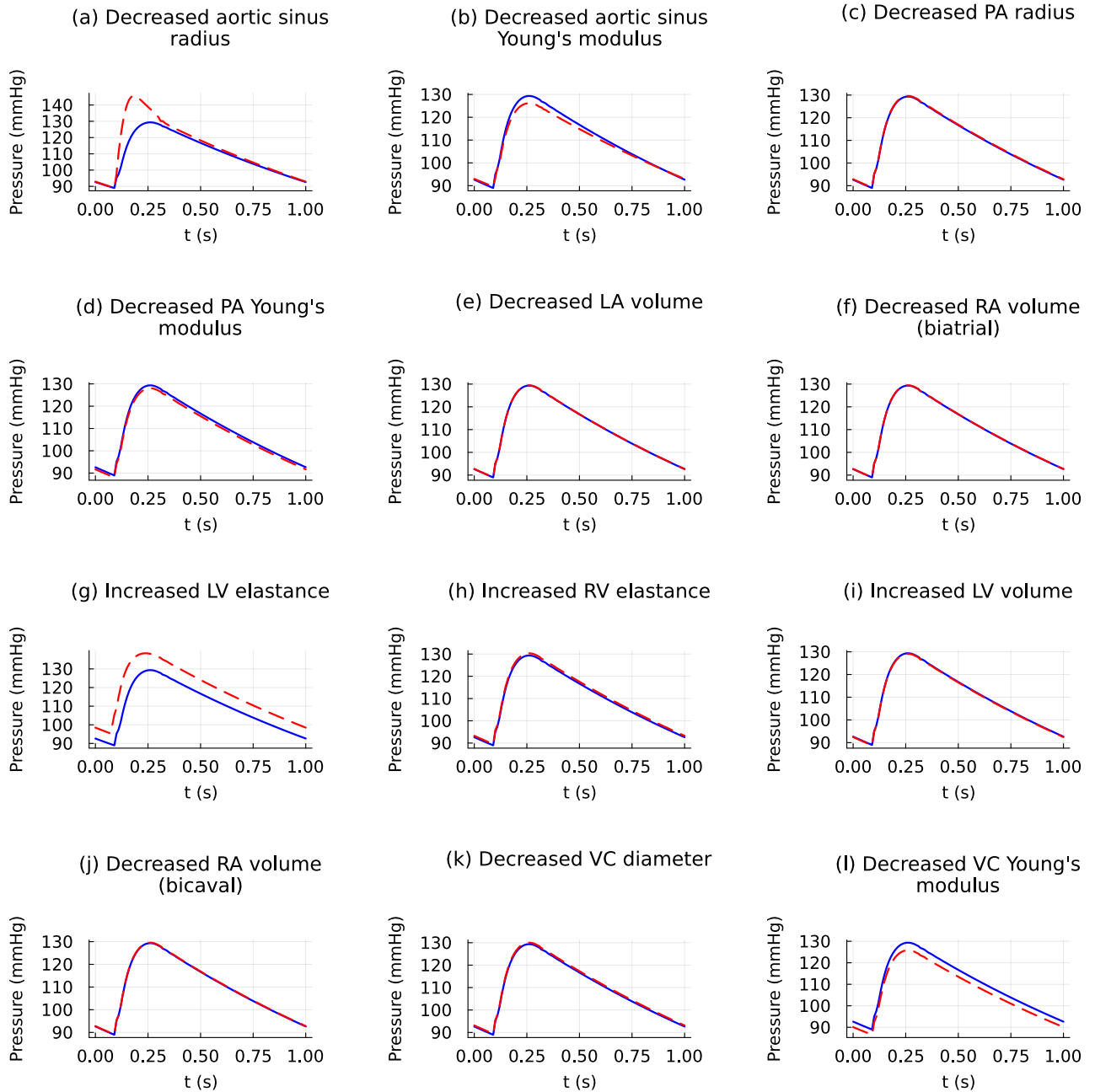


**Figure C.2:** Pressure in the aortic sinus of a reference healthy human (blue) and altered model (red).

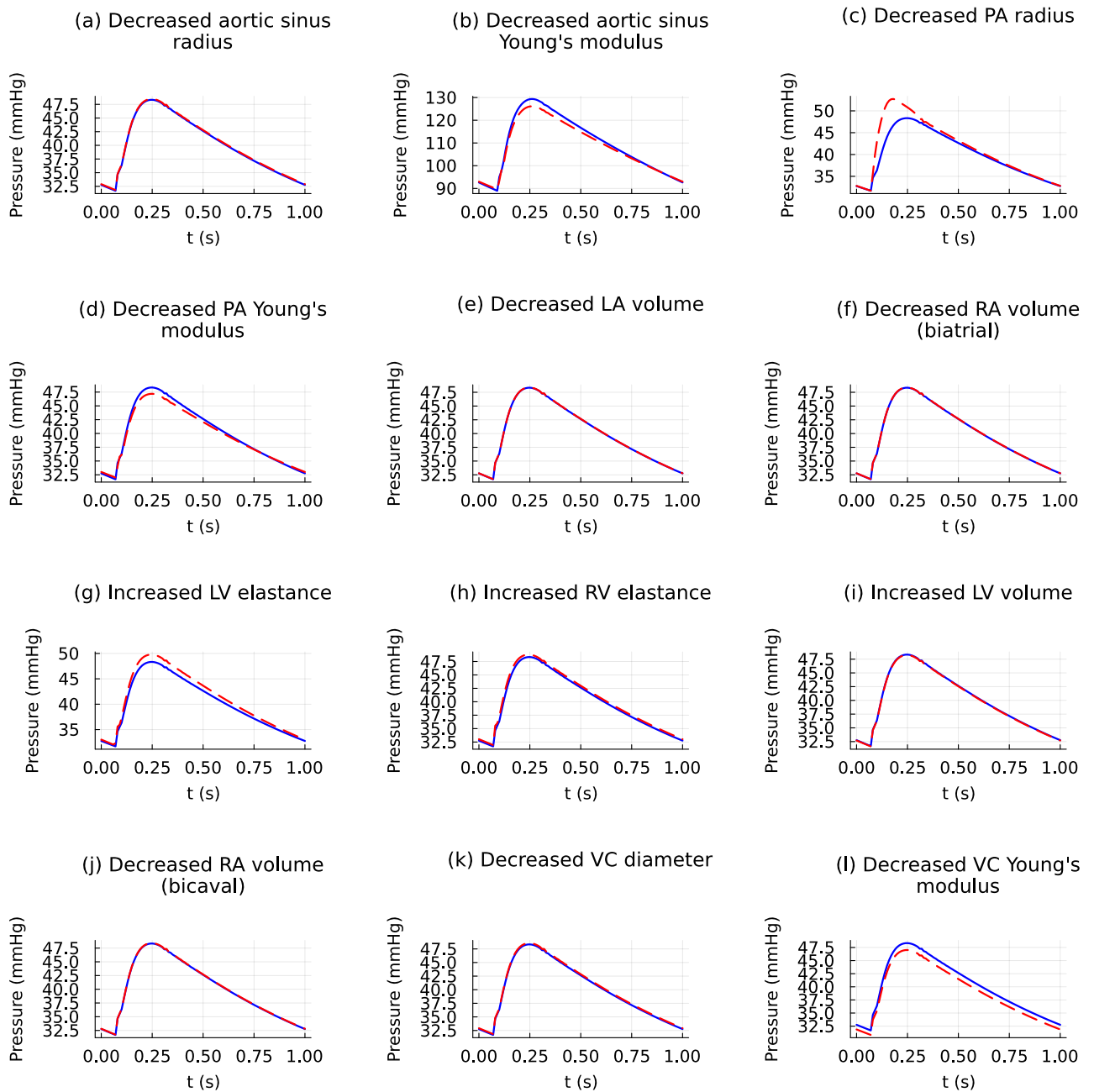


**Figure C.3:** Pressure in the pulmonary sinus of a reference healthy human (blue) and altered model (red).

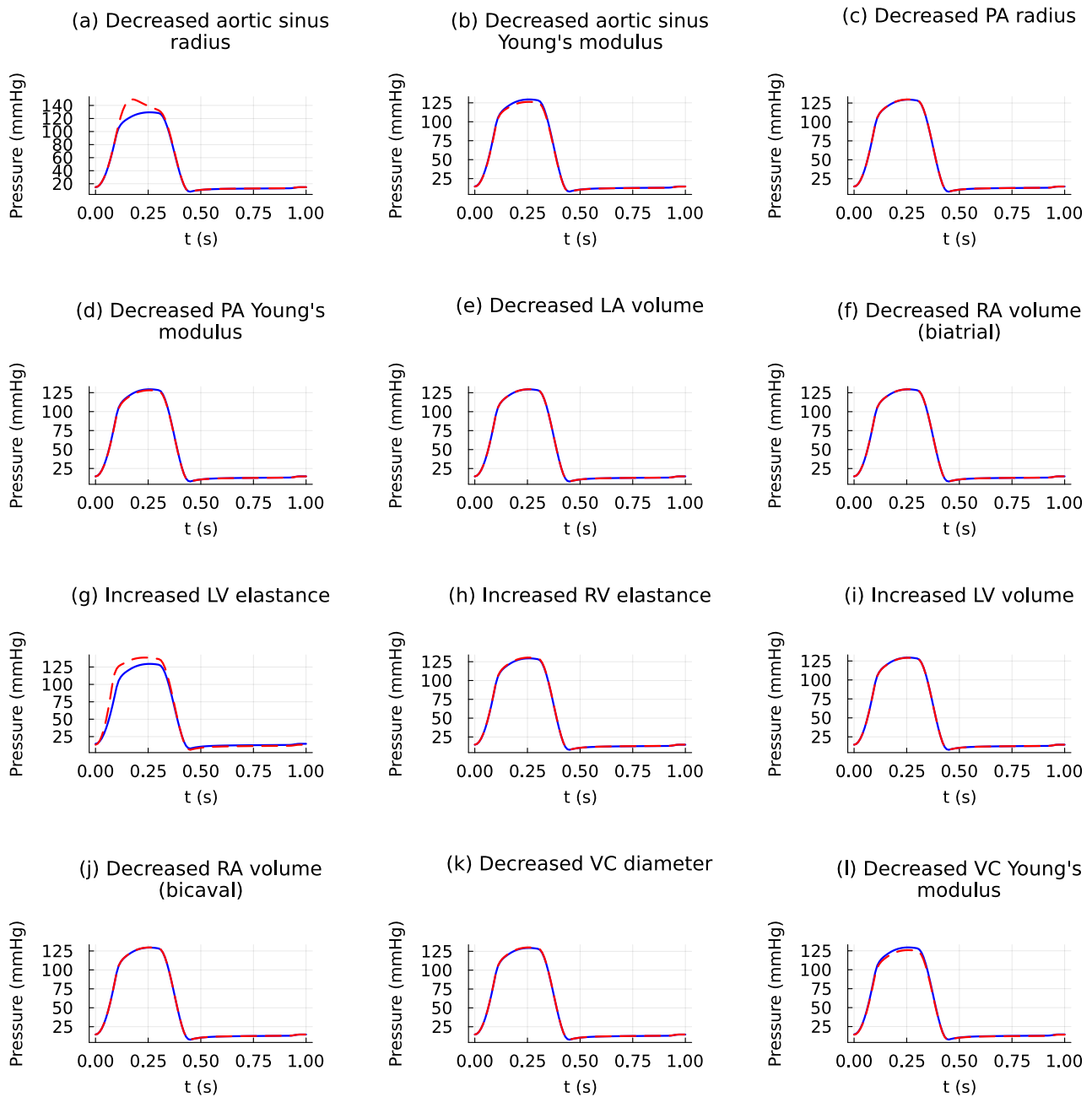


**Figure C.4:** Pressure in the left ventricle of a reference healthy human (blue) and altered model (red).

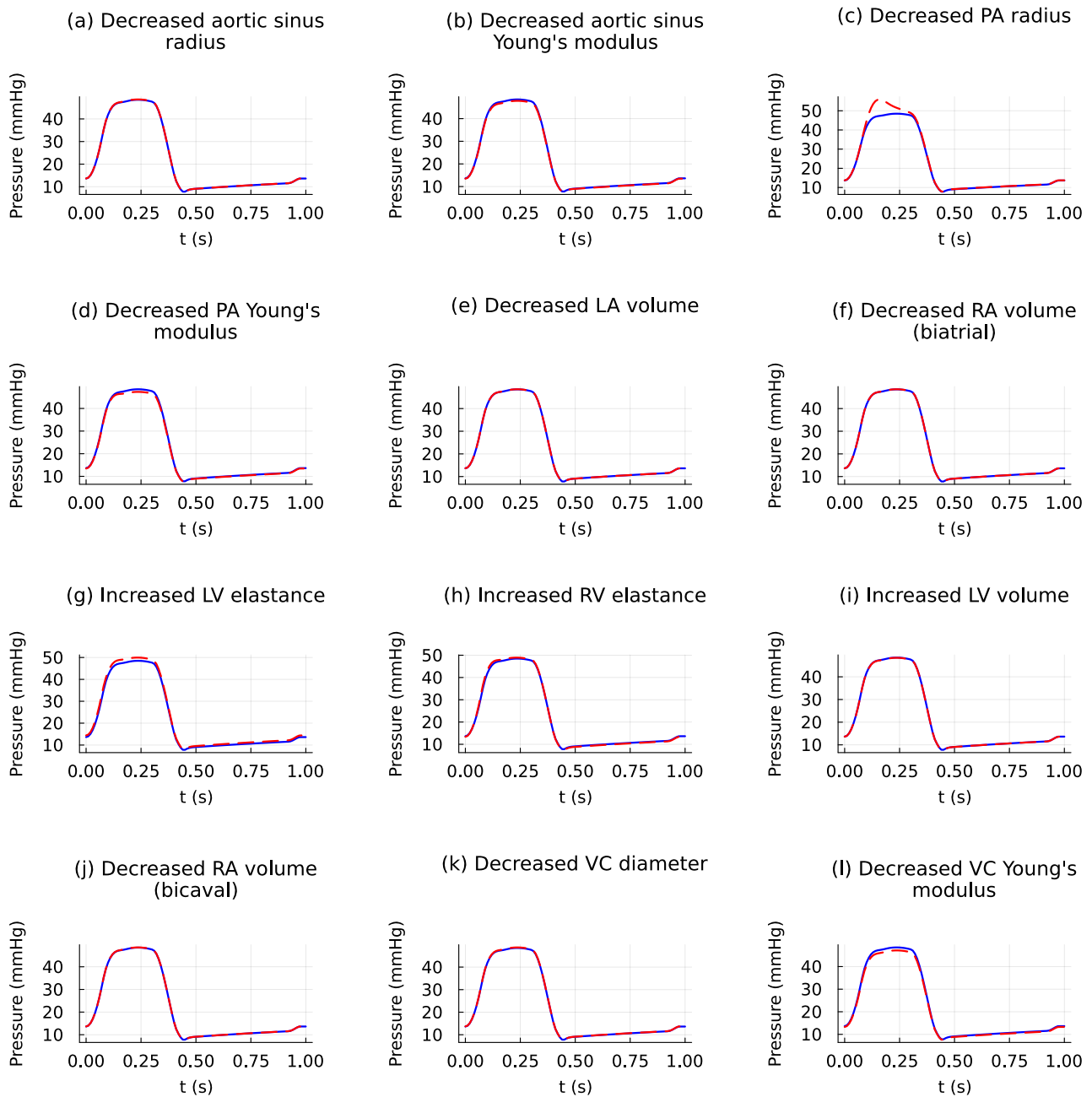


**Figure C.5:** Pressure in the right ventricle of a reference healthy human (blue) and altered model (red).

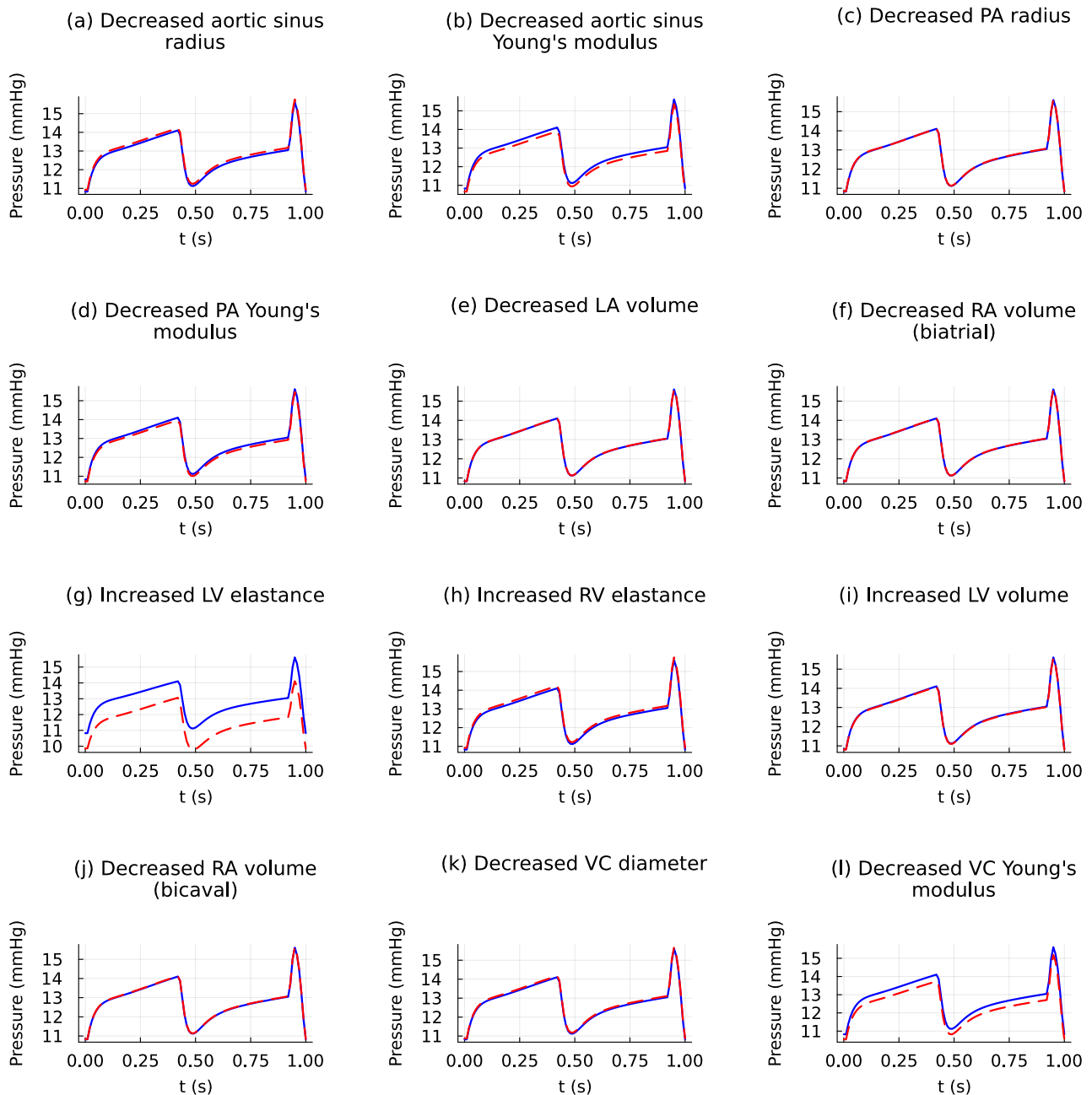


**Figure C.6:** Pressure in the left atrium of a reference healthy human (blue) and altered model (red).

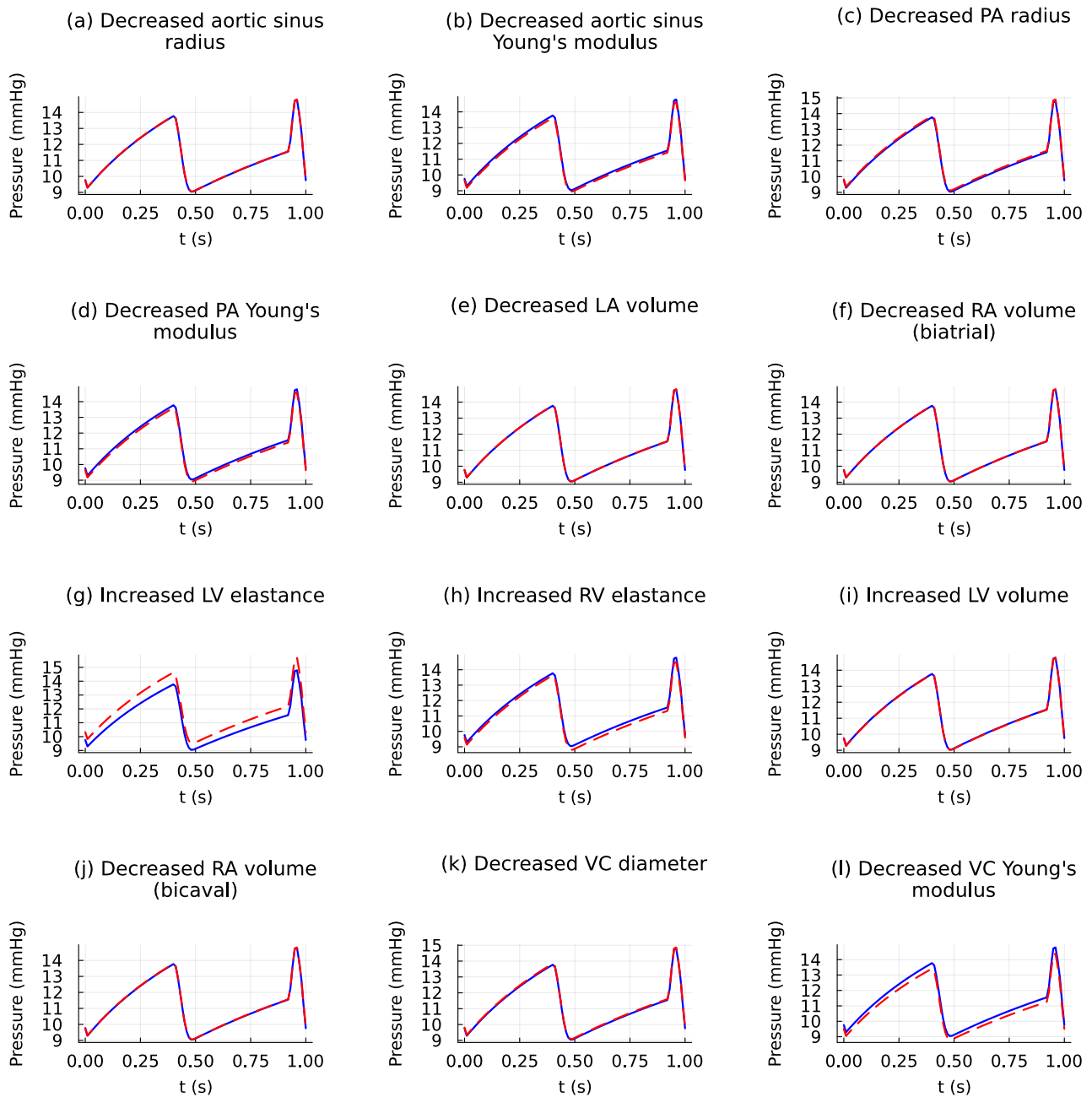


**Figure C.7:** Pressure in the right atrium of a reference healthy human (blue) and altered model (red).

## C.2.2 Volume curves

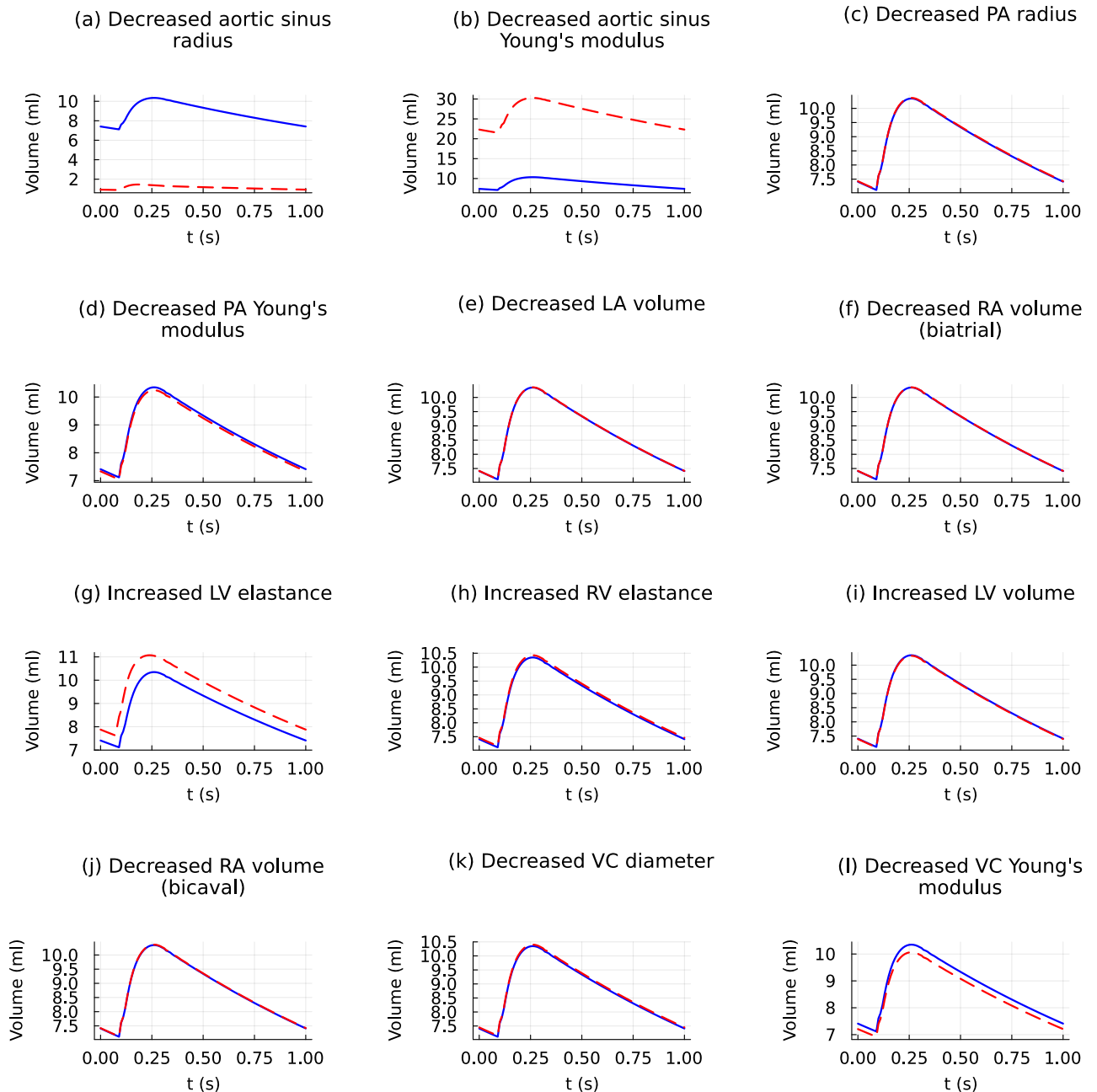


**Figure C.8:** Volume of blood in the aortic sinus of a reference healthy human (blue) and altered model (red).

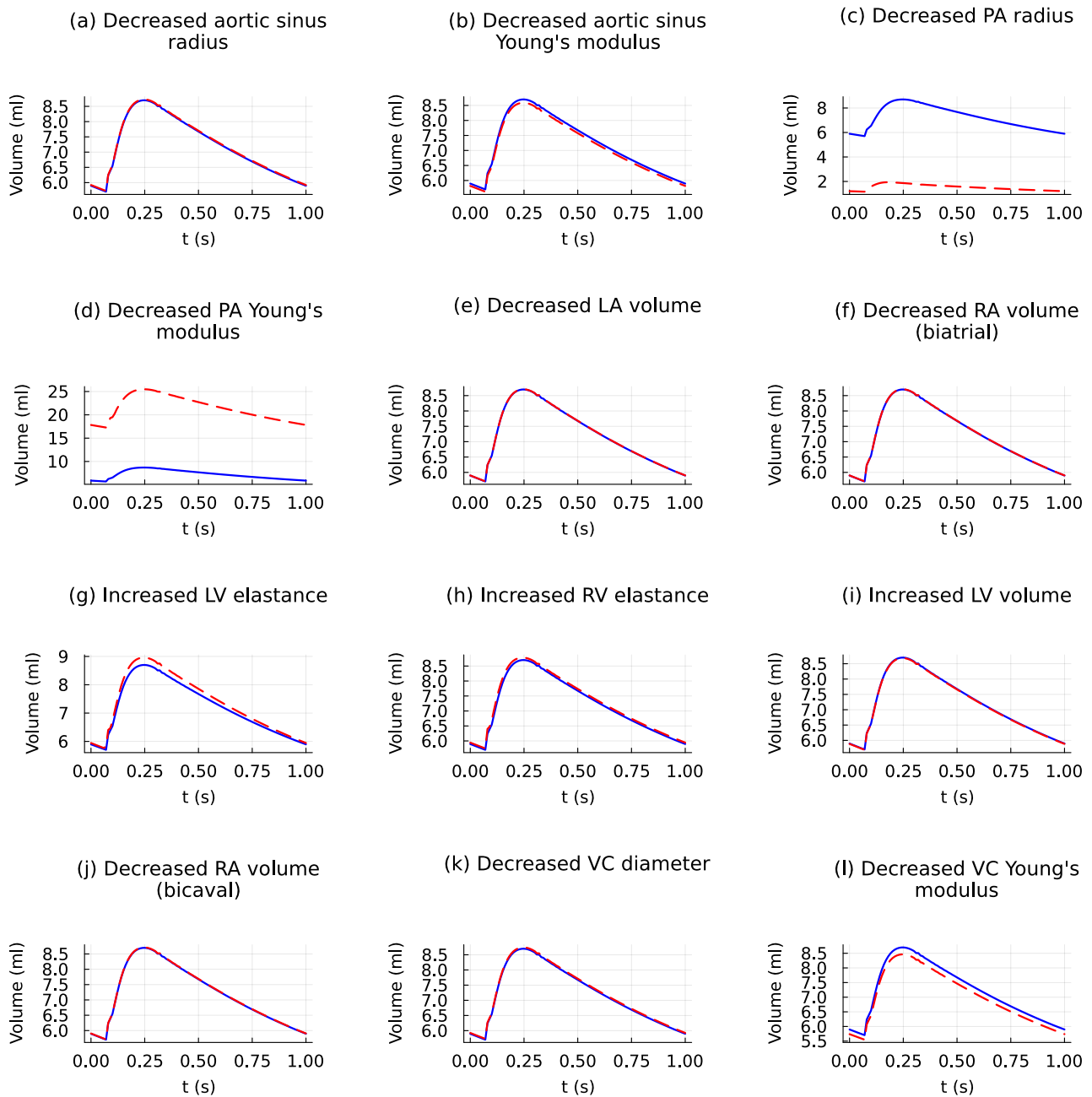


**Figure C.9:** Volume of blood in the pulmonary sinus of a reference healthy human (blue) and altered model (red).

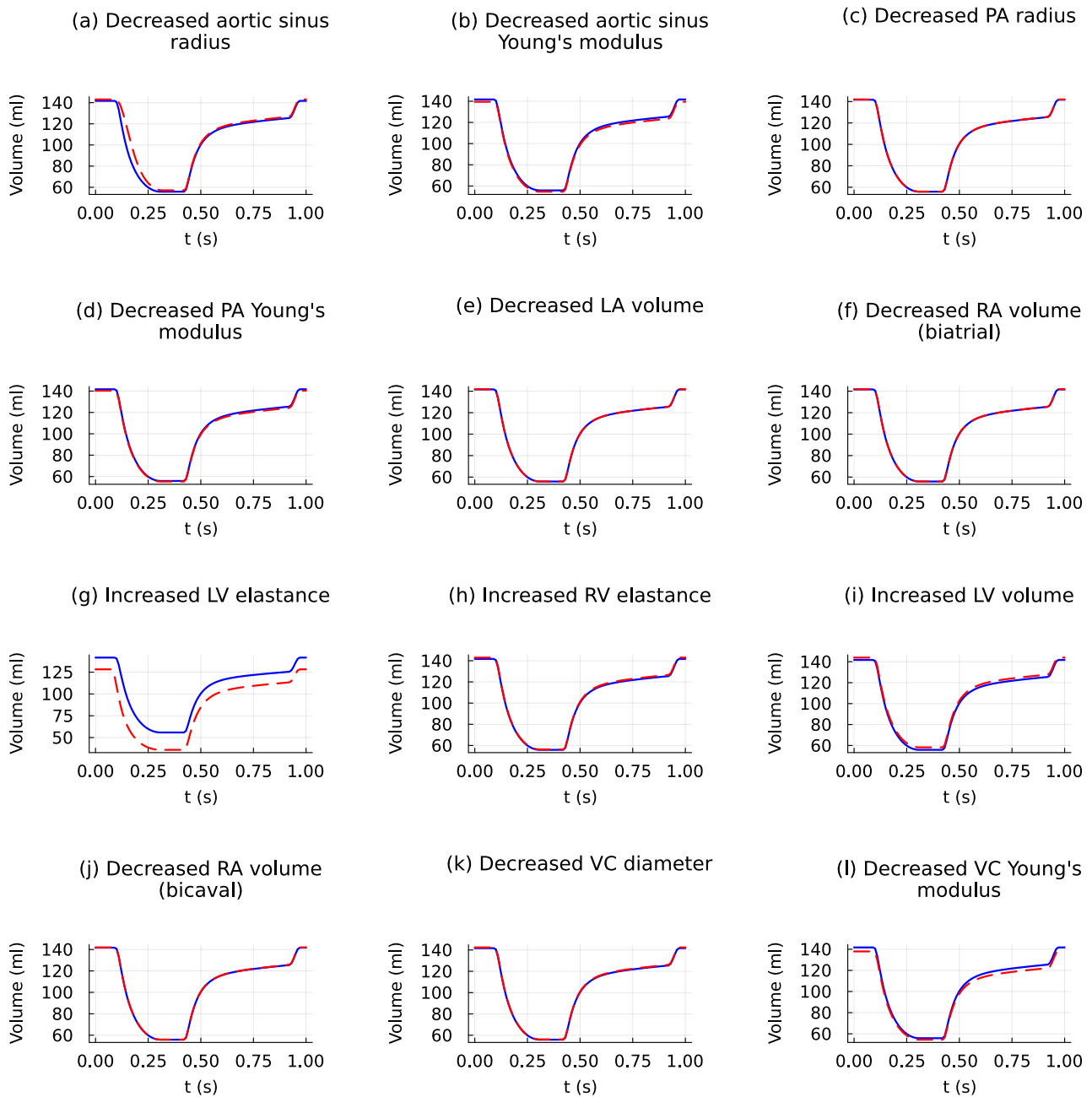


**Figure C.10:** Volume of blood in the left ventricle of a reference healthy human (blue) and altered model (red).

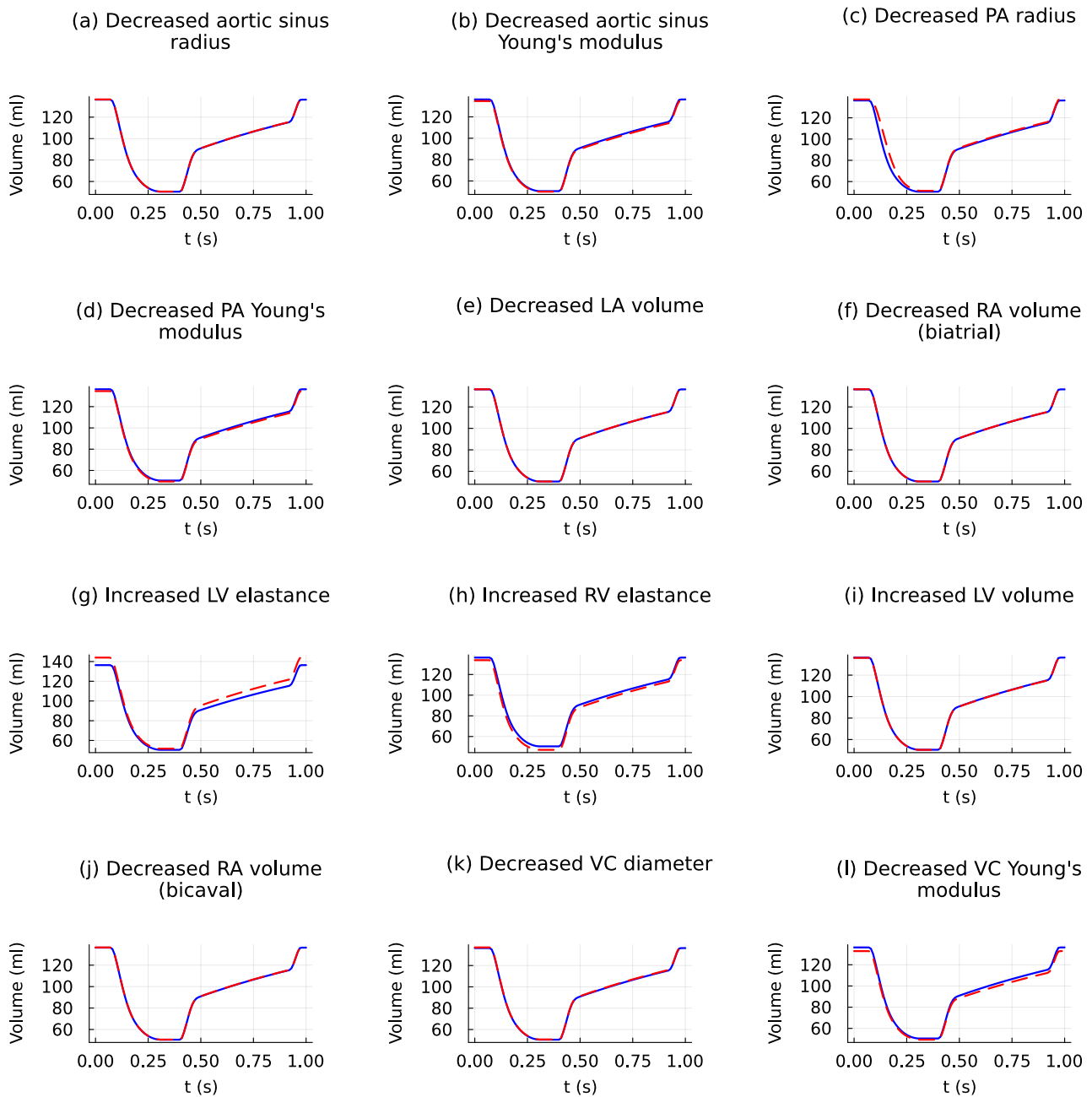


**Figure C.11:** Volume of blood in the right ventricle of a reference healthy human (blue) and altered model (red).

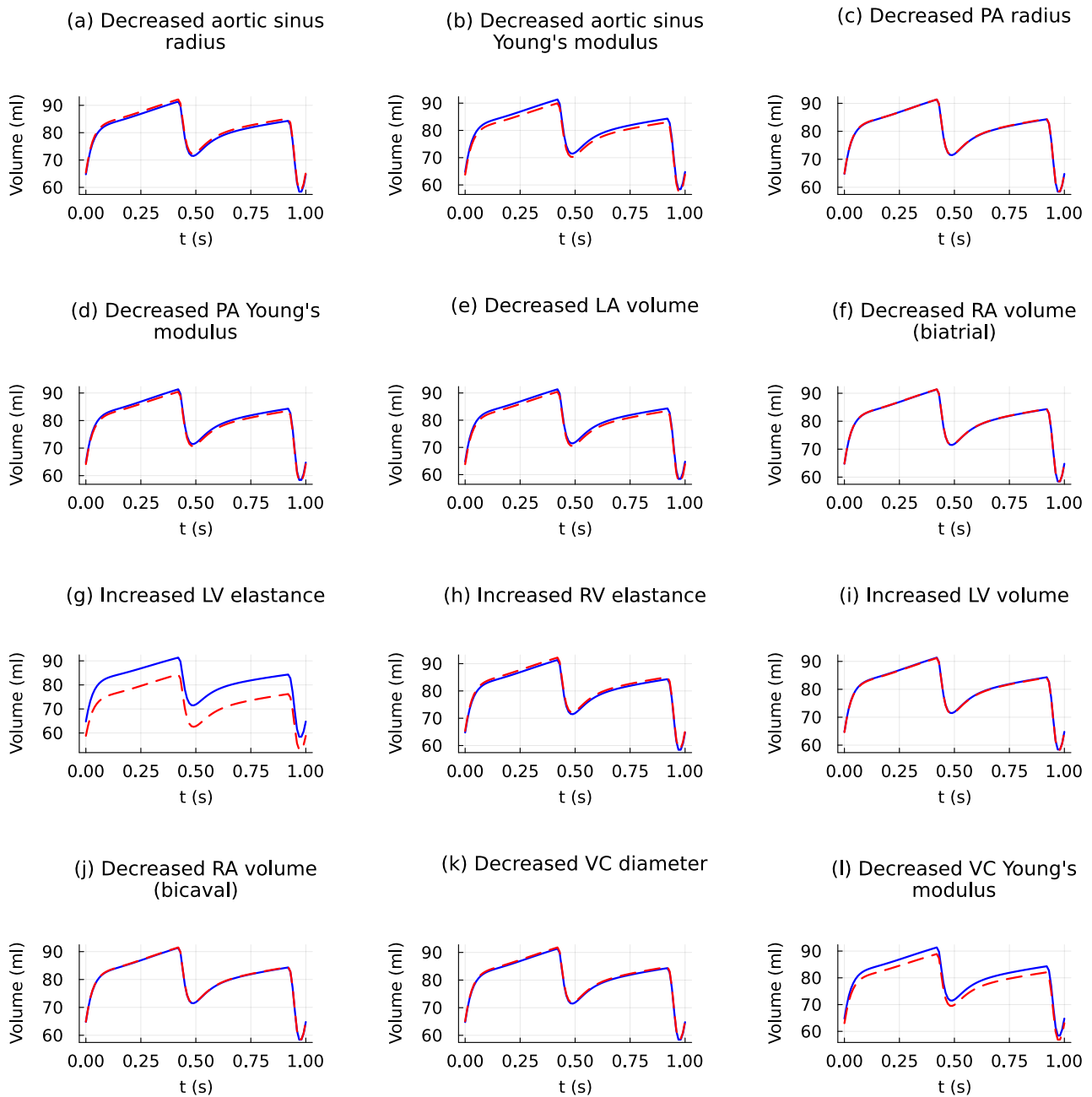


**Figure C.12:** Volume of blood in the left atrium of a reference healthy human (blue) and altered model (red).

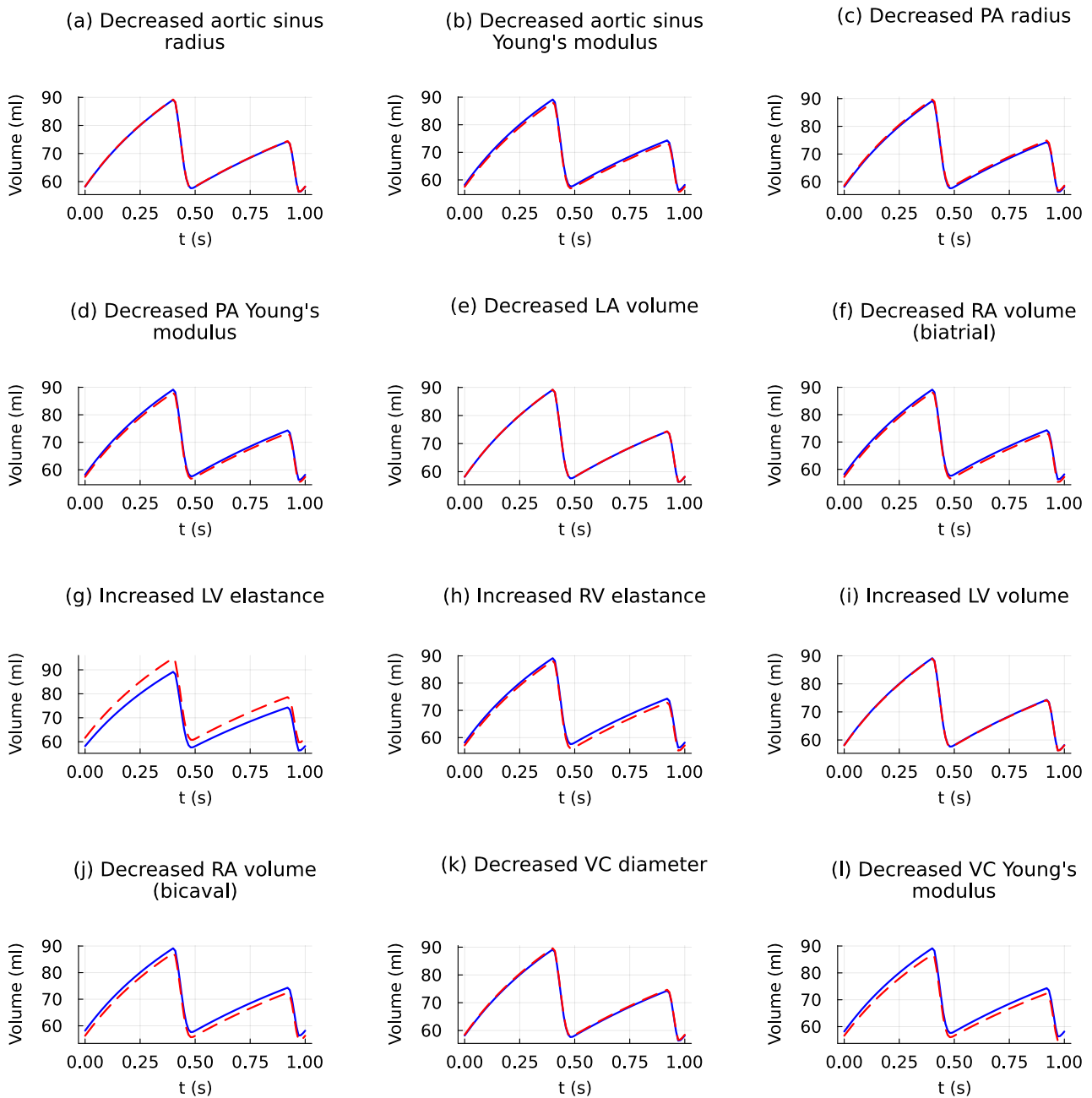


**Figure C.13:** Volume of blood in the right atrium of a reference healthy human (blue) and altered model (red).

### C.2.3 Pressure-Volume loops

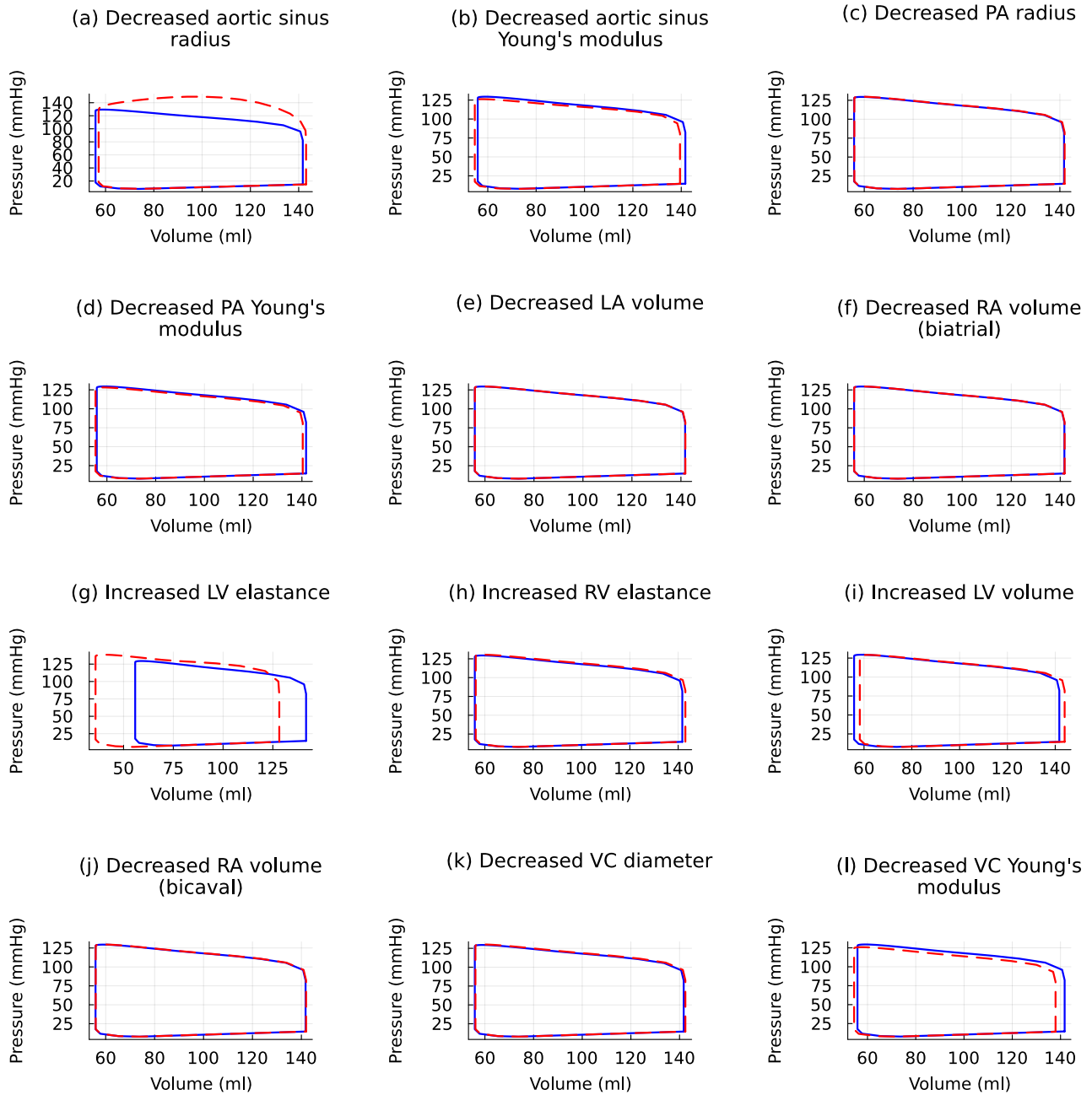


**Figure C.14:** PV loop of the left ventricle of a reference healthy human (blue) and altered model (red).

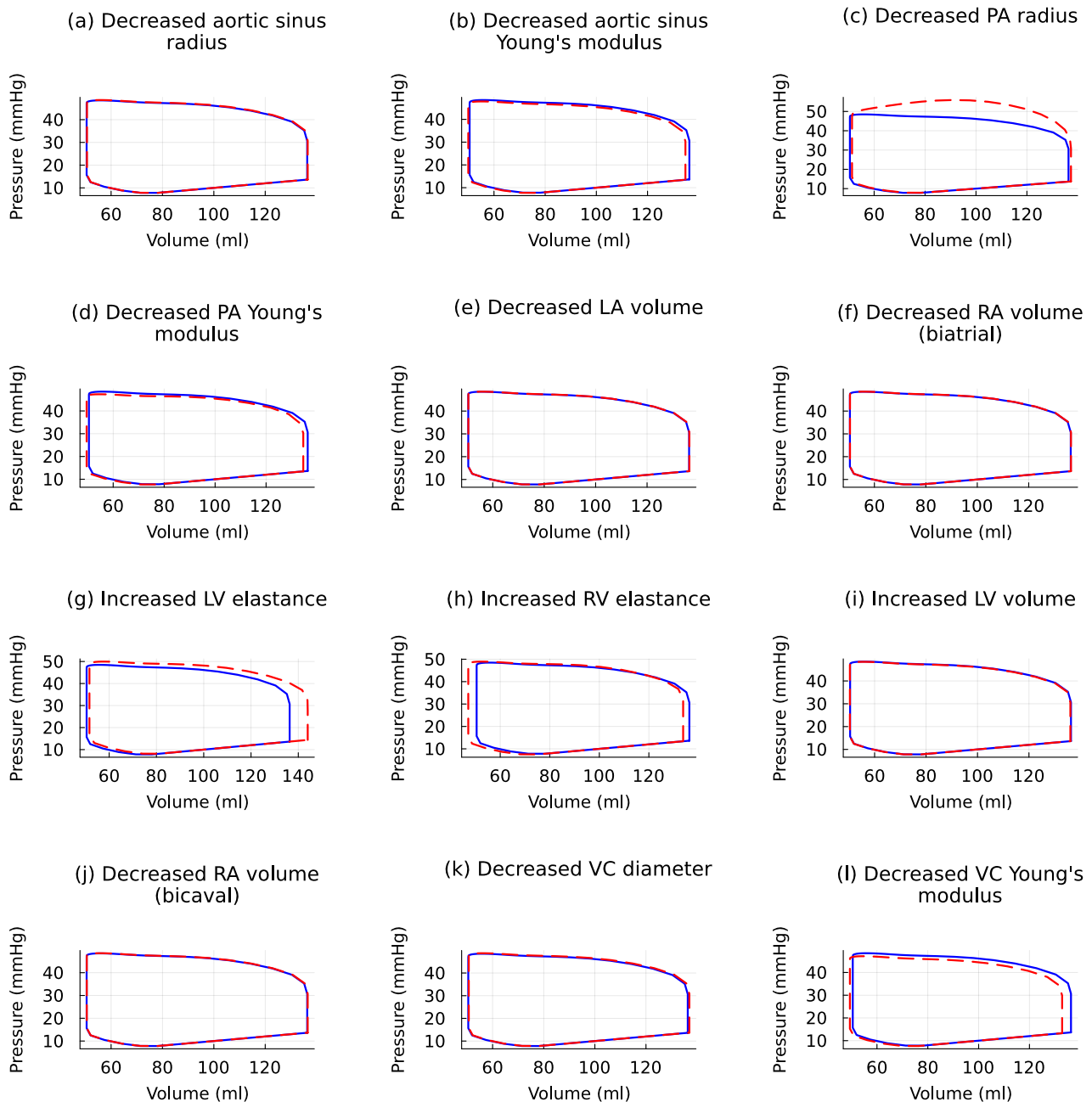


**Figure C.15:** PV loop of the right ventricle of a reference healthy human (blue) and altered model (red).

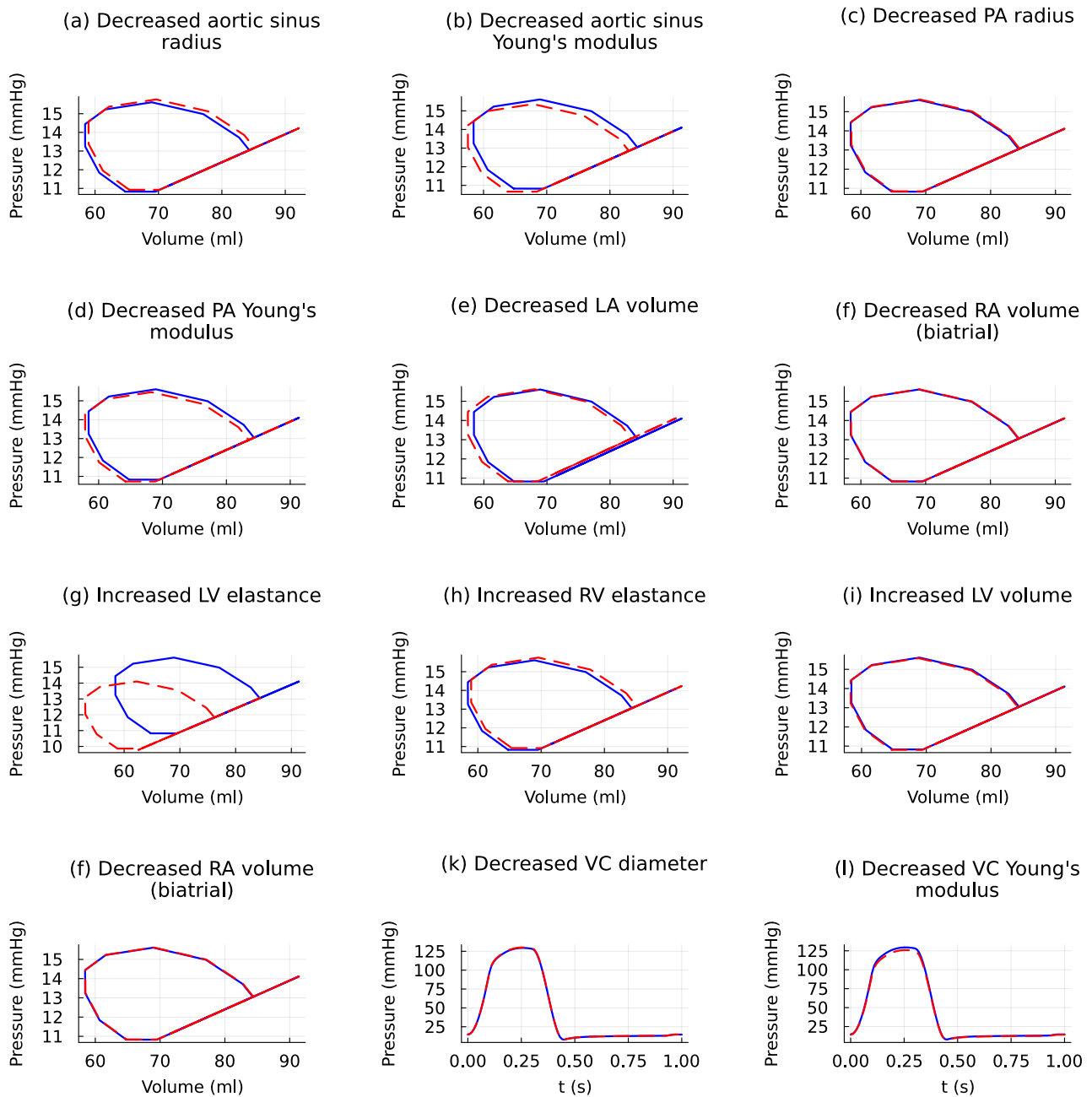


**Figure C.16:** PV loop of the left atrium of a reference healthy human (blue) and altered model (red).

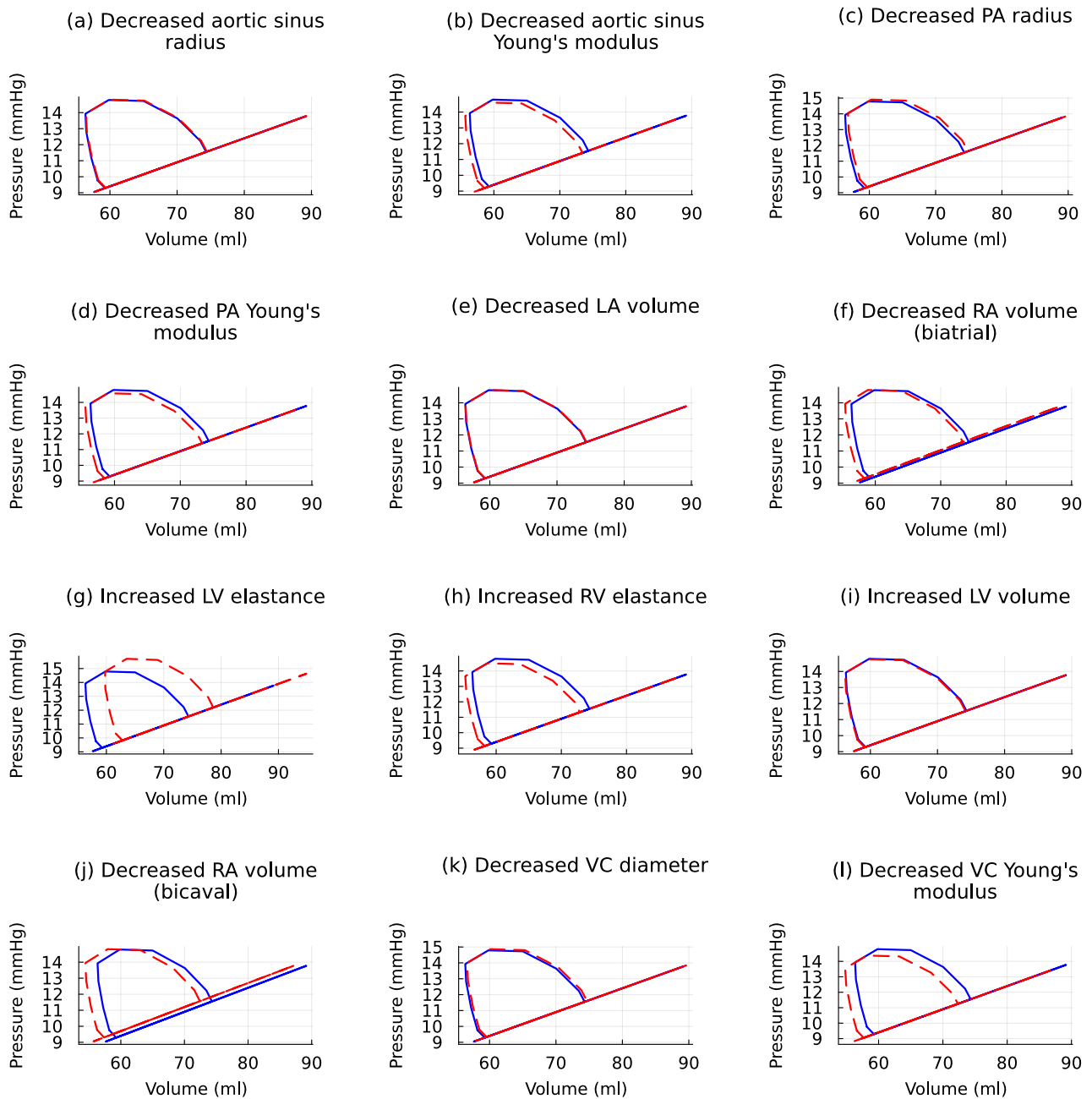


**Figure C.17:** PV loop of the right atrium of a reference healthy human (blue) and altered model (red).

---

## APPENDIX

---

# D

---

## CODE

### D.1 Comparison of Julia vs Python processing speed

#### D.1.1 Julia

```
1 using Printf  
2  
3 C = 1.1  
4 R = 0.9  
5 A = 1e-4  
6 B = 60/72  
7 r = 0.01  
8 L = 0.002  
9  
10 #####  
11 # RUNGE-KUTTA FUNCTION #  
12 #####  
13  
14 """  
15 runge_kutta_4o(h,t0,tn,y0,func)
```

```

17 Performs the fourth-order Runge-Kutta method for solving first order
18 differential equations.

19
20     Inputs:
21     h   Step size
22     t0  Initial condition time value
23     tn  Final time
24     y0  Initial condition y value

25
26     Returns:
27     t   Vector of values of t for which y is calculated
28     y   Vector of values of y
29 """
30
31
32     function runge_kutta_4o(h,t0,tn,y0,func)
33
34
35         t = [convert(Float64,t0)]
36         y = [convert(Float64,y0)]
37
38         n = floor(Int,((tn-t0)/h))
39
40         for i in range(1,n)
41             k1 = h*func(t[i], y[i])
42             k2 = h*func((t[i]+0.5*h),(y[i]+0.5*k1))
43             k3 = h*func((t[i]+0.5*h),(y[i]+0.5*k2))
44             k4 = h*func((t[i]+h),(y[i]+k3))
45
46             y_n = y[i] + (1/6) * (k1 + 2*k2 + 2*k3 + k4)
47             append!(t, t[i]+h)
48             append!(y,y_n)
49         end
50
51
52         return t,y
53     end

```

```

51 #####
52 # BLOODFLOW FUNCTION AND DERIVATIVES #
53 #####
54
55 function flow(t)
56     return A*sin(2*pi*t/(B)-pi/2)+A
57 end
58
59 function flow_dot(t)
60     return (2*A*pi/(B))*cos(2*pi*t/(B)-pi/2)
61 end
62
63 function flow_dotdot(t)
64     return -(4*A*(pi^2)/((B)^2))*sin(2*pi*t/(B)-pi/2)
65 end
66
67 #####
68 # WINDKESSEL PRESSURE FUNCTIONS #
69 #####
70
71 function pressure_2_element(t,P)
72     return flow(t)/C - P/(C*R)
73 end
74
75 function pressure_3_element(t,P)
76     I = flow(t)
77     Idot = flow_dot(t)
78     return (I/C)*(1+r/R) + r*Idot - P/(R*C)
79 end
80
81 function pressure_4_element(t,P)
82     I = flow(t)
83     Idot = flow_dot(t)
84     Idotdot = flow_dotdot(t)

```

```

85     return L*Idotdot + (L/(C*R)+r)*Idot + (1/C+r/(R*C))*I - P/(C*R)
86 end
87
88 #####
89 # SOLVING #
90 #####
91
92 h = 0.01
93 t0 = 0
94 tn = 3000
95 p0 = 78
96
97 start = time()
98 t_rk,P_rk = runge_kutta_4o(h, t0, tn, p0, pressure_2_element);
99 fin = time()
100 @sprintf("Time elapsed: %f", fin-start)
101
102 start = time()
103 t_rk,P_rk = runge_kutta_4o(h, t0, tn, p0, pressure_3_element);
104 fin = time()
105 @sprintf("Time elapsed: %f", fin-start)
106
107 start = time()
108 t_rk,P_rk = runge_kutta_4o(h, t0, tn, p0, pressure_4_element);
109 fin = time()
110 @sprintf("Time elapsed: %f", fin-start)

```

## D.1.2 Python

```

1 import time
2 import math
3 import numpy as np
4
5 C = 1.1
6 R = 0.9

```

```

7 A = 90
8 B = 1
9 r = 0.05
10 L = 0.004
11
12 #####
13 # RUNGE-KUTTA FUNCTION #
14 #####
15
16 def runge_kutta(h, t0, tn, y0, func):
17     """
18         runge_kutta_4o(h,t0,tn,y0,func)
19
20     Performs the fourth-order Runge-Kutta method for solving first order differential eqns
21
22     Inputs:
23         h      Step size
24         t0    Initial condition time value
25         tn    Final time
26         y0    Initial condition y value
27
28     Returns:
29         t      Vector of values of t for which y is calculated
30         y      Vector of values of y
31     """
32
33     t = [t0]
34     y = [y0]
35
36     n = math.floor((tn-t0)/h)
37
38     for i in range(0,n):
39         k1 = h*func(t[i], y[i])
40         k2 = h*func((t[i]+0.5*h),(y[i]+0.5*k1))

```

```

41     k3 = h*func((t[i]+0.5*h),(y[i]+0.5*k2))
42     k4 = h*func((t[i]+h),(y[i]+k3))
43
44     y_n = y[i] + (1/6) * (k1 + 2*k2 + 2*k3 + k4)
45     t.append(t[i]+h)
46     y.append(y_n)
47
48     return t,y
49
50 #####
51 # BLOODFLOW FUNCTION AND DERIVATIVES #
52 #####
53
54 def bloodflow(t):
55     return A*np.sin((2*np.pi*t/B)-(np.pi/2))+A
56
57 def bloodflow_dot(t):
58     return (2*A*np.pi/B)*np.cos((2*np.pi*t/B)-(np.pi/2))
59
60 def bloodflow_dotdot(t):
61     return -(4*A*(np.pi**2)/(B**2))*np.sin((2*np.pi*t/B)-np.pi/2)
62
63 #####
64 # WINDKESSEL PRESSURE FUNCTIONS #
65 #####
66
67 def pressure_2_element(t,P):
68     return bloodflow(t)/C -P/(C*R)
69
70 def pressure_3_element(t,P):
71     q = bloodflow(t)
72     qdot = bloodflow_dot(t)
73     return (q/C)*(1+r/R) + r*qdot - P/(R*C)
74

```

```

75 def pressure_4_element(t,P):
76     q = bloodflow(t)
77     qdot = bloodflow_dot(t)
78     qdotdot = bloodflow_dotdot(t)
79     return L*qdotdot + (L/(C*R)+r)*qdot + (1/C+r/(R*C))*q - P/(C*R)
80
81 #####
82 # SOLVING #
83 #####
84
85 h = 0.01
86 t0 = 0
87 tn = 3000
88 p0 = 78
89
90 start = time.time()
91 t,y = runge_kutta(h, t0, tn, p0, pressure_2_element)
92 end = time.time()
93 print('Time elapsed: {:.4f}'.format(end-start))
94
95 start = time.time()
96 t,y = runge_kutta(h, t0, tn, p0, pressure_3_element)
97 end = time.time()
98 print('Time elapsed: {:.4f}'.format(end-start))
99
100 start = time.time()
101 t,y = runge_kutta(h, t0, tn, p0, pressure_4_element)
102 end = time.time()
103 print('Time elapsed: {:.4f}'.format(end-start))

```

## D.2 circulatory\_system\_components.jl

```
1  using ModelingToolkit
2  using DifferentialEquations
3
4  export Pin, Ground, OnePort, Resistor, Capacitor, Compliance, Inductance,
5      DrivenFlow, HeartChamber, HeartValve, CRL, CR
6
7  @variables t
8  D = Differential(t)
9
10 """
11 Pin(; name)
12
13 Defines a node, at which pressure and flow rate is continuous
14 """
15 @connector function Pin(; name)
16     sts = @variables p(t) = 1.0 q(t) = 1.0 [connect = Flow]
17     ODESSystem(Equation[], t, sts, []; name=name)
18 end
19
20 """
21 Ground(; name)
22
23 Defines the ground node, or a reference node. Pressure defaults to zero.
24 """
25 @component function Ground(; name, P=0.0)
26     @named g = Pin()
27     ps = @parameters P = P
28     eqs = [g.p ~ P]
29     compose(ODESystem(eqs, t, [], ps; name=name), g)
30 end
31
32 """
33 OnePort(; name)
```

```

34
35 Defines a generic 'electrical' element by applying Kirchhoff's circuit
36 laws.
37
38 Parameters calculated:
39 del_p Pressure drop across element (mmHg)
40 q Blood flow through element (ml/s)
41 """
42 @component function OnePort(; name)
43     @named in = Pin()
44     @named out = Pin()
45     sts = @variables del_p(t) = 0.0 q(t) = 0.0
46     eqs = [
47         del_p ~ out.p - in.p
48         0 ~ in.q + out.q
49         q ~ in.q
50     ]
51     compose(ODESystem(eqs, t, sts, []; name=name), in, out)
52 end
53 """
54
55 Resistor(; name, R=1.0)
56
57 Defines a resistor by applying Ohm's law to a generic element.
58
59 Arguments:
60 R Resistance of blood vessel (mmHg*s/ml)
61
62 Parameters calculated:
63 del_p Pressure drop across resistance element (mmHg)
64 q Blood flow through resistance element (ml/s)
65 """
66 @component function Resistor(; name, R=1.0)
67     @named oneport = OnePort()

```

```

68 @unpack del_p, q = oneport
69 ps = @parameters R = R
70 eqs = [
71     del_p ~ -q * R
72 ]
73 extend(ODESystem(eqs, t, [], ps; name=name), oneport)
74 end
75
76 """
77 Compliance(; name, V_0=0.0, C=1.0, p_0=0.0)
78
79 Defines a compliant vessel.
80
81 Arguments:
82 V_0      Stress-free (zero pressure) volume (ml)
83 C        Compliance of blood vessel (ml/mmHg)
84 p_0      Offset pressure value (mmHg)
85
86 Parameters calculated:
87 p        Pressure in compliance vessel (mmHg)
88 V        Volume in compliance vessel (ml)
89 """
90 @component function Compliance(; name, V_0=0.0, C=1.0, p_0=0.0)
91     @named in = Pin()
92     @named out = Pin()
93
94     sts = @variables begin
95         V(t) = V_0
96         p(t) = 0.0
97     end
98
99     ps = @parameters begin
100        V_0 = V_0
101        C = C

```

```

102     p_rel = p_θ
103
104
105     D = Differential(t)
106
107     eqs = [
108         θ ~ in.p - out.p
109         p ~ in.p
110         p ~ ((V - V_θ) / C) + p_rel
111         D(V) ~ in.q + out.q
112     ]
113
114     compose(ODESystem(eqs, t, sts, ps; name=name), in, out)
115 end
116
117 """
118 Inductance(; name, L=1.0)
119
120 Defines a capacitor by applying the inductors's pressure-flow
121 relationship to a generic element to represent inertia.
122
123 Arguments:
124 L           Inductance of blood vessel (mmHg*s^2/ml)
125
126 Parameters calculated:
127 del_p        Pressure drop across capacitance element (mmHg)
128 q            Blood flow through capacitance element (ml/s)
129 """
130 @component function Inductance(; name, L=1.0)
131     @named oneport = OnePort()
132     @unpack del_p, q = oneport
133     ps = @parameters L = L
134     D = Differential(t)
135     eqs = [

```

```

136     D(q) ~ -del_p / L
137   ]
138   extend(ODESystem(eqs, t, [], ps; name=name), oneport)
139 end
140
141 """
142 DrivenFlow(; name, Q=1.0)
143
144 Defines a blood flow source.
145
146 Arguments:
147 Q      Magnitude of blood flow (ml/s)
148
149 Parameters calculated:
150 q      Blood flow through source element (ml/s)
151 """
152 @component function DrivenFlow(; name, Q=1.0)
153   @named oneport = OnePort()
154   @unpack q = oneport
155   ps = @parameters Q = Q
156   eqs = [
157     q ~ Q * flow(t)
158   ]
159   extend(ODESystem(eqs, t, [], ps; name=name), oneport)
160 end
161
162 """
163 HeartChamber(; name, V_0, p_0, E_min, E_max, T, T_es, T_ep, Eshift=0.0)
164
165 Defines a chamber of the heart
166
167 Arguments:
168 V_0          Stress-free (zero pressure) volume (ml)
169 p_0          Pressure offset value (mmHg)

```

```

170 E_min           Minimum elastance (mmHg/ml)
171 E_max           Maximum elastance (mmHg/ml)
172 T               Period of cardiac cycle (s)
173 T_es            End systolic time (s)
174 T_ep            Peak systolic time (s)
175 Eshift          Time shift of contraction (s)

176
177 Parameters calculated:
178 p                Pressure in chamber (mmHg)
179 V                Volume in chamber (ml)
180 """
181 @component function HeartChamber(; name, V_0, p_0, E_min, E_max, T, T_es,
182 T_ep, Eshift=0.0)
183
184     @named in = Pin()
185     @named out = Pin()
186     sts = @variables V(t) = 0.0 p(t) = 0.0
187     ps = @parameters (V_0 = V_0, p_0 = p_0, E_min = E_min, E_max = E_max,
188                         T = T, T_es = T_es, T_ep = T_ep, Eshift = Eshift)
189
190     D = Differential(t)
191     E = Elastance(t, E_min, E_max, T, T_es, T_ep, Eshift)
192
193     p_rel = p_0
194
195     eqs = [
196         0 ~ in.p - out.p
197         p ~ in.p
198         p ~ ((V - V_0) * E) + p_rel
199         D(V) ~ in.q + out.q
200     ]
201
202     compose(ODESystem(eqs, t, sts, ps; name=name), in, out)
203 end

```

```

204
205 """
206 HeartValve(; name, CQ=1.0)
207
208 Defines the heart valves as orifice valves
209
210 Arguments:
211 CQ Flow coefficient (ml/(s*mmHg^0.5))
212
213 Parameters calculated:
214 del_p Pressure drop across capacitance element (mmHg)
215 q Blood flow through capacitance element (ml/s)
216 """
217 @component function HeartValve(; name, CQ=1.0)
218     @named oneport = OnePort()
219     @unpack del_p, q = oneport
220     ps = @parameters CQ = CQ
221     eqs = [
222         q ~ (del_p < 0) * CQ * sqrt(abs(del_p))
223     ]
224     extend(ODESystem(eqs, t, [], ps; name=name), oneport)
225 end
226
227 """
228 CRL(; name, C=1.0, R=1.0, L=1.0)
229
230 Defines compliace, resistor, inductance subsystem
231
232 Arguments:
233 C Blood vessel compliace (ml/mmHg)
234 R Blood vessel resistance (mmHg*s/ml)
235 L Blood vessel inductance (mmHg*s^2/ml)
236
237 Parameters calculated:

```

```

238 del_p Pressure drop across subsystem (mmHg)
239 q Blood flow through subsystem element (ml/s)
240 """
241 @component function CRL(; name, C=1.0, R=1.0, L=1.0)
242     @named in = Pin()
243     @named out = Pin()
244
245     sts = @variables del_p(t) = 0.0 q(t) = 0.0
246     ps = []
247
248     @named C = Compliance(C=C)
249     @named R = Resistor(R=R)
250     @named L = Inductance(L=L)
251
252     eqs = [
253         del_p ~ out.p - in.p
254         q ~ in.q
255         connect(in, C.in)
256         connect(C.out, R.in)
257         connect(R.out, L.in)
258         connect(L.out, out)
259     ]
260
261     compose(ODESystem(eqs, t, sts, ps; name=name), in, out, C, R, L)
262 end
263 """
264 CR(; name, C=1.0, R=1.0)
265
266 Defines compliance, resistor subsystem
267
268 Arguments:
269 C Blood vessel compliance (ml/mmHg)
270 R Blood vessel resistance (mmHg*s/ml)

```

```

272
273 Parameters calculated:
274 del_p Pressure drop across subsystem (mmHg)
275 q Blood flow through subsystem element (ml/s)
276 """
277 @component function CR(; name, R=1.0, C=1.0)
278     @named in = Pin()
279     @named out = Pin()
280
281     sts = @variables del_p(t) = 0.0 q(t) = 0.0
282     ps = []
283
284     @named R = Resistor(R=R)
285     @named C = Compliance(C=C)
286
287     eqs = [
288         del_p ~ out.p - in.p
289         q ~ in.q
290         connect(in, C.in)
291         connect(C.out, R.in)
292         connect(R.out, out)
293     ]
294
295     compose(ODESystem(eqs, t, sts, ps; name=name), in, out, R, C)
296 end

```

### D.3 Solving Windkessel circuits using *ModelingToolkit.jl*

```
1  using ModelingToolkit
2  using DifferentialEquations
3  using Plots
4
5  @variables t
6  D = Differential(t)
7  include("circulatory_system_components.jl")
8
9  ######
10 # DEFINING PARAMETERS THAT WILL BE USED IN WINDKESSEL MODELS #
11 #####
12
13 A = 90          # Blood flow rate mL/s
14 B = 1           # Period of cardiac cycle (s)
15 C_2elem = 1.05
16 C_3elem = 1.1
17 C_4elem = 1.1  # Compliance (ml/mmHg)
18 Rp_2elem = 0.95
19 Rp_3elem = 0.9
20 Rp_4elem = 0.9 # Peripheral resistance (mmHg*s/ml)
21 Rc = 0.05       # Characteristic Resistance (mmHg*s/ml)
22 L = 0.008        # Blood inertia (mmHg*s^2/ml)
23 tspan = (0,10)   # Time period over which ODEs are solved
24 P0 = -78
25
26 #####
27 # BLOOD FLOW FUNCTION (SIMPLE SINE WAVE) #
28 #####
29
30 function flow(t)
31     return A*sin(2*pi*t/(B)-pi/2)+A
32 end
33
```

```

34 # Create vector with blood flow over time for plotting
35
36 t1 = 0.0:0.01:10.0
37 i = []
38 for t in t1
39     append!(i,flow(t))
40 end
41
42 #####
43 # 2 ELEMENT WINDKESSEL #
44 #####
45
46 @mtkmodel WK2model begin
47     @components begin
48         resistor = Resistor(R = Rp_2elem)
49         capacitor = Capacitor(C = C_2elem)
50         source = DrivenCurrent(Q = 1.0)
51         ground = Ground()
52     end
53     @equations begin
54         connect(source.out, resistor.in, capacitor.in)
55         connect(resistor.out, source.in, capacitor.out, ground.g)
56     end
57 end
58
59 @mtkbuild wk2model = WK2model()
60 u0 = [
61     wk2model.capacitor.del_p => P0
62 ]
63 prob = ODEProblem(wk2model, u0, tspan)
64 sol_2_elem = solve(prob, RK4(), reltol=1e-6)
65
66 #####
67 # 3 ELEMENT WINDKESSEL #

```

```

68 #####
69
70 @mtkmodel WK3model begin
71     @components begin
72         resistor_p = Resistor(R = Rp_3elem)
73         resistor_c = Resistor(R = Rc)
74         capacitor = Capacitor(C = C_3elem)
75         source = DrivenCurrent(Q = 1.0)
76         ground = Ground()
77     end
78     @equations begin
79         connect(source.out, resistor_c.in)
80         connect(resistor_c.out, resistor_p.in, capacitor.in)
81         connect(resistor_p.out, capacitor.out, source.in, ground.g)
82     end
83 end
84
85 @mtkbuild wk3model = WK3model()
86 u0 = [
87     wk3model.capacitor.del_p => P0
88 ]
89 prob = ODEProblem(wk3model, u0, tspan)
90 sol_3_elem = solve(prob, RK4(), reltol=1e-6)
91
92 #####
93 # 4 ELEMENT WINDKESSEL #
94 #####
95
96 @mtkmodel WK4model begin
97     @components begin
98         resistor_p = Resistor(R = Rp_4elem)
99         resistor_c = Resistor(R = Rc)
100        capacitor = Capacitor(C = C_4elem)
101        inductor = Inductance(L=L)

```

```

102     source = DrivenCurrent(Q = 1.0)
103     ground = Ground()
104
105 end
106
107 @equations begin
108     connect(source.out, resistor_c.in)
109     connect(resistor_c.out, inductor.in)
110     connect(inductor.out, resistor_p.in, capacitor.in)
111     connect(resistor_p.out, capacitor.out, source.in, ground.g)
112
113 end
114
115
116
117 @mtkbuild wk4model = WK4model()
118 u0 = [
119     wk4model.capacitor.del_p => P0
120 ]
121
122 prob = ODEProblem(wk4model, u0, tspan)
123 sol_4_elem = solve(prob, RK4(), reltol=1e-6)
124
125 #####
126 # PLOTTING #
127 #####
128
129 plot(sol_2_elem, idxs = wk2model.source.del_p, labels="",
130       ylabel="Pressure", xlims=(7.0,10.0), ylims=(70.0,100.0))
131 plot!(sol_3_elem, idxs = wk3model.source.del_p, labels="",
132       xlims=(7.0,10.0))
133 plot!(sol_4_elem, idxs = wk4model.source.del_p, labels="",
134       xlims=(7.0,10.0))
135 plot!(twinx(), t1, i, c=:gray, ls=:dash, xlims=(7.0,10.0), label="",
136       ylabel="Flow Rate (ml/s)")
137 plot!((0, NaN), c=:gray, ls=:dash, label="")

```

## D.4 Building and solving an LPM of the cardiovascular system

```
1  using ModelingToolkit
2  using DifferentialEquations
3  using Plots
4
5  @variables t
6  D = Differential(t)
7  include("model_parameters.jl")
8  include("circulatory_system_components.jl")
9
10 #####
11 # ELASTANCE FUNCTION #
12 #####
13
14 function Elastance(t, E_min, E_max, T, T_es, T_ep, Eshift)
15     # Get time relative to start of cycle
16     t_i = rem(t + (1 - Eshift) * T, T)
17
18     E_p = (t_i <= T_es) * (1 - cos(t_i / T_es * pi)) / 2 +
19         (t_i > T_es) * (t_i <= T_ep) * (1 + cos((t_i - T_es) /
20                                         (T_ep - T_es) * pi)) / 2 +
21         (t_i > T_ep) * 0
22
23     E = E_min + (E_max - E_min) * E_p
24
25     return E
26
27
28 #####
29 # DEFINE COMPONENTS OF CIRCULATORY SYSTEM #
30 #####
31 #####
```

```

32
33 # Heart chambers
34 @named LV = HeartChamber(V_0=v0_lv, p_0=p0_lv, E_min=Emin_lv,
35                                     E_max=Emax_lv, T=T, T_es=Tes_lv,
36                                     T_ep=Ted_lv, Eshift=0.0)
37 @named LA = HeartChamber(V_0=v0_la, p_0=p0_la, E_min=Emin_la,
38                                     E_max=Emax_la, T=T, T_es=Tpww_la / 2,
39                                     T_ep=Tpww_la, Eshift=Tpwb_la)
40 @named RV = HeartChamber(V_0=v0_rv, p_0=p0_rv, E_min=Emin_rv,
41                                     E_max=Emax_rv, T=T, T_es=Tes_rv,
42                                     T_ep=Ted_rv, Eshift=0.0)
43 @named RA = HeartChamber(V_0=v0_ra, p_0=p0_ra, E_min=Emin_ra,
44                                     E_max=Emax_ra, T=T, T_es=Tpww_ra / 2,
45                                     T_ep=Tpww_ra, Eshift=Tpwb_ra)
46
47 # Valves
48 @named AV = HeartValve(CQ=CQ_AV)
49 @named MV = HeartValve(CQ=CQ_MV)
50 @named TV = HeartValve(CQ=CQ_TV)
51 @named PV = HeartValve(CQ=CQ_PV)
52
53 # Systemic circulation
54 @named SAS = CRL(C=Csas, R=Rsas, L=Lsas)
55 @named SAT = CRL(C=Csat, R=Rsat, L=Lsat)
56 @named SAR = Resistor(R=Rsar)
57 @named SCP = Resistor(R=Rscp)
58 @named SVN = CR(R=Rsvn, C=Csvn)
59
60 # Pulmonary circulatioin
61 @named PAS = CRL(C=Cpas, R=Rpas, L=Lpas)
62 @named PAT = CRL(C=Cpat, R=Rpat, L=Lpat)
63 @named PAR = Resistor(R=Rpar)
64 @named PCP = Resistor(R=Rpcp)
65 @named PVN = CR(R=Rpvn, C=Cpvn)

```

```

66
67
68 ######
69 # COMPOSE AND SOLVE ODE SYSTEM #
70 #####
71
72 # Connect components to form circuit
73 circ_eqs = [
74     connect(LV.out, AV.in)
75     connect(AV.out, SAS.in)
76     connect(SAS.out, SAT.in)
77     connect(SAT.out, SAR.in)
78     connect(SAR.out, SCP.in)
79     connect(SCP.out, SVN.in)
80     connect(SVN.out, RA.in)
81     connect(RA.out, TV.in)
82     connect(TV.out, RV.in)
83     connect(RV.out, PV.in)
84     connect(PV.out, PAS.in)
85     connect(PAS.out, PAT.in)
86     connect(PAT.out, PAR.in)
87     connect(PAR.out, PCP.in)
88     connect(PCP.out, PVN.in)
89     connect(PVN.out, LA.in)
90     connect(LA.out, MV.in)
91     connect(MV.out, LV.in)
92 ];
93
94 # Create ODE system
95 @named _circ_model = ODESSystem(circ_eqs, t)
96 @named circ_model = compose(_circ_model,
97     [LV, RV, LA, RA, AV, MV, PV, TV, SAS, SAT, SAR, SCP, SVN, PAS, PAT,
98      PAR, PCP, PVN])
99 circ_sys = structural_simplify(circ_model)

```

```

100
101 #Initial conditions for ODEs
102 u0 = [
103     LV.V => LV_Vt0
104     LV.p => (LV_Vt0 - v0_lv) * Emin_lv + p0_lv
105     RV.V => RV_Vt0
106     RV.p => (RV_Vt0 - v0_rv) * Emin_rv + p0_rv
107     LA.V => LA_Vt0
108     RA.V => RA_Vt0
109     SAS.C.p => pt0sas
110     SAS.C.V => pt0sas * Csas
111     SAS.L.q => qt0sas
112     SAT.C.p => pt0sat
113     SAT.C.V => pt0sat * Csat
114     SAT.L.q => qt0sat
115     SVN.C.p => pt0svn
116     SVN.C.V => pt0svn * Csvn
117     PAS.C.p => pt0pas
118     PAS.C.V => pt0pas * Cpas
119     PAS.L.q => qt0pas
120     PAT.C.p => pt0pat
121     PAT.C.V => pt0pat * Cpat
122     PAT.L.q => qt0pat
123     PVN.C.p => pt0pvn
124     PVN.C.V => pt0pvn * Cpvn
125 ];
126
127 # Solve system of ODEs
128 prob = ODAEProblem(circ_sys, u0, (0.0, 20.0))
129 sol = solve(prob, RK4(), reltol=1e-9, abstol=1e-12, saveat=19:0.01:20)
130
131 #####
132 # PLOTTING RESULTS EXAMPLES #
133 #####

```

```
134  
135 # Pressure in left ventricle  
136 plot((sol.t.-19.0), sol[circ_sys.LV.p], xlabel="t (s)",  
137     ylabel="Pressure (mmHg)", title = "Left Ventricle")  
138  
139 # Pressure in aortic sinus  
140 plot((sol.t.-19.0), sol[circ_sys.SAS.C.p], xlabel="t (s)",  
141     ylabel="Pressure (mmHg)", title = "Aortic sinus")  
142  
143 # Flow through mitral valve  
144 plot((sol.t.-19.0), sol[circ_sys.MV.q], xlabel="t (s)",  
145     ylabel="Flow rate (ml/s)", title = "Mitral valve")
```